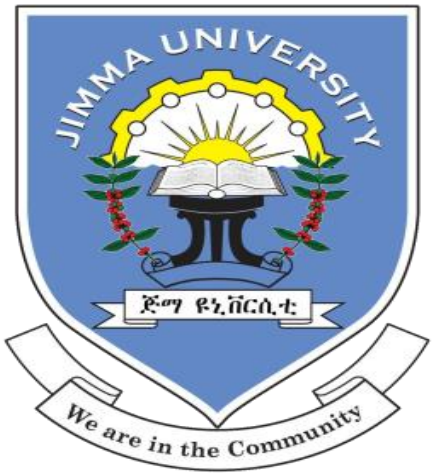


# Jimma University

## Jimma Institute of Technology

## Faculty of Electrical and Computer Engineering

## Control and Instrumentation Engineering (Stream)

A PSO-Based Optimization of a Fuzzy based MPPT Controller for a PV Water Pumping System

**By**

**Tesfaye Tereche**

*A thesis submitted to faculty of electrical and computer engineering, Jimma institute of technology in partial fulfillment of the requirements for the degree of masters of Science in control and instrumentation engineering*

**Advisor: Dr. Fitsum B.**

**Co-Advisor: Tesfabirhan S.**

**Jimma, Ethiopia**

**November, 2021**

**JIMMA UNIVERSITY**

**JIMMA INSTITUTE OF TECHNOLOGY**

**FACULTY OF ELECTRICAL AND COMPUTER ENGINEERING**

**GRADUTE PROGRAM IN CONTROL AND INSTRUMENTATION ENGINEERING**

# A PSO-BASED OPTIMIZATION OF A FUZZY BASED MPPT CONTROLLER FOR A PV WATER PUMPING SYSTEM

***By***

***TESFAYE TERECHE***

***APPROVED BY BOARD OF EXAMINERS***

| | | |
|---|---|---|
| _____ | _____ | _____ |
| *Chairman, Faculty of Electrical and Computer engineering* | Signature | Date |
| _____ | _____ | _____ |
| *External Examiner* | *Signature* | *Date* |
| _____ | _____ | _____ |
| *Internal Examiner* | *Signature* | *Date* |

# CERTIFICATE

This is to certify that the thesis titled “A PSO-based optimization of a fuzzy based MPPT controller for a PV water pumping system”, which was submitted to Jimma University Faculty of Electrical and Computer Engineering for the award of the degree of Master of Science (M.Sc) in Control and Instrumentation Engineering and is a record of genuine research work carried out by Tesfaye Tereche, under my guidance and supervision.

As a result, I hereby declare that no part of this thesis has been submitted for a degree or diploma to any other university or institution.

| Fitsum Bekele |  | 09/10/21 |
|---|---|---|
| Major Advisor Name | Signature | Date |
| _____ | _____ | _____ |
| *Dean of Faculty of Electrical and Computer Engineering* | Signature | Date |

## Declaration

I, the undersigned, declare that this thesis titled "A PSO-based optimization of a fuzzy based MPPT controller for a PV water pumping system" is my original work, has not been presented for the fulfillment of a degree or professional qualification in this or any other university, and all sources and materials used for the thesis have been acknowledged.

| Researcher Name | Signature | Date |
|---|---|---|

The thesis entitled, "A PSO-based optimization of a fuzzy based MPPT controller for a PV water pumping system" submitted by Tesfaye Tereche to Jimma University in partial fulfillment for the degree of MSc. in Control and Instrumentation Engineering is hereby recommended for final evaluation and examination.

| | | |
|---|---|---|
| Fitsum Bekele | | 09/10/21 |
| Major Advisor Name | Signature | Date |
| Tesfabirhan Shope | | 30/11/2021 |
| Co-Advisor Name | Signature | Date |

## Acknowledgement

Firstly and foremost, I would like to thank and praise the Almighty God and holy Virgin Mary for being savior and source of strength to successfully complete this study. Without him at my side I would not have been able to complete this thesis. Secondly, I have a great many thanks to many people who helped me during this work. My deepest appreciation and gratitude goes to my advisor Dr. Fistum Bekele, for guiding and motivating me. As great advisor, He is trying to provide me with guidance and feedbacks about my performance. I am truly honored by having him as teachers and advisors. I also like to thanks my co-advisor Mr. Tesfabirhan Shoga (M.Sc.) for his valuable guidance, support and motivation during my thesis work. Third I owe my greatest appreciation to my parents, who have been the inspirations of my life: your passion for love has contributed immensely to the completion of this study: this is for you. I am grateful to the Faculty of Electrical and Computer Engineering at the Jimma Institute of Technology for providing me the excellent work environment during my study. Let my acknowledgment extend to my classmates, friends, instructors and colleagues in and outside the University. I would like to appreciate all for their friendship and support during my stay at Jimma University. Finally, I acknowledge all other who have helped me and whose names could not be accommodated in this brief acknowledgment. Last, but not least, I would like to express my deep gratitude to Arba Minch University for their continuous encouragement, financial support and study environment that it provides.

# Table of Contents

# List of Figures

# List of Tables

## List of symbols and abbreviations

| | |
|---|---|
| **AC** | Alternating Current |
| **Cb** | Boost capacitor |
| **Cf** | Filter capacitance |
| **COG** | Centre of Gravity |
| **D** | Duty cycle ration |
| **DC** | Direct Current |
| **FIS** | Fuzzy Inference System |
| **FLC** | Fuzzy logic controller |
| $F_o$ | Resonant frequency |
| **G** | Photovoltaic cell's operating irradiation |
| **GTI** | Global tilted irradiation |
| **I*mp*** | Maximum power point current at reference condition |
| **IRC** | International Rescue Committee |
| **ISE** | Integral of square error |
| **Ipv** | Output current of the solar cell |
| **Isc** | Short Circuit current |
| **Lb** | Boost inductor |
| **MOM** | Mean of maximum method |
| **MPP** | Maximum Power Point |
| **MPPT** | Maximum Power Point Tracking |
| **ɳ** | Tracking efficiency |
| **NP** | Number of connected PV cells in parallel |
| **NS** | Number of connected PV cells in series |
| **Ph -** | Pump level head |

| | |
|---|---|
| **Pinv** | Inverter rated output power |
| **Pmax** | Maximum power point |
| **Pout** | Output power of the converter |
| **Ppv** | Output power of the solar cell |
| **PSO** | Particle swarm Optimization |
| **PV** | Photovoltaic |
| **PVWPS** | Photovoltaic water pumping system |
| **PWM** | Pulse Width Modulation |
| ***q*** **-** | Charge of electron |
| ***μ*** | Dynamic viscosity |
| **Rd** | Damping resistance |
| **RMS** | Root mean square |
| **SNNPR** | Southern Nation, Nationalities, and Peoples Region |
| **T** | Photovoltaic cell's operating temperature |
| **TC** | Photovoltaic cell's operating temperature in kelvin |
| **TH** | Total system dynamic head |
| **UNESCO** | United Nations Educational, Scientific and Cultural Organization |
| **Vdc** | Output voltage of the boost converter |
| **Vmp** | Voltage at maximum power of the PV array |
| **Voc** | Open Circuit voltage |
| **Vpv** | Output voltage of the solar cell |
| **VRh** | Vertical rise head |
| **WHO** | World Health Organization |

# ABSTRACT

As part of the sustainable development plan, there is a trend of shifting to a new energy paradigm, in which carbon-free technologies are being extensively used for renewable energy generation, transmission, and consumption. The driving force behind this energy paradigm are enabled by advancement in power switching devices and digital signal processing units that constitute power converters. However, to ensure energy efficiency and reliability from these power converters there is a need to maximum power point tracking (MPPT) in a PV system. To this end, conventional control such as incremental conductance, perturb and observe, constant voltage, load switching schemes find wide applications in distributed generation, microgrids, and power quality compensation. While much has been done to improve their performance, there remains a lot more to do to improve the performance of conventional control techniques for real-time application. In particular, poor performance and/or requirement for complete knowledge of model parameters as well as disturbances are the main drawbacks of conventional control methods. In this work, an alternative Perturb and observe (PO), Fuzzy Logic Control (FLC) scheme in power converters is designed and simulated in SIMULINK/MATLAB. Furthermore, particle swarm optimization (PSO) algorithm is used for fine tuning the FLC inputs and output scaling gains. The total PV panel capacity is 32 kW to supply desired motor rating of 22 kW to supply water demand of 478.4 $m^3$/day at the head of 98 m in the flow rate of 49.2 $m^3$/h. Based on the simulation result for a hypothetical photovoltaic water pumping application demonstrate the efficiency has been 84.99%, 95.65%, and 96.5% for perturb and observe, Fuzzy Logic, and PSO-based Fuzzy controller respectively. So that the results confirm that the proposed PSO-based fuzzy controller methods have the potential to significantly increase the total efficiency of the PV water pumping system. It is recommended to apply hybrid PSO-based Genetic algorithm to improve the speed of convergence and the ability to find the global optimum in the future research investigation in this area.



**Keywords:** Maximum power point tracking (MPPT), Perturb and Observe (PO), Fuzzy Logic Controller (FLC), Particle Swarm Optimization (PSO), power converters.

# CHAPTER ONE

# INTRODUCTION

## 1.1. Background

Water is vital for various human and agricultural needs such as drinking, cooking, washing, bathing, securing health, and guaranteeing food production vitality and the rebuilding of environments. It is critical to use environmentally friendly technology to supply water for drinking. This necessity necessarily requires the use of remote water pumping systems. It will also serve as the first stage of purification and desalination plants, which will create drinkable water. According to United Nation (UN) World Water Development Report in 2015, about one-fifth of the world's population who are nearly 1.2 billion people are lived in districts where water is physically uncommon. One-quarter of the around the world population as well live in developing countries that confront water shortages [1]. Throughout the evolution of civilization in human cultures, there has always been a necessity to supply drinking water and meet regular agricultural demands.

When AC power is available from a neighboring grid, an AC-powered system is cost-effective and requires little maintenance. However, in many rural locations, water sources are dispersed over several miles of land and are too far from existing grid lines. The cost of installing a new transmission line and transformers in remote areas is prohibitively high. In today's world, several diesel engines are employed to power stand-alone water pumping systems. These systems have similar advantages, such as being portable and easy to install, but they require frequent site visits for refueling and maintenance, supply is limited, causes environmental pollution and a high running costs. Furthermore, diesel is expensive and not readily available in rural areas of many developing countries, and even when the fuel is available within the country, transporting the fuel to remote, rural villages is difficult because most of the remote villages lack roads or supporting infrastructure [2].

The usage of fossil fuels has an environmental impact; because of their polluting effects, they are considered a major contributor to climate change. Energy consumption is accompanied by the release of carbon dioxide ($CO_2$) into the atmosphere, which accounts for more than 60% of the world $CO_2$ emissions each year [3]. The $CO_2$ emissions problem can be handled by implementing renewable energy technologies, which are already cost competitive with fossil

fuels in many instances [4]. As part of the sustainable development plan, there is a trend of shifting to a new energy paradigm, in which carbon-free technologies are being extensively used for renewable energy generation, transmission, and consumption. The driving force behind this energy paradigm are enabled by advancement in power switching devices and digital signal processing units that constitute power converters. As result, presently technology focuses on the development of renewable energy sources such as photovoltaic solar energy, wind energy, bioenergy and geothermal energy. Photovoltaic (PV) solar energy is the fastest growing energy source as it is freely available, inexhaustible, clean form of energy, operate silently, low running cost and can be scaled into desired output for specific purposes.

The photovoltaic system consists of interconnected components designed in a way to achieve the specific target of delivering the desired electricity from a small device to the load. Photovoltaic systems are categorized by the main categories of grid-connected, stand-alone systems and hybrid system which comprises different sources of energy such as PV arrays, diesel generators and wind generators. Hybrid and stand-alone systems are used increasingly in rural areas [5]. Therefore, the PV water pumping system considered in this thesis is a stand-alone system to fulfill the needs of people in the rural locations.

The power from the photovoltaic array in the stand-alone system is directly fed to the load without connection to the utility system. The stand-alone system is considered one of the most economic ways of implementing a photovoltaic system especially for application in rural areas that have large periods of intense solar radiation and have no access to the main utility grid. Stand-alone system are modelled and sized in a way that it can be used to power specific DC or AC electrical loads and it can be classified into two types: The direct coupled stand-alone system and stand-alone system that include battery storage. Application of stand-alone system are communication systems, water pumping systems, lighthouses and emergency services or military applications where the auxiliary power units are needed [5].

Photovoltaic water pumping systems have been explored and used in off-grid applications for more than 40 years [6], particularly for drinking purposes. Nevertheless, the extreme drop in costs of PV modules due to the rapid worldwide growth of the PV market over the past long time has boosted research and development of these systems, empowering greater system flexibility and bigger and modern applications [7]. This work focused on the design of Fuzzy PSO-based converter control to get the maximum amount of energy for the required quantity

of demand to pump water from the ground to 5200 residential household needs and to improve the energy conversion efficiency of the PVWPS. The size of system selected for the proposed system is 32kW, which is used to supply 478.4 $m^3$/day water demand of 5200 residential houses.

## 1.2. Statement of the problem

In 2018, UNESCO and Water.org estimated that 61 million Ethiopians lacked access to potable water and 65 million lacked better sanitation [8]. A whopping 27 million people conduct open defecation because they lack access to basic sanitation. People living in rural parts of Ethiopia are using Kerosene lamps or candles to light their home at night time and going long distances to fetch water for drinking and for their domestic utility. In the study location, students use these light options for self-learning or to do their homework at night time and going a minimum of 5-8 km to fetch water to help their family before and after class. Due to this, they waste their reading and home studies time. The PV system is basic in rural areas to generate electric sources for the purpose of the water pumping systems, however many factors limit the implementation of photovoltaic systems. These are high installation cost, power loss, and low efficiency of power conversion.

Out of the total installation cost of the PV system, the storage battery takes the highest one and this process leads to extra power loss because about 15-25% of the power is lost during charging and discharging processes and the PV array should be oversized to cover the energy losses. Furthermore, the batteries require everyday maintenance and degrade very rapidly if the electrolyte is not topped up. Therefore, these factors add significantly to the system price and maintenance burden. So that energy in a water pumping system can be alternatively stored using water tanks to store the water to be used at night time and on days when the solar radiation is insufficient to operate the system by the designed maximum load. On the other hand, altering atmospheric conditions have an impact on the output characteristics of the PV array, this is a challenge to track the exact MPPT with varying source and load conditions due to non-linear voltage-current characteristics of the PV array.

## 1.3. Contribution of the thesis

The utilization of photovoltaic systems for water pumping not only provides potable clean water, but it also helps to reduce global warming. In this thesis, PSO-based Fuzzy control

methods have the quickest time response for tracking the MPP and high efficiency for delivering maximum power to the load than fuzzy logic and conventional techniques. The proposed MPPT methods have the potential to substantially increase the total efficiency of the PVWPS and to enhance the performance of MPP tracking. Most remote and rural areas use diesel-driven pumps for water pumping applications. Diesel pumps consume fossil fuel, impact the environment, needs more maintenance, and are less reliable. Recently PVWP have received extensive concern, due to low operating cost, low maintenance, and flexibility. DC motor has the merit of direct coupling the PV panel for a water pumping system, however, it has limitations like periodic maintenance and high initial cost due to this, the Ac motor is used to pump the water due to the fact of its easy maintenance and low cost. The thesis provided a cost-effective solution by means of replacing the battery which makes the system costy by using a standalone PVWPS and storage tank instead of a battery for bad weather or nighttime conditions.

## 1.4. Thesis objectives

### General objective

The general objective of this thesis is to model and design PSO-based optimization of a fuzzy based MPPT controller for a PV water pumping system.

### Specific objectives

The specific objectives considered in thesis are as follows:

- To analyze the required amount of generated PV power
- To determine required size of motor, pump and required capacity of the water tank
- To model and design power converter for selected PV module
- To design PSO-based Fuzzy controller
- To determine the effect of irradiation and temperature changes on the PV array
- To analyze the efficiency of the proposed system.

## 1.5. Scope and limitation of the thesis

The scope of this thesis is intended to PSO-based optimization of a fuzzy based MPPT controller for a PV water pumping system for the village in Gamo Zone, Arbaminch Zuria

Woreda. From the available different control methods, this thesis has centered on P&O and Fuzzy, PSO-based Fuzzy MPPT controllers. MATLAB/Simulink software is used for modeling and simulation of the system. There are different types of pump technologies available. But, a submerged centrifugal pump is chosen due to its higher reliability, less prone to theft due to harder accessibility than surface pumps. As photovoltaic produces electricity solely when daylight exists, so standalone PV systems require backup energy storage which makes it accessible through the bad climate or night conditions. In standalone PV systems, among many possible storage mediums, batteries are commonly used as a storage aspect which makes the system costy and its charging and discharging losses, due to this storage tank (reservoir) is used for water storage to supply water in terrible weather or night conditions. Hence, the charging and discharging control technique of the battery bank is out of the scope of this thesis. The study additionally includes design, model, and simulation of P&O, fuzzy logic, and PSO-based Fuzzy MPPT control of PVWPS to supply 478.4 $m^3$/day water demand of 5200 residential houses.

## 1.6. Organization of the thesis

This paper is organized into six chapters and the contents of each chapter are discussed below. The first chapter is introductory chapter and presents an overview of the thesis background, the problem statement, objective, scope and contribution of the study, limitation of the study, and brief summary of the thesis. Chapter two discusses a review of literature on some components of the photovoltaic water pumping system and MPPT algorithm with controlling techniques and theoretical overviews of solar energy (PV system), power converters, pump motor, perturb and observe method, and fuzzy logic controller techniques. Chapter three gives the modelling and designing of PVWPS and the modelling of whole components and their operation discussed briefly in this chapter. Chapter four introduces the controller design for the MPPT of PVWPS. In this chapter three MPPT techniques are discussed in detail. It provides perturb and observe method, fuzzy logic control, particle swarm optimization operations. Chapter five presents the MATLAB/Simulink implementation results of the proposed system. This chapter discusses simulation results of the proposed MPPT techniques applied to the water pumping systems. In chapter six conclusions are drawn concerning the MATLAB/Simulink simulation result of three proposed MPPT techniques and recommendation and future work also produced as response to conclusions.

# CHAPTER TWO

# LITERATURE REVIEW AND THEORETICAL BACKGROUND OF PVWPS

## 2.1. Literature review

This chapter reviews and discuses several popular MPPT techniques for solar PV systems that are reviewed in the literature along with their advantages and disadvantages to get better understanding of each MPPT technique and its influence on the system performance. Researchers tried to identify various techniques for optimal allocation and sizing of PVWPS, for enhancing the efficiency of systems. Some reviews of research provided by different authors are mentioned below.

V. Mahes Kumar, and et.al, 2018 [9]. The MPPT approach was used to propose a solar PV-powered BLDC motor-driven water pump in this paper. It makes use of a voltage source inverter (VSI), which allows it to operate the solar PV array at full power. The recommended algorithm employs a single-stage solar energy conversion device with steady-state, starting, and dynamic functionality. It works without sacrificing performance, especially the MPP operation of the PV array, because it employs an incremental conduction (INC) MPPT approach to track MPP. The method's flaws include its inability to track changes, steady-state oscillation at MPP, and order competence.

V. Parimala, D. Ganeshkumar, M. Divya, 2020 [10]. The designs and simulations of an effective photovoltaic water pumping system using the PI and fuzzy logic controller are described in this study. An MPPT with P&O and Increment conduction algorithms is used in the system. Although the proposed algorithm works well with acceptable accuracy when using a fuzzy logic controller, it is unclear how the fuzzy membership functions are tuned to increase the performance of a solar water pumping system.

Abdulhamid Alshamani and Tariq Iqbal, 2017 [11]. This paper describes a study that was conducted in Riyadh, Saudi Arabia, to size a massive deep-water PV water pumping system. This system is linked to a typical Riyadh cultivate that uses 245 $m^3$/day on average. Some beneficial apparatuses, like as Homer and PVsyst, have been used to size such a framework.

The author of this research failed to account for climatic variation, which has an impact on the system's output. No controller is designed to track the maximum power point.

Quentin C., and et.al, 2019 [12]. The goal of this work is to develop a solar photovoltaic-based water pumping system that uses an induction motor. An intelligent speed control method for induction motors is provided to improve the efficiency of the suggested system. The proposed technique employs a fuzzy-PI controller for speed control and torque reference generation. The Perturb and Observe (P&O) approach is utilized to extract the most power out of the PV panel. The downside of this MPPT method is that it has a slow tracking ability, resulting in steady-state oscillation at maximum power.

R. Dahiya, and R. Kumari, 2018 [13]. An induction motor drive is used to power a solar array-based water pump in this paper. Stator current and rotor flux are used as state variables to estimate Induction motor speed. Despite climatic variations, an incremental conductance algorithm-based maximum power point tracker (MPPT) records maximum power from a solar PV array, which results in less efficient MPP tracking.

Ahmed C, Mohamed K, and Aldjia L, 2016 [14]. This document provides the FLC for solar water pumping system maximum power point tracking. A photovoltaic water pumping system with a solar module, a DC/DC converter, a fuzzy controller, and a resistive load is modeled for various environmental conditions. The water pumping system is fed by an induction motor and centrifugal pump, and the fuzzy logic MPP tracker is used. The author of this work does not mention how to increase the system's performance by optimizing the membership function.

D. Devaraj, and et.al, 2021 [15]. The Genetic Algorithm-based fuzzy logic MPPT technique is presented and discussed in this paper. The proposed Genetic algorithm simultaneously optimizes membership function ranges and the fuzzy controller's rule base. The solar photovoltaic system is built and simulated with a GA-based fuzzy logy MPPT controller. The results reveal that the Genetic algorithm-based FLC MPP tracking approach performs better in all climate conditions, with greater tracking accuracy and faster response. PSO, on the other hand, offers several appealing properties when compared to GA. Because PSO has memory, information of the best solutions is kept across all particles, but with GA, whenever the population changes, earlier knowledge of the problem is discarded. It has beneficial particle

collaboration; that is, particles inside the swarm share information with one another. In practice, PSO has been used to optimize a variety of continuous nonlinear functions.

N. Essounbouli, and et.al, 2016 [16]. The optimal scaling parameters of a fuzzy logic controller for maximizing the effectiveness of a photovoltaic water pumping system are found using a GA-based optimization in this research. The introduced GA-based fuzzy controller's performance is compared to that of a fuzzy controller that has not been optimized. FLC requires an expert to define its rules and ranges, and while the outcomes are often satisfactory, they are not ideal. As a result, the authors of this study used GA to optimize the fuzzy rules and membership functions in order to solve this problem. Because of the knowledge of good solution, the system efficiency improved when the fuzzy controller was optimized with PSO instead of GA.

Mustapha Errouha and et.al, 2020 [17]. The performance of an induction motor for a water pumping system driven by a PV system is improved in this paper. The proposed solution is based on a fuzzy logic controller and uses direct torque control. The maximum power point is tracked using a variable Perturb and Observe algorithm, which is not the optimum method for improving the performance of the PV water pumping system by observing the maximum power point of the PV system. As a result, as the insolation varies, the mechanical power is maximized, resulting in an increase in pumped water. Subsequently, the enhancement of the pumped water is achieved by the maximization of the mechanical power as the insolation varies. So, PSO-based fuzzy logic controller is the best technique for the improvement of the pumped water for PV water pumping system.

## 2.2. Theoretical background of PVWPS

### 2.2.1. Basic theories of renewable energy

The electricity which is harvested from natural assets like sunlight, wind, tides, geothermal, heat, etc. is called renewable energy. Renewable electricity sources include solar energy, biomass energy, wind energy, and hydropower, among others [18]. The sun provides all life forms on the planet with a free, silent, and nonpolluting source of energy. Solar energy affords a compelling solution for all societies to meet their needs for clean, considerable sources of energy in the future. Sunlight is easily available, invulnerable from geopolitical tensions, and poses no hazard to our environment and our global climate systems from air pollution

emissions. Electromagnetic waves, which can also be represented by particles or photons, are the primary means through which solar energy is conveyed to the planet. The earth is really a massive photovoltaic power collector receiving large portions of solar energy that occur in more than a few forms, such as direct sunlight used for plant photosynthesis, heated air masses causing wind, and evaporation of the oceans resulting as rain, which forms rivers and offers hydropower. The most frequent solar cells are essentially large pn (thought of as positive-negative) junction diodes that use light energy (photons) to produce DC electricity. No voltage is utilized across the junction; rather, a current is produced in the connected load when the cells are illuminated. The solar cell is made up of n- and p-layers that meet at a junction to form the solar cell (Figure 2.1 and Figure 2.2). Combining doped semiconductor materials like Si or GaAs results in a pn junction [5].

PV cells convert solar energy into direct current power by generating electricity with semiconductors that exhibit the photovoltaic effect. Materials used in solar energy generation include monocrystalline silicon, polycrystalline silicon, cadmium telluride, copper indium gallium sulfide/selenide, and amorphous silicon. The manufacturing of photovoltaic cells and arrays has advanced significantly in recent years due to the renewable energy sources increasing demand [19]. The photovoltaic effect describes a process that produces direct electric current from the radiant energy of the solar. The PV effect can occur in solid, liquid, or gaseous materials, but the best conversion performance has been found in solids, particularly semiconductor materials. Solar cells are made by enlarging semiconductor material and adding certain chemicals. Crystallized silicon is the most widely utilized material for various types of fabrication, accounting for approximately 90% of global commercial PV module output in its many forms. In full sunlight, a conventional silicon cell with a diameter of 10 cm may produce more than 1 W of direct current (DC) energy.

The amount of current generated by a PV cell is determined by its efficiency (kind of PV cell), size (surface area), and the amount of daylight striking the surface. Because a single cell produces a lower electrical output, multiple cells are linked and enclosed (typically with glass) to make a module (also referred to as a panel). Cells can be connected in a series or in a parallel configuration [20]. Using low-power solar PV cells, higher power can be obtained by connecting cells in series and parallel. When connecting PV cells in parallel and series, it is believed that all cells have the same characteristics, i.e. they are identical in all aspects [21].

When two identical cells are connected in series, the output voltage of the two cells is added, while the current flowing through the combination is the same as the current flowing through the single cell. The current from both cells is combined when two cells are connected in parallel, but the voltage of the combination stays the same as a single cell.

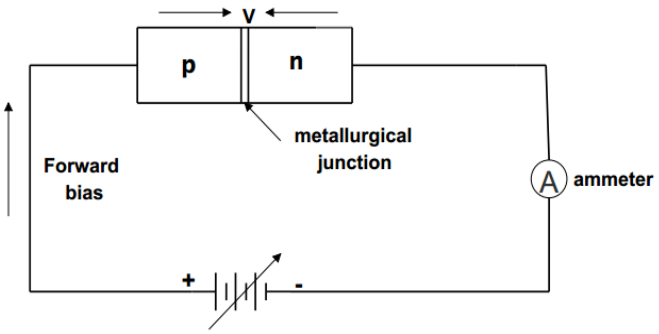


Figure 2.1. P-N junction in a simple circuit [5]

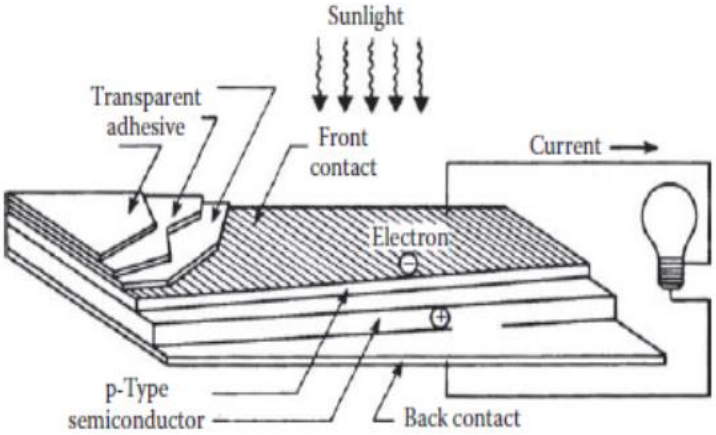


Figure 2.2. PV cell formed by N- and P-layer [5]

Solar cells for terrestrial purposes commonly use single-crystal, poly-crystalline, and amorphous silicon materials. Single-crystal silicon is the most efficient because it is free of grain boundaries, which are flaws in the crystal structure induced by changes in the lattice that tend to impair the material's electrical and thermal conductivity. The sections of single crystals are apparent to the human eye in polycrystalline silicon, which has distinct grain boundaries. Amorphous silicon (a-Si) is the non-crystalline shape of silicon atoms that are organized in a relatively haphazard way. Amorphous silicon has lowest power conversion efficiency of the

three types, however is the least expensive to produce. Figure 2.3 depicts these types of solids pictorially. Mono-crystalline silicon cells are created by cutting, doping, and etching a single crystal silicon ingot in a high-tech facility. The efficiency of industrial terrestrial modules is typically between 15-20%. At 80 percent of nameplate rating, reliable manufacturers of this type of PV module provide guarantees of up to 20-25 years. Polycrystalline silicon cells are made up of various silicon crystals formed from an ingot. They are also sliced and, then doped and etched. They reveal conversion efficiency slightly lower than those of monocrystalline cells, generally from thirteen to fifteen percent. Reliable producers typically guarantee polycrystalline PV modules for 20 years. Amorphous silicon refers to the lack of any geometric cell structure. When compared to crystalline silicon, amorphous modules lack the ordered pattern that crystals have. Commercial modules typically have conversion efficiency from 5-10%. Depending on the manufacturer, most products come with a 10-year guarantee. The technology has yet to achieve big acceptance for larger power applications mostly due to shorter lifetimes from accelerated cell degradation in sunlight (degradation to 80% of original output in most cases). However, amorphous PV has found wide appeal for use in consumer devices (e.g., watches and calculators).

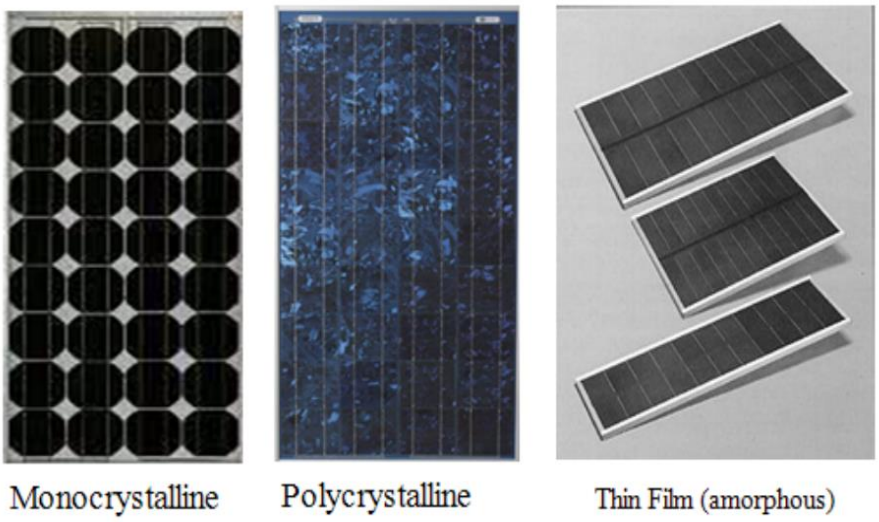


Figure 2.3 Monocrystalline, polycrystalline, and amorphous solids [5]

## 2.2.2. Water pump system

The water pump framework incorporates the motor, the pump, and the couplings. Depending on the type of application and the water demand for water pumping purposes, different types

of coupling are used. The majority of PVWPS are specially connected to solar arrays and use DC motor-driven pumps. This system is straightforward to use, however it is inefficient and in need of constant maintenance. The solar pump with AC drive is powered by an inverter and an AC motor. The solar arrays DC electricity is amplified and sent to an inverter, which converts it to AC for the motor driving the water pump. The majority of PVWPS are specially connected to solar arrays and use DC motor-driven pumps. This system is simple to function but is inefficient and requires frequent maintenance. Different motors and pumps are used based on the daily water requirement, the suction head (for surface-mounted), the pumping head, and the water resource. The more popular are direct current (DC) motors, alternative current (AC) motors, or BLDC motors. Brushless DC (BLDC) motor drives have garnered a lot of attention since their performance is superior to that of traditional brushed DC and AC motors. BLDC motors are best in small units up to 5 kW and have increased the request in photovoltaic water pumping systems because of their higher working efficiency and good starting torque and AC motors (incorporated with inverters) are more attractive for medium to larger installations [22]. As photovoltaic produces electricity only when daylight exists, so standalone PV systems require backup energy storage which makes it accessible through the bad climate or night conditions.

Motors are generally grouped into two types DC-motors and AC-motors. Wound-field DC motors and permanent magnets are the two types of DC motors (brushed and brushless). A permanent magnet is used to deliver the magnetic field in a permanent magnet DC-motor, thus no power is wasted in the field windings, resulting in increased efficiency. As a result, this engine is better suited to smaller solar installations. The squirrel-cage induction motor is the simplest and most affordable type of AC motor. It is the most often used engine for wind/PV systems due to its low cost and sturdy design. Squirrel-cage (asynchronous) motors and wound-rotor motors are the two types of induction motors. In mechanical applications, wound-rotor motors are extensively utilized [23].

An induction motor is a type of electric transformer that has two magnetic fields separated by an air gap, one carrying the primary winding and the other the secondary winding. The primary difference between an induction machine and other types of electric motors is that the secondary currents are generated exclusively by induction, as in a transformer, rather than by a DC exciter or other external power source, as in synchronous and DC machines. The

secondary windings on the rotor of squirrel-cage motors are made of conductor bars that are short-circuited by end rings or are cast in place from conductive alloy. Because the revolving squirrel cage has no electrical connection, there are no brushes or slide rings to wear out or adjust. AC motors are typically employed in applications with medium to high power demands. Induction motors with squirrel-cage rotors are available in single-phase and three-phase configurations. An induction motor's speed is practically constant. Electronic converters, on the other hand, can change the speed of an induction motor (inverters). Inverters are particularly efficient in controlling induction motor speeds over a wide range of speeds and loads. Induction motors were chosen as the components for this study for these reasons.

Photovoltaic pumping is one of the early potential ideas in solar applications. Pump technologies come in a variety of shapes and sizes. The type of pump to use is determined on the application. The most common commercially available configurations of motor pump subsystems are positive displacement (volumetric), centrifugal, and floating-point motor pumps. In the centrifugal pump, water is forced into the tube by the rotation of an impeller. Positive displacement pumps use a piston or a screw to control the water flow, whereas rotating impeller mechanical power and total dynamic head determine pressure and water velocity. The positive displacement pump is far more efficient than the centrifugal pump in low-power situations. Various sorts of driving systems can be used to power the water pumps.

## 2.3. MPPT controller algorithms

There are numerous strategies for maximizing the output power from the PV modules either ordinary techniques like incremental conductance method, P&O method, open-circuit voltage, and short-circuit current method, or intelligent methods like fuzzy control [24] [25]. Using ordinary strategy the MPP can be found for specified solar irradiation and temperature conditions but they show oscillatory behavior around the maximum power point under typical operating conditions. Additionally, the system will not react rapidly to fast changes in temperature or irradiance.

Several MPPT algorithms for PV power systems have been presented in recent years to detect the MPP and improve system efficiency. Direct control or "real tracking techniques" and indirect control or "quasi following techniques" are the two types of MPPT algorithms” [26].

The maximum power point is computed in indirect control systems by measuring the photovoltaic array's current and voltage, as well as solar insolation, or by using mathematical formulae derived from empirical data. As a result, current methods can't track MPP changes in response to irradiation or temperature. Indirect control methods include the look-up table approach, constant voltage technique, fractional short-circuit current, and fractional open-circuit voltage. In any event, because they don't rely on past knowledge of or derived data from the PV array V-I characteristics, true following techniques have the ability to discover the optimum operating point even under changing atmospheric conditions. The true tracking techniques include P&O and incremental conductance. One or two variables from the tracking process are used to determine the MPP. The PV array output voltage or current is used in only one variable in the fractional open-circuit voltage and fractional short-circuit current techniques, whereas the MPP is calculated using both variables in the P&O and INC methods.

### 2.3.1. Classical control techniques

### A. Simple panel load matching

The simple panel load matching technique is one of the simplest techniques to operate a PV array close to its maximum power point. In this technique the optimum operating point of the PV array is determined either by a series of measurements under average operating conditions or theoretical calculation. The load is designed to produce the values of PV voltage and current corresponding to the MPP. There is another commonly used simple method that is widely used all over the world in PV battery charger systems, which involves choosing the average battery voltage close to the average solar panel [27]. This method has the advantages of simplicity and no additional circuitry is used, therefore, the power loss between the panel and the battery is reduced and the risk of component failure is kept low for the whole system. However, the system does not take into consideration the changes of solar irradiation or temperature [27].

### B. Load switching technique

Different panels are connected in series and parallel in a suitable way to construct a PV array using the load switching technique setup. To complete the load matching procedure, the PV cluster is next connected to a series of controlled battery cells. The batteries are used to store the energy generated by the solar panels. The control unit detects the PV array's output in real time, determines the optimum operating point, and switches the battery connection to maintain

operation as close to this as possible. This method has the disadvantages of requiring additional switching circuits and wiring, and the stepwise, switched operating voltage cannot ensure exact tracking of MPP. Additionally, maintaining an equal charge level on all battery cells is difficult, resulting in battery life degradation over time.

## C. Constant voltage method (CV)

If the PV system is implemented without a battery to tie the bus voltage to an approximately constant level, a simple control scheme of the constant voltage method can be applied as presented in [28]. The PV voltage feedback is compared to a set reference voltage in this approach, and the resulting signal adjusts the duty ratio of the DC-DC converter to keep the PV array operating point as close to the MPP as possible. This technique has the disadvantage that it does not correct for environmental variables such as a change in irradiation and temperature it fixes the reference voltage to a best-fixed voltage value and holds it constant beneath any operating condition rather than following the MPP [29].

## D. Perturb and observe (P&O) algorithm

Perturb and observation algorithm is considered to be the most commonly used MPPT algorithm, among the other techniques since of its simple structure and ease of implementation. It is based on the concept that on the power-voltage curve, the change in the PV array output power is equal to zero ($\Delta P_{PV} = 0$) on the top of the curve as shown in Figure 2.4 below.

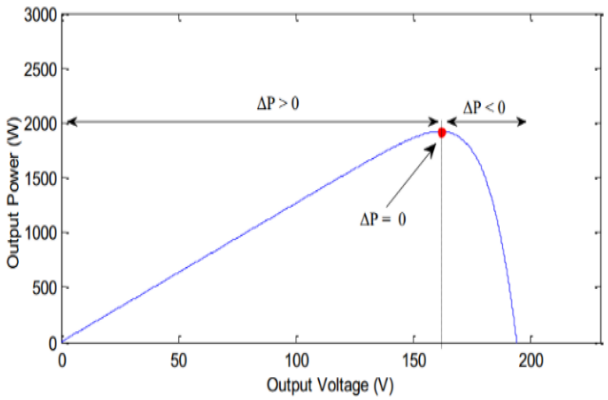


Figure 2.4. Perturbs and observes technique

The P&O works by periodically perturbing (incrementing or decrementing) the PV array terminal current or voltage and comparing the corresponding output power of the PV array. If the perturbation in terminal voltage leads to extend in the PV power ($\Delta P_{PV} > 0$) the perturbation

ought to be kept in the same direction, otherwise, the perturbation is moved to the inverse direction. The perturbation cycle is repeated until the maximum power i.e. $\Delta P_{PV} = 0$ is reached. The advantages of this technique are simplicity, ease of implementation and it does not require a previous knowledge of the PV array. On the other hand, P&O will not stop perturbing when the MPP is reached and will oscillate around it resulting in some unnecessary power loss.

### 2.3.2. Fuzzy logic control techniques

Recently artificial intelligence-based schemes have been introduced. In a control system, fuzzy logic is utilized to simulate human-like decisions. Due to its heuristic character linked to simplicity and efficacy for both linear and nonlinear systems, fuzzy logic techniques have been widely applied in a wide range of engineering applications [30]. It can be implemented in either hardware or software, or a combination of both. Fuzzy logic is a modified version of Boolean logic designed to deal with partial truth. We can see that any action in Boolean logic can provide true or false results. If we refer to true by (1) and the false by (0) then the result may be (1) or (0) [31]. Figure 2.5 shows an example of a classical set that has two values true or false. We see that the classical set has crisp boundaries. And this example shows an age example: the man is old if he is between 50 years and 60 years in that interval all age has the same degree (1). And outside of this interval, it has (0) degrees. However, there is an issue; at 49 years and 11 months, is the man still young? No, he is elderly, yet his degree is less than 50 years, but there are no degrees in the Classical sets; instead, there are only two values: 1 or 0. So what is the solution, fuzzy sets give the solution.

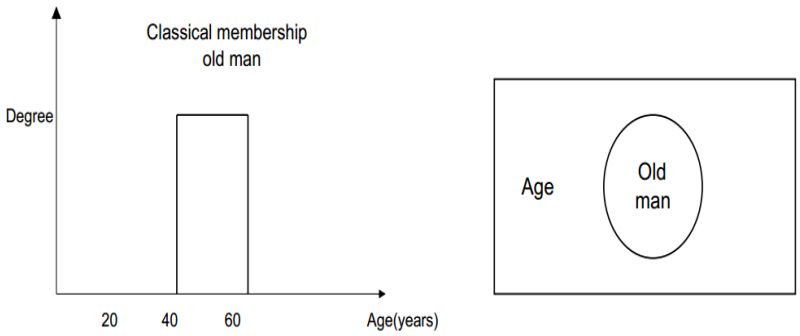


Figure 2.5 Classical set [32]

Sets that lack crispness are referred to as fuzzy [32]. There are no two values (true or false), but there are two limitations: (1) fully true and (0) completely false, with the outcome falling

somewhere between these two limits. The ages between the intervals (50, 60) have the same degree, as indicated in Figure 2.6 below. However, the man is old outside of this interval, but to a different degree, and this set solves the problem of 49 years and 11 months. In Figure 2.6 we see two circles the small circle is (old man) set. Every element inside it has the same degree (1), and there are varying degrees of (old man) between the tiny circle and the big circle, and every element outside the huge cycle has the same degree (0). The second definition is the mathematical representation of fuzzy sets. The fuzzy control system's brain, fuzzy sets, are in charge of converting analog input values to a scale of 0 to 1.

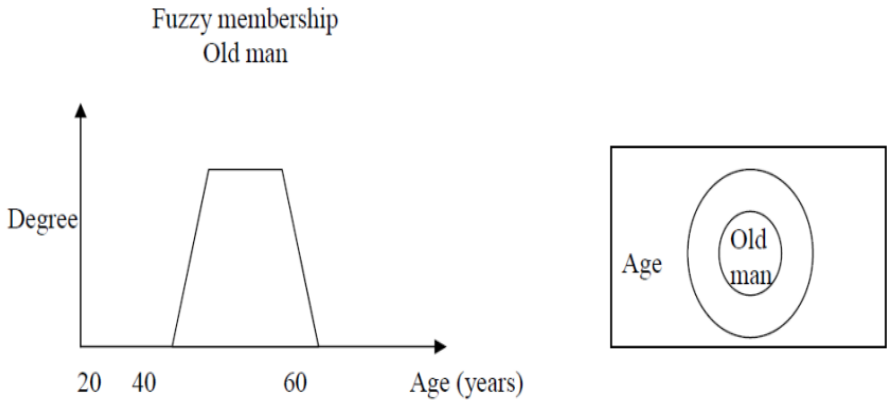


Figure 2.6 Fuzzy sets [32]

A fuzzy logic controller has its own advantages among the intelligent control methods such that the MPPT algorithm can be effectively formed. Fuzzy control systems have been tested in many practical and industrial applications as an important modeling tool since they can work with imprecise inputs, do not require correct mathematical modeling, and can handle the nonlinearities and uncertainties [33]. The main demerits of the fuzzy logic techniques are its challenge for choosing the number of optimum tuning parameters. In this paper, a method has been introduced for finding the optimized membership functions, input and output gain of a fuzzy controller using PSO. PSO has seen a lot of success in recent years, particularly in optimization and search issues; the main reason for this success is that it can start from any solution and develop the best solutions that converge to the optimal solution in less time than other traditional search tools.

# CHAPTER THREE
# MODELLING AND DESIGN OF STANDALONE PV WATER PUMPING SYSTEM

This chapter covers the PV water pumping system's component characteristics, circuit design, and mathematical modeling. The effect of atmospheric conditions on the I-V and P-V output characteristics of the solar cell and module are shown and analyzed using a mathematical model of the solar cell and module. This chapter introduces and explores several DC-DC converters, which are often used in MPPT power converters in PV systems, in order to determine which converter is best for an AC motor pump load. The AC motor and pump that will be utilized in the system are discussed in this chapter, as well as how to choose the most appropriate and efficient AC motor pump combination. When linked to the MPPT, the load characteristics will be examined and discussed with the PV module characteristics.

## 3.1. Water pumping system design

The designer of a solar pumping system must fit the separate components together. As depicted in Figure 3.1, a solar water pumping system consists of three primary components: the solar array, pump controller, and electric water pump (motor and pump).

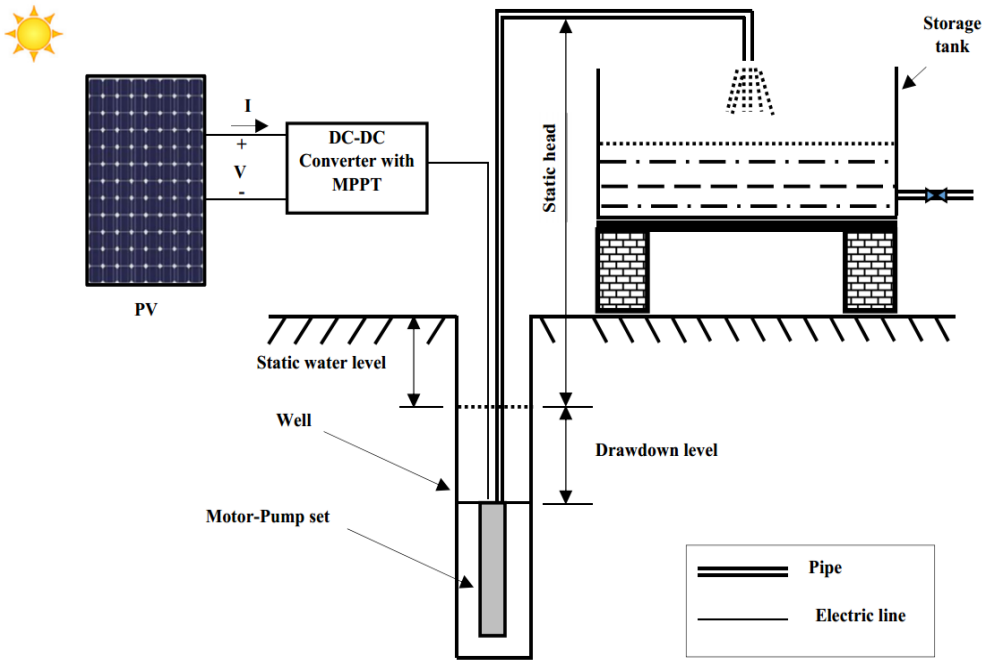


Figure 3.1 Schematic diagram of proposed system

The information of the site location, including sun irradiation, how many gallons of water must be pumped per day and the total system dynamic head is essential for designing and selecting the right PV pumping system. So that, this thesis focused on a solution to the water problems that plagued 5200 residential homes. The Water level data were compiled from UNESCO and IRC [34]. From the site survey, the number of households and population has been corrected as shown in Table 3.3 and Table 3.4 below. The framework that is followed in this thesis are shown by Figure 3.2 below.

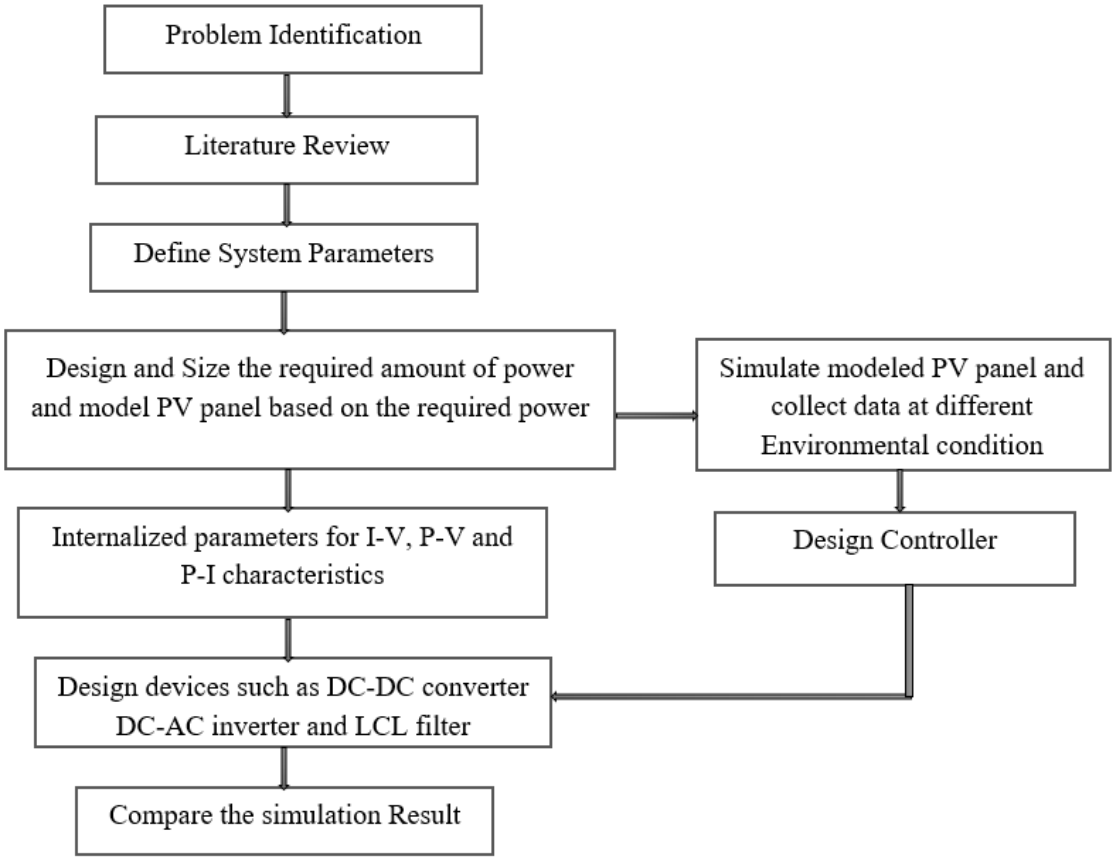


Figure 3.2 Framework of proposed system

Table 3.1. Water requirement activities per person

| Activities | Drinking | Cooking | Personal washing | Cleaning Home | Average Number of family/Home | Total |
|---|---|---|---|---|---|---|
| Water used L/day | 3 | 5 | 10 | 5 | 4 | 92 |

Table 3.2 Number of residential households

| Population | Quantity |
|---|---|
| Number of households | 1182 |
| Average population per household | 4 |
| Current population | 4728 |
| Expected rise in population in the future (10%) | 472 |
| Total population | 5200 |

According to WHO, the minimum water requirement for drinking, cooking, personal washing, washing clothes, cleaning home and sanitation is 70 liters/person/day [35]. For this thesis minimum water requirement is to be 92 Liters/person/day. From this, taking the maximum population to be 5200, the total water requirement per day is 478400 liters/day.

$$Q_{day} = N_r * 92 = 5200 * 92 = 478{,}400\,{}^{L}/_{day} \quad 3\text{-}1$$

Where, $N_r$ is number of residential i.e. 5200.

Uncertainty of data: ±7 to 10%, [36]. Drinking water system design is more delicate than irrigation system design. In the case of irrigation, supplementary rainfall adds to the water output of the SWPS whereas, for the drinking water system, the demand is constant throughout the year and must be fulfilled by the pump. Because of this, the minimum average GTI is taken as the basis of peak sun hours. From Table 3.4, the minimum average GTI is 4.5 kWh/m2/day in the month of July. This is reasonable since July is the rainstorm season and the climate is for the most part cloudy. In expansion, the maximum uncertainty of data (10%) is further factored in for safety. The daily average GTI (kW h/$m^2$/day) can also be interpreted as 'peak sun hours' since the accumulation of total irradiation over a day represents equivalent hours of rated radiation, i.e. 1,000 W/$m^2$. In other words, 4.5 kW h/m2/day can be interpreted as 1,000 W/$m^2$ of radiation over 4.5 hours (1,000 W/$m^2$ * 4.5 hours = 4,500 Wh/$m^2$ = 4.5 kWh/$m^2$). Presently, the peak sun hours for design basis is: $4.5 * (1 - 10\%) = 4.05$ kWh/$m^2$/day. Guaranteeing that the system can deliver water demand in 4.05 kWh/$m^2$/day will ensure that it can meet the water demand in any other month of the year.

Table 3.3. Average temperature of Arba Minch [34]

| | Ann | Jan | Feb | Mar | Apr | May | Jun | Jul | Aug | Sep | Oct | Nov | Dec |
|---|---|---|---|---|---|---|---|---|---|---|---|---|---|
| $^0$C | 25.2 | 25.6 | 26.6 | 27.4 | 26.1 | 25.2 | 24.6 | 23.9 | 24.2 | 25 | 24.9 | 25 | 24.6 |

## Global tilted irradiation profile

Table 3.4. Daily averages of GTI of Arba Minch [34]

| Month | Max | Min | Average (MJ/m$^2$ ) | Average (kWh/m$^2$ ) |
|---|---|---|---|---|
| Jan | 22.5 | 19.7 | 21.1 | 5.86 |
| Feb | 23.8 | 20.2 | 22 | 6.11 |
| Mar | 23.2 | 20.3 | 21.75 | 6.04 |
| Apr | 21.4 | 19.5 | 20.45 | 5.68 |
| May | 20.9 | 19.8 | 20.35 | 5.65 |
| Jun | 19.2 | 16.4 | 17.8 | 4.94 |
| Jul | 17.5 | 14.9 | 16.2 | 4.50 |
| Aug | 18.6 | 15.6 | 17.1 | 4.75 |
| Sep | 20.4 | 18.9 | 19.65 | 5.45 |
| Oct | 20.5 | 17.5 | 19 | 5.28 |
| Nob | 22 | 18.5 | 20.25 | 5.62 |
| Dec | 22.2 | 18.8 | 20.5 | 5.69 |

## Total system dynamic head ( $T_h$)

In solar pumping system, the total lifting height ( $T_h$) is the main parameter to decide the necessary power to move the water from the well depth level to the desired place.

$$T_h = P_h + VR_h + f_h + V_h + D_h + H_{pipe} \quad 3\text{-}2$$

Where $T_h$ is total system dynamic head, $VR_h$ Vertical rise head, $P_h$ is pump level head, $f_h$ is a head due to friction loss, $V_h$ is velocity head, $D_h$ is dynamic head loss, and $H_{pipe}$ is the length of pipe in horizontal surface.

## Determination of head due to friction ($f_h$)

To calculate $f_h$ apply Darcy-Weisbach formula

$$f_h = \frac{4fl}{d}\frac{c^2}{2g} \quad 3\text{-}3$$

Where f is friction factor, l is length of pipe, d is pipe diameter and c is velocity of fluid. But determine the friction factor, f‟ is more debatable, for smooth flow and smooth pipes, Blasius equation is applicable. For turbulent flow equation 3.7 is applicable.

$$f = \frac{0.079}{Re^{1.4}} \quad 3\text{-}4$$

Where Re is Reynolds number.

If Re < 2,000, then flow is laminar. If Re > 4,000, then flow is turbulent.

Most simplify form of Blasius equation is i.e. for laminar flow:

$$Re = \frac{\rho * V * d}{\mu} \quad 3\text{-}5$$

Where ρ is density of water (1000kg/m$^3$), μ is dynamic viscosity (1.14x10$^{-3}$Ns/m), V is velocity of fluid (m/s) i.e. $0.44\ \mathrm{m/s}$, d is internal diameter of pipe (m) i.e. 0.2m and e is the roughness of the pipe take PVC (0.009)

$$Re = 1000 * 0.44 * \frac{0.2}{1.14*10^{-3}} = 7.7192 * 10^4 \quad 3\text{-}6$$

If Re > 4000 then the flow is turbulent and if Re < 2000 the flow is laminar [37].

$$f = \begin{cases} \frac{64}{Re}, & \mathrm{Re} < 2000 \\ \frac{1.325}{\left[\ln\left(\frac{e}{3.7d} + \frac{5.74}{Re^{0.9}}\right)\right]^2}, & \mathrm{Re} > 4000 \end{cases} \quad 3\text{-}7$$

Since Re > 4000 equation 3-8 is used

$$f = \frac{1.325}{\left[\ln\left(\frac{e}{3.7d} + \frac{5.74}{Re^{0.9}}\right)\right]^2} \quad 3\text{-}8$$

$$f = 0.783 \quad 3\text{-}9$$

$$f_h = \frac{4*0.783*86}{0.2}\frac{0.354^2}{2*9.81} = 8.6m \quad 3\text{-}10$$

Where,

$$l = P_h + VR_h + H_{pipe} = 70 + 6 + 10 = 86m \quad 3\text{-}11$$

## Determination of velocity head ($V_h$)

$$V_h = \frac{c^2}{2*g} \quad 3\text{-}12$$

Where water velocity ($c = \frac{Q_{pump}}{A}$) but cross section area ( $A = \frac{\pi}{4}d^2 = 0.0314m^2$) but, pump capacity or flow rate can be calculated as ($Q_{day} = 478400\,{}^{L}/_{day}$) water required per day;

If the pump works 10 hours per day and the average peak-sun-hours in Arbaminch is 4.05 kWh/m$^2$/day [36].

$$Q_{pump} = \frac{hw}{psh} * Q_{day} = \frac{10}{4.05} * 478400 = 1{,}181{,}234.57\,{}^{L}/_{day} \quad 3\text{-}13$$

$$Q_{pump} = 13.7\,{}^{L}/_{sec} = 0.0137\,{}^{m^3}/_{sec} = 49.2\,{}^{m^3}/_{h} \quad 3\text{-}14$$

Therefore, the required hourly flow of pump is 49.2 m$^3$/h.

$$c = \frac{0.0137\ m^3/sec}{0.0314m^2} = 0.44\,{}^{m}/_{sec} \quad 3\text{-}15$$

Then velocity head loss will be

$$V_h = \frac{C^2}{2*g} = \frac{0.44^2}{2*9.81} = 0.01m \quad 3\text{-}16$$

## Determination of dynamic head loss ( $D_h$)

Using Darcy Weisbach equation given by:

$$D_h = \frac{kc^2}{2*g}\ , k = k_{pipe} + k_{fitting} \quad 3\text{-}17$$

$k_{pipe}$ is associated with the straight length of pipe used in the system and defends as

$$k_{pipe} = \frac{fl}{d} = 336.69 \quad 3\text{-}18$$

$k_{fitting}$ is the fittings used in the pipe works of the system to pump the water from ground to the receiving tank and $k_{pipe}$ values are received from standard tables and a total $k_{fitting}$ values can be calculated by adding all the $k_{fitting}$ values for each individual fitting within the system. The calculation of $k_{fitting}$ for the system under discussion is shown in Table 3.5.

$$D_h = \frac{(336.69+2.8)}{2*9.81} * 0.44^2 = 3.3m \quad 3\text{-}19$$

$$T_h = 70 + 6 + 10 + 8.6 + 0.01 + 3.3 = 98m \quad 3\text{-}20$$

Table 3.5. The calculation of $k_{fitting}$ for the system

| Fitting items | No of item | $k_{fitting}$ value | Total item |
|---|---|---|---|
| No return valves | 1 | 1 | 1 |
| $90^0$ bend | 2 | 0.75 | 1.5 |
| Valves (fully open) | 1 | 0.3 | 0.3 |

### 3.1.1. Pump power determination and selection

This step is an important step to estimate what amount of power is required to take the ground water to the surface.

$$P_h = \frac{q*\rho*g*T_h}{3.6*10^6} \quad 3\text{-}21$$

Where $P_h$ hydraulic power (kW), q fluid flow rate ($^{m^3}/_h$), ρ density of fluid (kg/m$^3$), g acceleration due to gravity (m/s$^2$), $T_h$ total dynamic head (m)

$$P_h = 13.13kW \quad 3\text{-}22$$

Therefore, the PV generator power (kW) necessary can be written as

$$P_s = \frac{P_h}{\mu_{pump}} kW = 22kW \quad 3\text{-}23$$

Now, the efficiency of pump is dependent on the producer. For preliminary estimation, engine to shaft efficiency of 60% is taken for this thesis. In this manner, the theoretical pump size is 22 kW. The actual pump size may differ slightly due to different efficiency point at given head and flow.

$$P_{pv} = \frac{P_s}{\delta} = 24kW \quad 3\text{-}24$$

Where,δ is the PV mismatch factor values range between 0.85 and 0.90, the value of δ selected is 0.9 for this thesis [38].

Considering operating factor (OF=0.75) (to reimburse for the energy falling due to warm, dirt and ageing) [38].

$$Total\ PV\ panel\ Capacity\ = \frac{P_{pv}}{OF} \quad 3\text{-}25$$

$$Total\ PV\ panel\ Capacity = 24\ kW/0.75\ = 32\ kW \quad 3\text{-}26$$

The pump should fulfill the desired flow rate and move waters in to the total dynamic head of the system to fill the specified liters of water. That's to lift 478.4 m$^3$ water at the head of 98m

in the flow rate of 49.2 $m^3$/h with the rating up to 22kW motor standard. The motor for this thesis is three-phase induction motor.

### 3.1.2. Water storage tank sizing

Nowadays, effective water management becomes more imperative all over the world [37]. Reservoirs have become more important in water resource management as a result of global climate change and population increase. Irrigation, hydropower generation, industrial and municipal water supply, recreation, flood protection, water quality control, low flow augmentation, and so on can all be done using a water storage tank. It was assumed that cloudy days or the absence of lighting are only two. Hence, the size of tank is to be evaluated as:

$$\text{Water tank size} = \text{Number of Cloudy days} * \text{average amount of Water}$$

$$= 2 * 478.4\ m^3 = 956.8 m^3 \qquad 3\text{-}27$$

## 3.2. General modeling of solar cell

The one-diode/two-resistors circuit model as shown in Figure 3.3 below is one of the most commonly used to model and study the behavior of solar cells [39].

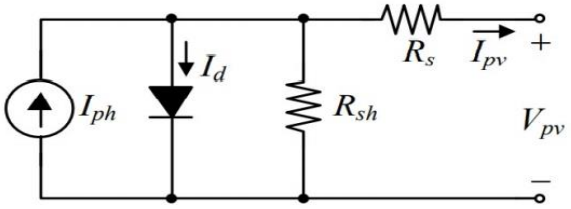


Figure 3.3. 1-diode/2-resistors solar cell electrical equivalent circuit model

$$I_{pv} = I_{ph} - I_s\left(\exp\left(\frac{V_{pv} + I_{pv}R_s}{\alpha V_t}\right) - 1\right) - \frac{V_{pv} + I_{pv}R_s}{R_{sh}} \qquad 3\text{-}28$$

Where $I_{ph}$ photon current, $I_s$ saturation current, $R_s$ is the series resistance, $R_{sh}$ is the shunt resistance, and $\alpha$ *is* the ideality factor of the diode. A common value for $\alpha$ is 1.2 for Silicon mono and 1.3 for Silicon poly, 1.3 for AsGa, and 1.5 for CdTe, and (Id) is diode current [39].

$$V_t = \frac{kT}{q} \qquad 3\text{-}29$$

Where q is the electron charge (1.602 × 10−19 C), k is Boltzmann's constant (1.381 × 10−23 J/K), and T is the junction temperature (K).

The five-parameter model of the solar photovoltaic module is utilized (Figure 3.3). Thus, the PV array is composed of an association of Ns modules in series and in parallel $N_p$ to attain the desired current and voltage, hence, the output current is given by

$$I_{pv} = I_{ph} - I_d - I_{sh} \quad 3\text{-}30$$

$$I_{sh} = \frac{V_{pv}+I_{pv}R_s}{R_{sh}} \quad 3\text{-}31$$

$$I_d = I_s\left(\exp(\frac{V_{pv}}{V_t}) - 1\right) \quad 3\text{-}32$$

The saturation current ($I_s$) also depends on the temperature according to the following expression:

$$I_s = I_{rs}\left(\frac{T}{T_{ref}}\right)^3 exp\left[\frac{q.E_{go}}{nk}\left(\frac{1}{T_{ref}} - \frac{1}{T}\right)\right] \quad 3\text{-}33$$

$T_{ref}$ is reference temperature in kelvin (298.15K) and $I_{rs}$ is the cell reverse saturation current in ampere at reference temperature and Ego is the band-gap energy of the semiconductor used in the cell. $E_{go}$~1.12 for polycrystalline silicon panels.

$$I_{rs} = \frac{I_{sc}}{\exp\left(\frac{V_{oc}}{V_t N_s}\right)-1} \quad 3\text{-}34$$

The photovoltaic current is linearly dependent on the irradiance (G) and is also influenced by the temperature T according to the following equation.

$$I_{ph} = \left(I_{ph,ref} + K_i\left(T - T_{ref}\right)\right).\frac{G}{G_{ref}} \quad 3\text{-}35$$

$I_{ph,ref}$ is the photovoltaic current generated at nominal conditions (T = 298.15 K and $G$=1000 W/m²), and $K_i$, coefficient of variation of current as a function of temperature.

$$I_{ph,ref} = \left(\frac{R_{sh}+R_s}{R_{sh}}\right).I_{sc,ref} \quad 3\text{-}36$$

Where $I_{sc,ref}$ is rated short-circuit current under nominal conditions of temperature and irradiation. Then from the above equations Current $I_{pv}$ generated by the panel is expressed as a function of $R_s$ and $R_{sh}$ resistors, voltage and currents and as follows:

$$I_{pv} = N_p I_{ph} - N_p I_s\left(\exp\left(\frac{1}{V_t}\left(\frac{V_{pv}}{N_s} + \frac{R_s}{N_p}I_{pv}\right)\right) - 1\right) - \frac{N_p}{R_{sh}}\left(\frac{V_{pv}}{N_s} + \frac{R_s}{N_p}I_{pv}\right) \quad 3\text{-}37$$

Obviously, prior to the use of this model to simulate the cell behavior it is necessary to identify the five parameters $I_{ph}$, $I_o, R_s$, $Rsh$, and $a$. Boundary conditions obtained from either manufacturer's data, or by testing the solar cell are used to calculate this parameters.

The short circuit current $I_{sc}$, is defined as the current that flows when the terminals are shorted together. This is equal to the magnitude of the ideal current source and the open-circuit voltage $V_{oc}$ is defined as the voltage across the terminals when the loads are left open.

The short-circuit conditions once introduced in equation (3.28), lead to the following expression,

$$I_{sc} = I_{ph} - I_s\left(\exp(\frac{I_{sc}R_s}{\alpha V_t}) - 1\right) - \frac{I_{sc}R_s}{R_{sh}} \quad 3\text{-}38$$

The second term of the right side of (3.38) can be neglected, and the expression in equation 3.38 can be rewritten as:

$$I_{ph} = \frac{R_s+R_{sh}}{R_{sh}} I_{sc} \quad 3\text{-}39$$

From the open circuit conditions, equation (3.28) can be rewritten as:

$$0 = I_{ph} - I_s\left(\exp\left(\frac{V_{oc}}{\alpha V_t}\right) - 1\right) - \frac{V_{oc}}{R_{sh}} \quad 3\text{-}40$$

From equations (3.39) and (3.38), the saturation current, Io, can be reduced to:

$$I_s = \frac{(R_s+R_{sh})I_{sc}-V_{oc}}{R_{sh}\exp\left(\frac{V_{oc}}{\alpha V_t}\right)} \quad 3\text{-}41$$

The following expression is obtained, if equation (3.28) is evaluated at the MPP:

$$I_{mp} = I_{ph} - I_s\left(\exp(\frac{V_{mp}+I_{mp}R_s}{\alpha V_t}) - 1\right) - \frac{V_{mp}+I_{mp}R_s}{R_{sh}} \quad 3\text{-}42$$

Once more, analyzing relative magnitude of the different terms of the expression above, it is possible to neglect the second term inside the brackets. Finally, the following expression without dependence of $I_{pv}$ and $I_s$ can be derived from equation (3.39), (3.41) and (3.42).

$$I_{mp} = I_{sc} - \left(I_{sc} - \frac{V_{oc}-I_{sc}R_s}{R_{sh}}\right)\left[exp\left(\frac{V_{mp}+I_{mp}-V_{oc}}{\alpha V_t}\right)\right] - \frac{V_{mp}+I_{mp}R_s-I_{sc}R_s}{R_{sh}} \quad 3\text{-}43$$

Taking also into account equation (3-28) differentiated once with respect to V, and the following expression obtained as given in equation 3-44.

$$\frac{dI}{dV} = -\frac{I_s}{\alpha V_t}\left(1 + \frac{dI}{dV}R_s\right)\left(exp\left(\frac{V+IR_s}{\alpha V_t}\right)\right) - \frac{1}{R_{sh}}\left(1 + \frac{dI}{dV}R_s\right) \quad 3\text{-}44$$

On the other hand, taking into account expressions (3-39), (3-41) and (3-43), it is possible to derive from equation. (3-44) an implicit expression of the series resistor, *Rs*, as a function of the initial parameters:

$$\frac{\alpha V_t V_{mp}(2I_{mp}-I_{sc})}{(V_{mp}I_{sc}+V_{oc}(I_{mp}-I_{sc}))(V_{mp}-I_{sc}R_s)-\alpha V_t(V_{mp}I_{sc}-V_{oc}I_{mp})} = exp\left(\frac{V_{mp}+I_{mp}R_s-V_{oc}}{\alpha V_t}\right) \quad 3\text{-}45$$

And finally, equation (3-44) combined with equation (3-42) leads to the final expression of the shunt resistor,$R_{sh}$ as a function of $R_s$ and the initial parameters:

$$R_{sh} = \frac{(V_{mp}+I_{mp}R_s)(V_{mp}-R_s(I_{sc}-I_{mp})-\alpha V_t)}{(V_{mp}+I_{mp}R_s)(I_{sc}-I_{mp})-\alpha V_t I_{mp}} \quad 3\text{-}46$$

$$R_{sho} = -\left(\frac{\partial V}{\partial I}\right)|I = I_{sc} \quad 3\text{-}47$$

$$R_{so} = -\left(\frac{\partial V}{\partial I}\right)|V = V_{oc} \quad 3\text{-}48$$

It appears that using the slope at the short circuit point $R_{sho}$, rather than the slope at the open circuit point $R_{so}$ as the extra boundary condition for calculating the ideality factor, a, is preferable. In this way, the ultimate expressions of the method have a more simple form. It should also be cited that some writers prefer to use this boundary conditions in their calculations to fit their models to the I-V curve, instead of the slope of the curve at the open circuit point (expression (3-48). Once the value of $R_{sho}$ has been estimated, the extra boundary condition at the short circuit point can be expressed as:

$$\frac{1}{R_{sho}} - \frac{1}{R_{sho}-R_s} + \frac{I_s}{\alpha V_t} exp\left(\frac{I_{sc}R_s}{\alpha V_t}\right) = 0 \quad 3\text{-}49$$

Taking into account a magnitude analysis of the terms included in the above equation it can be simplified as:

$$R_{sho} = R_{sh} + R_s \quad 3\text{-}50$$

With equations (3-50) and (3-46) it is possible to derive an expression that gives the ideality factor as a function of constants already known, $R_s$ and the slope $R_{sho}$

$$\alpha V_t = \frac{(V_{mp}-I_{mp}R_s)(V_{mp}+(I_{mp}-I_{sc})R_{sho})}{V_{mp}-I_{mp}R_{sho}} \quad 3\text{-}51$$

Finally, introducing equation (3.51) in expression (3.45) and reorganizing the remaining terms, the value of the series resistor, $R_s$ is obtained

$$R_s = \frac{(A-B)}{(A+B)}\frac{V_{mp}}{I_{mp}} + \frac{B}{(A+B)}\frac{V_{oc}}{I_{mp}} \quad 3\text{-}52$$

Where,

$$A = \left(V_{mp} + \left(I_{mp} - I_{sc}\right)R_{sho}\right)log\left(\frac{V_{mp}+\left(I_{mp}-I_{sc}\right)R_{sho}}{V_{oc}-I_{sc}R_{sho}}\right) \quad 3\text{-}53$$

$$B = V_{mp} - I_{mp}R_{sho} \quad 3\text{-}54$$

## Photovoltaic module parameters determination in 245W module

The PV panel output current Ipv depends on many parameters such as the type of material that the PV panel is made (ideality factor n), shunt and series resistance, number of parallel and series solar cells (Ns & Np), temperature and illumination variations are the main factors in PV panel models to gate the required voltage, power or current. Starting from the above parameters and estimation we ought to design a 245 watt of PV modules. A single cell produces only a voltage of 0.5-0.6V and few watts of power for small use.

In common a single solar cell generates very low output power. It is normally less than 2W at 0.6V. Hence, the photovoltaic cells are connected in particular configurations so as to form an array which is called a photovoltaic module. The modules consist of a group of cells connected in series and parallel to provide the required output power and voltage. The combination of cells in series or parallel forms a module. As needed, a typical module may have 36, 54, 60, 72, or 96 cells in sequence [39]. In expansion to that, for a photovoltaic system, a group of several PV modules is connected in parallel and series in form of a PV array to generate the desired voltage and current values for the system. When two or more solar modules are wired in series, the same current flows through each module, and the output voltage is the sum of the voltages produced by each module. On the other hand, when two or more solar modules are connected in series the same voltage would have across each module and the output current is the sum of each generated current. The overall module voltage $V_{pv,module}$ is found by.

$$V_{pv,module} = N_s\left(V_d - I_{pv}R_s\right) \quad 3\text{-}55$$

Different modules can be wired in series to increase voltage and in parallel to increase current, in this case we want to realize a control of 245 watt with 8.1 amps of current and determine the required cells and compare with the “Soltech 1STH-245-P” data sheet values. Solar cell data have taken from MATLAB/Simulink library.

Then $V_{module}$ =245W/8.1A =29.94V Ns=29.94/0.5 ≈ 60 cells in series where 8.1A is the required current to produce by the photon.

$$N_{modules/String} = 32000W/245W = 132 \quad 3\text{-}56$$

## Calculating the maximum arising open circuit voltage ( $V_{oc,max}$)

The most established and most effortless way to calculate the maximum dc voltage (maximum open-circuit voltage) is to use the STC value from the datasheet with a certain estimated lowest happening cell temperature (from datasheet Temperature Coefficient ( $V_{oc}$= -0.36%/°C ) and Temperature Coefficient of ( $I_{sc,}$= 0.53%/°C). As a matter of fact, STC (1000W/m²) doesn't take under consideration the influence from the irradiation. The lower voltage at lower irradiation.

$$V_{oc,max} = \left(V_{oc,STC}[V] + V_{oc,STC}[V]\left(\frac{(T_{cell,min}[°C] - T_{stc}[°C]) * T_{C,Voc}[\%/°C]}{100}\right)\right) \quad 3\text{-}57$$

## Determine the size of the module in the strings and the number of strings

As described, calculating maximum DC Voltage with a lower ambient temperature enables sizing the strings and more flexibility, which decreases investment costs and leads to higher yields. When building a PV system with sizing strings regularly the number of strings can be reduced and therefor the costs for inverter, cabling, mounting and supporting systems, connections, fuses, and so on can be saved. With less cabling (and other current-carrying components) also the energy losses are decreased.

$$\text{Maximum number of Modules/Strings} = \text{rounded off}\left(\frac{\text{Maximum System Voltage}}{V_{oc,max}}\right) \quad 3\text{-}58$$

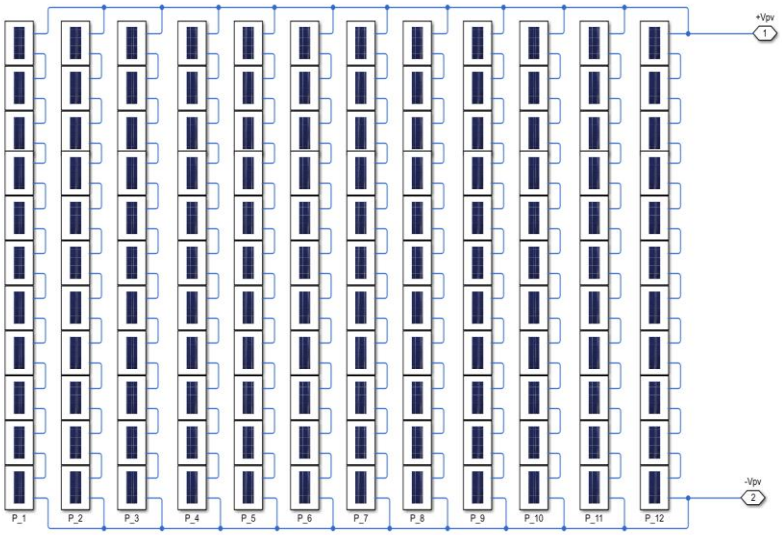


Figure 3.4. The PV array series-parallel structure [source: Author of thesis]

Table 3.6. Modeled and data sheet parameters comparison [source: Author of thesis]

| Parameters | Modeling value | Datasheet value | Unit |
|---|---|---|---|
| Maximum power ($P_{max}$) | 244.6932 | 244.62 | W |
| Open circuit voltage ($V_{oc}$) | 36 | 37.2 | V |
| Short circuit current ($I_{sc}$) | 8.6199 | 8.62 | A |
| Maximum current ($I_{max}$) | 7.983 | 8.1 | A |
| Maximum voltage ($V_{max}$) | 30.65 | 30.2 | V |
| Number of cells ($N_s$) | 60 | - | - |
| Series resistance ($R_s$) | 0.1900 | - | Ω |
| Shunt resistance ($R_{sh}$) | 112.3416 | - | Ω |

The minimum string size is the minimum number of series-connected modules, required to keep running the inverter during hot summer months. To get the minimum string size, first determine the minimum output voltage that each module will provide for the specified installation site, then divide the minimum inverter voltage by the estimated module minimum voltage to determine the minimum number of modules.

## 3.3. PV module I-V characteristics

The current and voltage (I-V) properties of a photovoltaic PV cell, module, or array are shown in I-V curves in Figure 3.5 and Figure 3.6, which provide a point-by-point description of its solar energy conversion ability and efficiency. Recognizing a solar cell's or panel's solar I-V characteristics (especially( $P_{max}$)) is essential for determining the device's output performance and solar efficiency. The relationship between the current and voltage produced on a specific solar cell I-V characteristics curve summarizes the overall PV cell or module electrical properties. The current (I) is controlled by the amount of solar radiation (insolation) that strikes the cell, whereas increases in the solar cell's temperature reduce its voltage (V). Characteristics I-V Curves are a graphical illustration of solar cell or module activity, describing the relationship between current and voltage under current irradiance and temperature circumstances.

Power is generated when the current and voltage of a solar cell are multiplied. The power curve for a particular radiation level can be derived by doing the product point-by-point for all voltages from short-circuit to open-circuit circumstances. In other words, the maximum

voltage accessible from a cell is at the open circuit and the maximum current at the closed circuit. These two conditions cannot produce any electrical power, but there must be points somewhere in between where the solar cell generates maximum power.

## Factors that affecting solar PV system performance

Understanding these factors will help us to make accurate predictions for controlling them and smart decisions on how to eliminate those issues as much as possible. There are many factors that affect the photovoltaic systems.

### A. Irradiance

Irradiance is a measure of the sum of sunlight falling on a given surface. The higher the irradiance, the more energy solar cell will produce. It is clear that as the irradiation level increases the PV output voltage and current increase with it. In general, the increase in the irradiation level leads to a theoretical increase in the maximum power voltage when there's no change in the cell temperature as shown in Figure 3.5 below.

On the other hand, the short circuit current ISC depends totally and linearly on the irradiance level hence the maximum power is changed as appeared underneath. Regardless, the total amount of energy absorbed from the sun by the system remains relatively consistent from year to year. Irradiance levels can be affected by the sun's angle, passing clouds, cloudy weather, and air pollution.

### B. Temperature

As temperature increases, the open-circuit voltage ($V_{oc}$) decreases, and the bandgap of the inborn semi-conductor reduces next the p-n junction voltage temperature dependence seen in the diode factor circuit. The temperature coefficient of $V_{oc}$ for solar cells made this way is negative [29]. As temperature increases, once more the bandgap of the inborn semiconductor shrinks meaning more incident energy is absorbed since a greater rate of the incident light has enough energy to raise charge carriers to the conduction band from the valence band. As a result, for a given amount of insolation $I_{sc}$ increases, and solar cells exhibit a positive temperature coefficient of short circuit current. In general, when the temperature rises with a constant irradiation level, the short circuit current ($I_{sc}$), rises slightly, as the bandgap energy lowers and more photons have enough energy to form electron-hole pairs. On the other hand,

the increase of temperature has an obvious reduction in the PV panel output power due to the drop in the fill factor and the open-circuit voltage as shown in Figure 3.6 below; therefore the module efficiency is reduced [29].

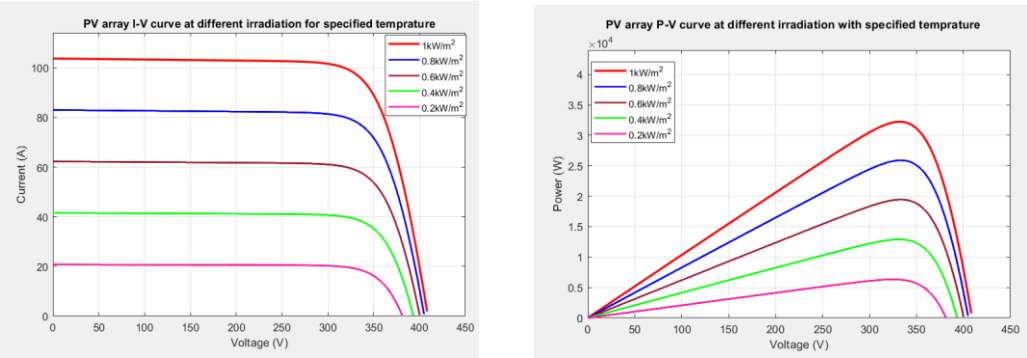


a) b)

Figure 3.5 Soltech 1STH-245-WH module with varying irradiation a) I-V b) P-V curve

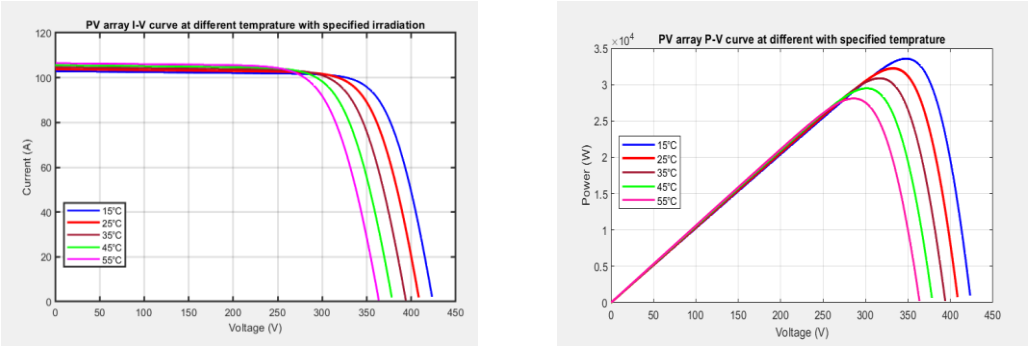


a) b)

Figure 3.6 Soltech 1STH-245-WH module with varying Temperature a) I-V b) P-V curve

## PV systems' maximum DC voltage

When sizing a solar system, the maximum DC voltage is usually used as a safety restriction. All components (modules, inverters, cables, connections, fuses, surges, and so on) have a maximum voltage that they can safely withstand. If this voltage is surpassed, it might cause injury or even worse harm can result. From an economic point of view, a high voltage makes sense, by causing lower investments (fewer strings) and higher earnings (lower losses and

mostly higher efficiencies). So the problem is to size a PV system with the highest possible and safe DC voltage. In this case, the desired voltage to produce from the PV panel is 332.2volt.

## PV module open circuit voltage

On the datasheet of a PV module, the open-circuit voltage is indicated most times at STC. (Standard Test Conditions) characterizing the irradiation at 1000W/m² and a cell temperature at 25°C). As the voltage relates mainly with the cell temperature, also a temperature coefficient is indicated, either in V/°C or %/°C. This is an inverse relationship, meaning the highest voltage occurs with the lowest cell temperature. Naturally, also irradiation is essential to produce voltage and power. So the voltage shows also a nonlinear dependency from the irradiation, meaning low voltage at low irradiation. Modern PV Modules have an efficiency of 15% to 20% of the sunshine. While 80% - 95% of the irradiation is mostly converted into heat, meaning the PV cell or module gets heated up very quickly. As a matter of truth, with irradiation, the cell temperature always will be higher than the ambient temperature in the day time.

Table 3.7 The proposed module and array value [source: Author of thesis]

| Parameters | Modelled Module value | Proposed array value | Unit |
|---|---|---|---|
| Maximum power ($P_{max}$) | 0.245 | 32.34 | kW |
| Open circuit voltage ($V_{oc}$) | 37.2 | 409.2 | V |
| Short circuit current ($I_{sc}$) | 8.62 | 103.4 | A |
| Maximum current ($I_{max}$) | 8.1 | 97.2 | A |
| Maximum voltage ($V_{max}$) | 30.2 | 332.2 | V |
| Number of cells ($N_s$) | 60 | 7260 | - |

The cell temperature limits built upon the international market for the design of a photovoltaic system are minimum -10 °C and maximum +70 °C. Generally, these temperatures are used with the STC values of a module for the calculation of extreme voltages. As the voltage of a PV cell (module) has a high dependency on its temperature but also a dependency on the irradiation (particularly at low irradiation levels) and further the cells own temperature has a high dependency on the irradiation, the minimum cell temperature can be chosen higher than the minimum ambient temperature. Taking into account the lowest day temperatures are

higher, modules are mounted on roofs where the surrounding air temperature is higher or heated up from the building, less dissipation of heat and so on, indeed a higher difference (> +10°C) between the lowest minimum ambient temperature and the lowest minimum cell temperature can be assumed.

## 3.4. DC link design

The solar converter is divided into two general components in many applications. The principal component is the DC/DC converter, which is responsible for ensuring that the second component, the DC/AC converter, receives the appropriate minimum DC input voltage. These two components are connected by a DC link capacitor, which smooth's the DC link voltage [40]. The DC link capacitor is assessed using equation 3.61 [28].

DC link voltage of the system is designed as,

$$V_{dc} = \frac{2\sqrt{2}}{\sqrt{3}} V_{L-L} = \frac{2\sqrt{2}}{\sqrt{3}} * 400V = 653.2V \qquad 3\text{-}59$$

Where, $V_{L-L}$ is the motor input line voltage, the minimum DC link voltage is 653.2V. In this thesis it is chosen to be 680V.

$$\frac{1}{2} C_{dc} \left[ {V_{dc}}^2 - {V_{dc,ref}}^2 \right] = 3\alpha VIt \qquad 3\text{-}60$$

Where, $V_{dc}$ is the reference DC bus voltage of VSI, α is the overloading factor, $V_{dc,ref}$ is minimum DC link voltage, *I* is IMD phase current and *t* is the time duration in which voltage reduces to minimum allowable DC link voltage.

$$C_{dc} = \frac{6\alpha VIt}{\left[ {V_{dc}}^2 - {V_{dc,ref}}^2 \right]} = \frac{6*1.2*230.9*42}{\left[ 680^2 - 653.2^2 \right]} \qquad 3\text{-}61$$

The capacitor value is selected as 16288μF.

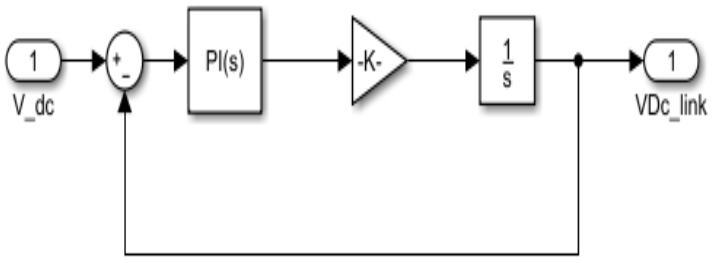


Figure 3.7. DC link design [source: Author of thesis]

## 3.5. Design of DC-DC boost converter for photovoltaic system

The applications of boost converter operation are the regenerative braking circuit of DC motors and in regulated DC power supplies. In this type of converter the output voltage ($V_o$) is greater than the source voltage ($V_d$). As a result, the step up converter can be used with MPPT systems that require a higher output voltage than the input voltage. In a grid-connected system, for example, the boost converter ensures a high output voltage even if the PV array voltage drops to low levels.

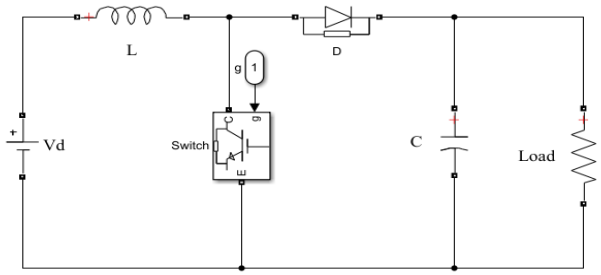


Figure 3.8. Step-up boost converter [source: Author of thesis]

During the switch is ON, the diode D is reverse biased. Subsequently, as shown in Figure 3.8 the current within the inductor L rises linearly due to the input voltage source, and in this case the output stage is disconnected and the capacitor (C) is somewhat discharged supplying the current load. When the switch is off during the second interim the diode is conducting, and during this time the output stage gets energy from both the inductor and the input source. The wave form of the inductor current during continuous conduction mode is shown below in Figure 3.9, where the inductor current flows continuously, i.e. IL (t) > 0. A dual stage power electronic system incorporate a boost converter and an inverter feed the power generated by the PV array to the load. To preserve the load voltage constant a DC-DC step up converter is presented between the PV array and the inverter. The DC-DC converter is considered the main portion of a MPPT system which used for generating duty cycle D depending on the converter switching frequency. These are broadly used to convert unregulated DC inputs into a regulated DC output at a desired voltage and current levels in DC power supplies The voltage over the DC-DC converter is fed to a three-phase, sine wave six step inverter a three-phase fixed amplitude and fixed frequency supply is gotten to feed an inverter as input. When the converter

is working at steady-state condition, duty ratio, the input and the output voltages of the converter can be expressed by equation (3-62) and (3-63) [20].

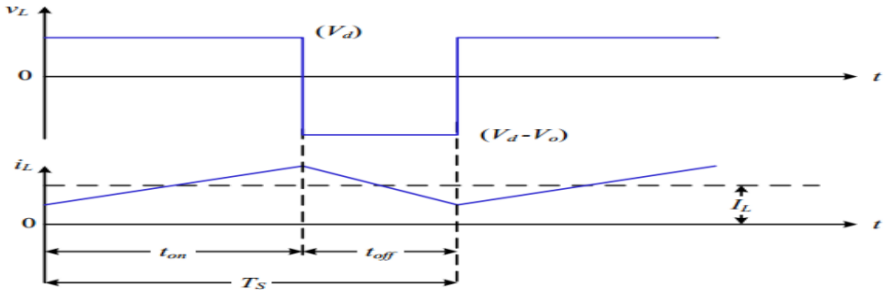


Figure 3.9. Step-up converter wave form of the inductor current and voltage in CCM [20]

The applications of boost converter operation are the regenerative braking circuit of DC motors and in regulated DC power supplies. In a boost converter, the input voltage is always less than the output voltage. The step-up converter can be used in MPPT systems where the output voltage must be higher than the input voltage in this sort. Such as in a grid-connected system where the boost converter maintains a high output voltage even in case the PV array voltage falls to low values.

$$D_{min} = 1 - \frac{V_{in,max}}{V_{out}} * \eta \qquad 3\text{-}62$$

$$D_{max} = 1 - \frac{V_{in,min}}{V_{out}} * \eta \qquad 3\text{-}63$$

Where D denotes the duty ratio, efficiency, $V_{in}$ and $V_{out}$ denotes the input and the output voltages of the converter, respectively. From the above equation it can be seen that, the increase in the duty ratio D will increase the value of the output voltage $V_{out}$. Moreover the change in the duty ratio results in change in the input and the output current of the converter. The filter inductor and capacitor to operate the converter in the CCM can be calculated by the following equations.

$$L_{min} = \frac{V_{in,min}}{\Delta I_L f_s} D_{min} \qquad 3\text{-}64$$

$$C_{min} = \frac{I_o}{\Delta V_o f_s} D_{min} \qquad 3\text{-}65$$

Where $f_s$ is switching frequency $I_o$ and $I_L$ is output and input current respectively.

This section provides an overview into the design of the boost converter that will be utilized for real-time implementation. A boost model is created to test the suggested MPPT algorithm

in order to reduce the physical system's costs. The inverter peak output phase voltage is chosen to be 500V. This inverter output voltage requires a dc inverter input voltage of 680V (the dc link voltage). Hence, the converter must be designed to be able to have 680V as its output voltage. The input voltage of the converter (or solar panel maximum power point voltage) is chosen as 332.2V. The output voltage ripple is chosen as 6.8V (or 1%) and the inductor current ripple is chosen as 14.12A (or 30%). The converter is designed as if it has a 10Ω stack resistor. In practice, however, the converter is operating as an impedance matcher and is connected to the inverter. In this manner, the actual load isn't 10Ω but the design still holds with the unknown load on the converter. The switching frequency ($f_s$) of the converter is chosen as 5 kHz. To increase the voltage, cells are set in series and to increase the current, the cells are put in parallel. In this manner, the emulator can output a maximum of 32kW. The source voltage at the MPP is chosen to be 332.2V and the source current at the MPP is chosen to be 97.2A. The specifications of the design are summarized in Table 3.8 below.

Numerous sorts of DC-DC converters have been considered to see which converter is suitable for the MPPT stage of the PV system. The Buck-Boost converter has the advantage over individual Buck and Boost converters of following the MPP at all times, beneath any conditions of solar global radiation, cell temperature and connected load. However, the person Boost and Buck types are the foremost efficient converters for a given price. The Cuk and SEPIC converters have the advantage that their input current is continuous, and they can draw ripple free current from a PV array. However, Cuk, SEPIC, and Buck-Boost converters have a higher number of passive components and high current, voltage and switched power stresses within the switch or transistor compared to the Boost converter. This too affects the entire system efficiency [29], since the switched current and voltage are higher for the same output power as an individual buck or boost. Additionally it needs the higher Voltages to feed the inverter in order to induce the desired AC voltages which is supply to the Ac machines.

Boost converters developed to maximize the energy gather for photovoltaic systems. For voltage conversion of 50/60 Hz at main frequencies transformers used must be large and heavy for powers exceeding some watts. This bring them costy, and they are subject to energy losses or core loss in their windings due to eddy currents in their cores. In this manner, it was chosen to utilize a boost converter since the DC-DC boost converter is an imperative stage in the PV inverter system since it increments the overall efficiency of the system. In truth, the working

with higher input voltage leads to lower input current required for a given power and consequently decreases the losses. It is responsible to regulate and boost the DC output voltage of the PV system. In this work, a boost converter working in continuous conduction mode has been designed to step up the voltage of the PV system to a higher constant voltage of 680V to feed an inverter.

Table 3.8. Boost converter parameters [source: Author of thesis].

| Parameters | Values | Units |
|---|---|---|
| Power Rating ( $P_{max}$) | 32.34 | kW |
| Input voltage range ( $V_{in}$= $V_{pv}$) | 150-332.2 | V |
| Output voltage ( $V_{dc}$= $V_{out}$) | 680 | V |
| Max, input current ($I_{pv}$ = $P_{max}$/ $V_{in}$) | 97.2 | A |
| Max. load current = $P_{max}$/ $V_{out}$) | 47.56 | A |
| Switching frequency ($f_s$) | 5 | kH |
| $V_{out}$ ripple ($\Delta V_{out}$) | 1% -5% | - |
| $I_{in}$ ripple ($\Delta I_L$) | 20% -40% | - |
| Inductance (L) | ≥1.2 | mH |
| Output capacitance (C) | ≥367 | µF |
| Minimum Duty ($D_{min}$) | 0.511 | - |
| Maximum Duty ($D_{max}$) | 0.853 | - |

The MPPT system's key component is the switch-mode DC-DC converter. These are broadly used to convert unregulated DC inputs into a controlled DC output at the desired voltage and current levels in DC power supplies and DC motor drives or as input of the inverter. The same converter is used for the MPPT to provide load coupling for the maximum power transfer by regulating the input voltage at the PV array by controlling the duty ratio D. DC-DC converters are used to interface the photovoltaic module with an inverter, in order to guarantee the photovoltaic module is always operating at the maximum power point to get the desired input voltage level to the inverter. This is often done by controlling the converter duty ratio (D) with maximum control point tracking algorithms (MPPT).

## 3.6. Design of DC-AC converter for photovoltaic system

Three phase inverters are frequently used to supply three-phase loads, such as ac motors. Three-phase inverter essential structure is shown in Figure 3.10 below. Each of the three legs produces an output which is displaced by $120^0$ with respect to each other. The output of each leg depends on the position of the switch and DC input voltage (Vdc). Since one of the two switches in each leg is always on, the output voltage is independent of the output load current. In Figure 3.10 below three-phase VSI topology shown, and the eight valid switch states are given in Table 3.9. Like single-phase voltage source inverter, the switches of upper and lower switch of three phase inverter i.e. switch (1 and 6), (3 and 4) or (5 and 2) cannot be switched ON simultaneously, because it result in a short circuit across the dc-link voltage source. As clarified earlier in order that the circuit satisfies the KVL and the KCL, in this way the nature of the two switches in the same leg is complementary [41].

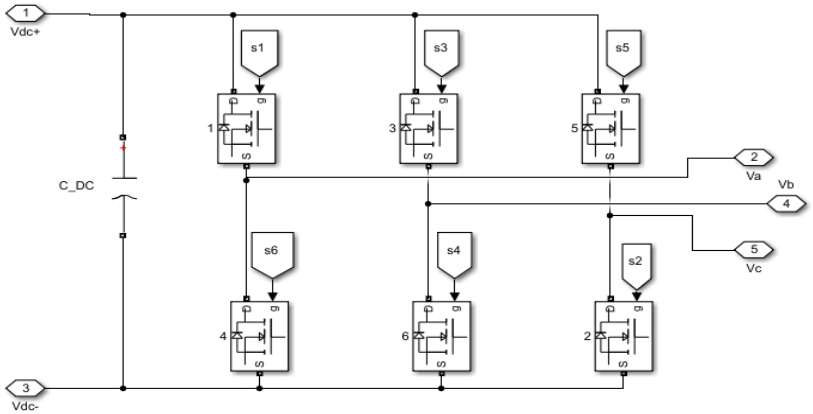


Figure 3.10. Three-phase full-bridge inverter topology [source: Author of thesis]

$$S_1 + S_6 = 1 \quad \text{3-66}$$

$$S_3 + S_4 = 1 \quad \text{3-67}$$

$$S_5 + S_2 = 1 \quad \text{3-68}$$

Among the eight valid states, two of them produce zero ac line voltages because, the ac line currents drift through either the lower or upper components. The remaining states deliver non-zero ac output voltages. Inverter moves from one state to another state in order to generate a given voltage wave form. Hence the resulting ac output line voltages consist of discrete values of voltages that are Vdc, 0, and -Vdc for the topology shown in Table 3-9. Choosing the states

is done by the modulating procedure that ought to ensure the use of only the valid states in order to generate the given waveform [41].

Table 3.9 Eight state of three phase inverter [source: Author of thesis]

| | $S_1$ | $S_3$ | $S_5$ | $V_{ab}$ | $V_{bc}$ | $V_{ca}$ |
|---|---|---|---|---|---|---|
| 1 | 0 | 0 | 0 | 0 | 0 | 0 |
| 2 | 0 | 0 | 1 | 0 | $-V_{dc}$ | $V_{dc}$ |
| 3 | 0 | 1 | 0 | $-V_{dc}$ | $V_{dc}$ | 0 |
| 4 | 0 | 1 | 1 | $-V_{dc}$ | 0 | $-V_{dc}$ |
| 5 | 1 | 0 | 0 | $V_{dc}$ | 0 | $-V_{dc}$ |
| 6 | 1 | 0 | 1 | $V_{dc}$ | $-V_{dc}$ | 0 |
| 7 | 1 | 1 | 0 | 0 | $V_{dc}$ | $-V_{dc}$ |
| 8 | 1 | 1 | 1 | 0 | 0 | 0 |

$$\frac{V_{dc}}{2}(S_1 - S_6) = V_{an} + V_{no} \quad 3\text{-}69$$

$$\frac{V_{dc}}{2}(S_3 - S_4) = V_{bn} + V_{no} \quad 3\text{-}70$$

$$\frac{V_{dc}}{2}(S_5 - S_2) = V_{cn} + V_{no} \quad 3\text{-}71$$

Expressing the equations above in terms of modulation signals and making use of conditions

$$\frac{V_{dc}}{2}(M_1) = V_{an} + V_{no} \quad 3\text{-}72$$

$$\frac{V_{dc}}{2}(M_3) = V_{bn} + V_{no} \quad 3\text{-}73$$

$$\frac{V_{dc}}{2}(M_5) = V_{cn} + V_{no} \quad 3\text{-}74$$

Where M is the modulation signal, which can be any sine or cos term (in accordance with the Fourier series) depending on the control we wish to implement. The general fundamental component for M is given as:

$$M = m_\alpha cos(\omega t - \alpha) \quad 3\text{-}75$$

And $m_\alpha$ is called the modulation index which can vary from 0 to 1 and for values of $m_\alpha$ less than 1 a linear modulation range is supposed to exist and it is operated in the over modulation range for values of $m_\alpha$ greater than one.

Then adding the valid state equation above which is equal to;

$$\frac{V_{dc}}{2}\left((S_1 + S_3 + S_5) - (S_6 + S_4 + S_2)\right) = V_{an} + V_{bn} + V_{cn} + 3V_{no} \quad 3\text{-}76$$

As we know the balanced voltages $V_{an} + V_{bn} + V_{cn} = 0$ and making use of the conditions from equations above the equation becomes:

$$\frac{V_{dc}}{6}(2S_1 + 2S_3 + 2S_5) = V_{no} \quad 3\text{-}77$$

Substituting for $V_{no}$ then each phase voltage becomes

$$\frac{V_{dc}}{3}(2S_1 - S_3 - S_5) = V_{an} \quad 3\text{-}78$$

$$\frac{V_{dc}}{3}(-S_1 + 2S_3 - S_5) = V_{bn} \quad 3\text{-}79$$

$$\frac{V_{dc}}{3}(-S_1 - S_3 - 2S_5) = V_{cn} \quad 3\text{-}80$$

## Sinusoidal pulse width modulation in three-phase VSI

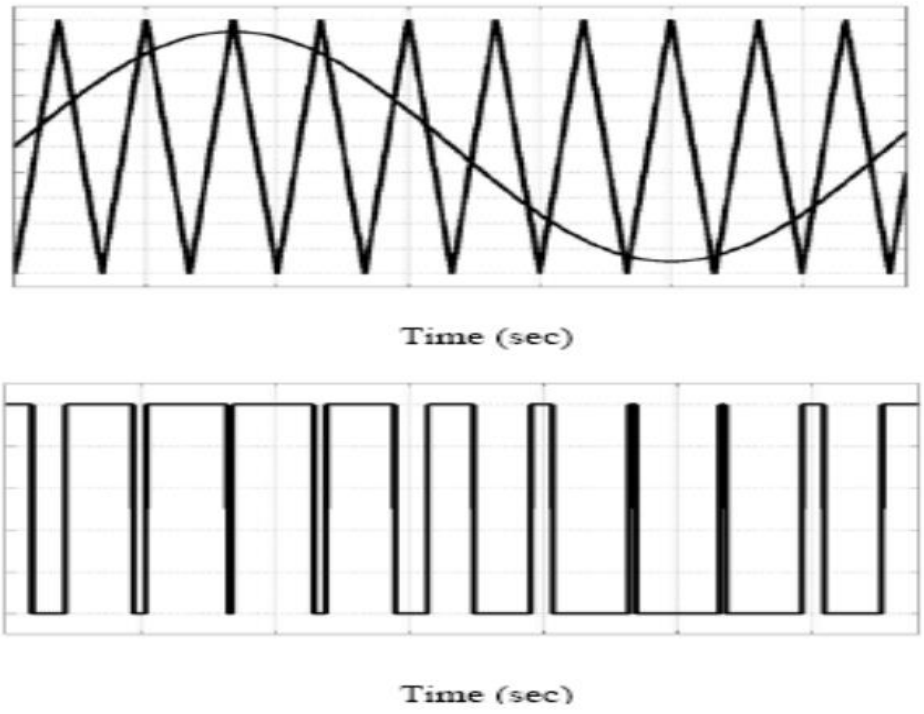


Figure 3.11. PWM illustration by the sine-triangle comparison method [41]

As in the single phase inverter PWM procedure can be used in three-phase inverters, in which three sine waves are phase shifted by $120^0$ with the frequency of the specified output voltage is compared with a very high frequency carrier triangle as shown in Figure 3.11 above. Both

carrier signals and sine wave signals are mixed in a comparator whose output is high, when the sine wave is greater than the carries signal and low, when the sine wave smaller than the carrier signal as shown in Figure 3.12 below [41]. This signal is produced by phase-shifting the reference signal by180 degrees. For a three-phase, three reference signals are required to produce the six pulses. The reference signals can also be produced by the PWM generator. In this case, specify a modulation index, a voltage output frequency, and phase.

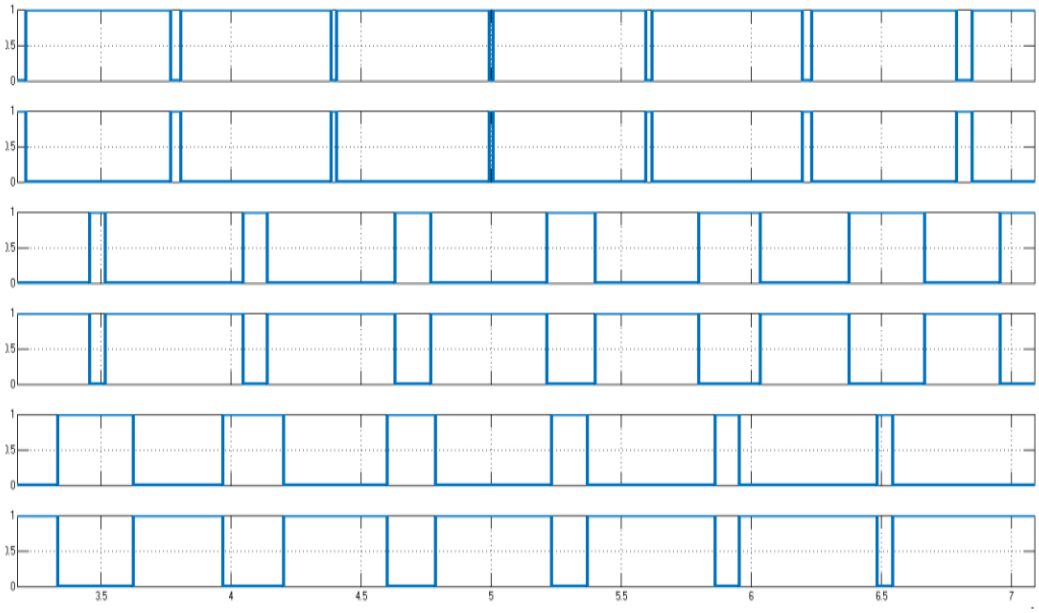

Figure 3.12. Pulse generated by 2-level PWM in three-phase VSI [41]

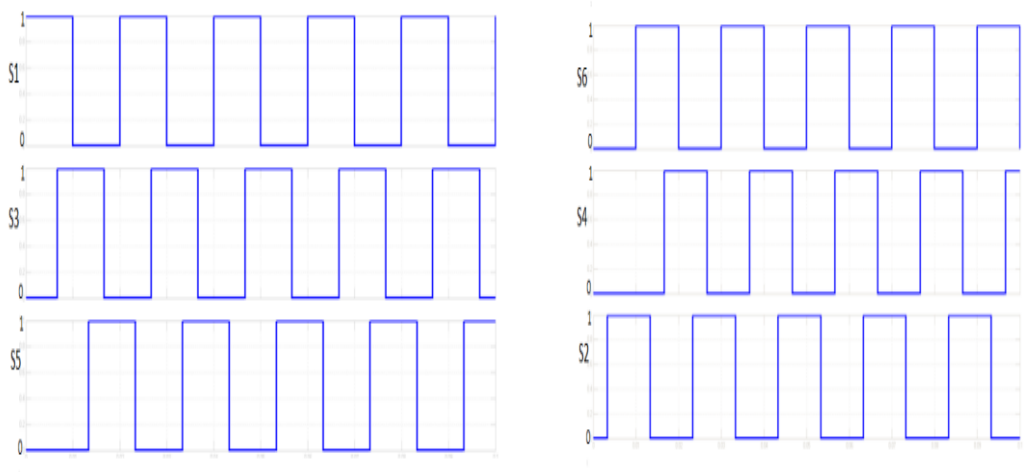


a) b)

Figure 3.13. $180^0$ mode switching signals for (a) Top devices, (b) Bottom devices [41]

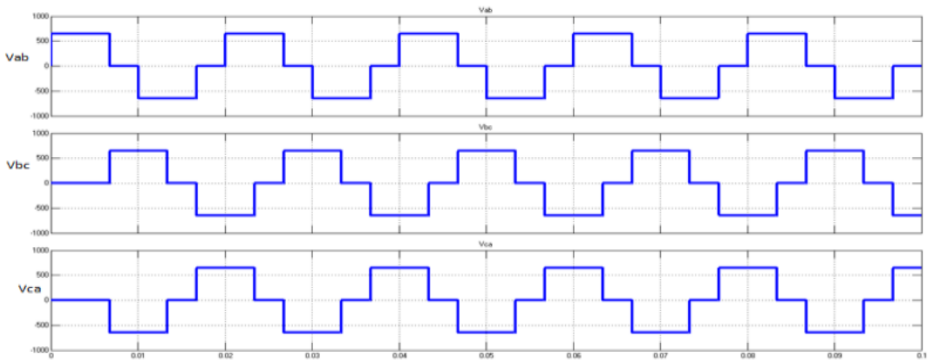


Figure 3.14. $180^0$ conduction mode six step inverter line voltage ($V_{ab}$, $V_{bc}$ & $V_{ca}$) [41]

### 3.6.1. Six step voltage source inverter

Three phase inverters are mostly used in AC-Motor drives and general purpose AC-Supplies. The circuit for the six-step VSI is as shown in Figure 3.10 above, which consists of three half-bridges, which are phase-shifted mutually by $120^0$ point. The square wave phase voltages with dc center tap expressed by using Fourier series as:

$$V_{an} = \frac{2V_{dc}}{\pi}\left(cos\omega t - \frac{1}{3}cos3\omega t - \frac{1}{5}cos5\omega t - \cdots\right) \quad 3\text{-}81$$

$$V_{bn} = \frac{2V_{dc}}{\pi}\left(cos\left(\omega t - \frac{2\pi}{3}\right) - \frac{1}{3}cos3\left(\omega t - \frac{2\pi}{3}\right) - \frac{1}{5}cos5cos\left(\omega t - \frac{2\pi}{3}\right) - \cdots\right) \quad 3\text{-}82$$

$$V_{cn} = \frac{2V_{dc}}{\pi}\left(cos\left(\omega t + \frac{2\pi}{3}\right) - \frac{1}{3}cos3\left(\omega t + \frac{2\pi}{3}\right) - \frac{1}{5}cos5cos\left(\omega t + \frac{2\pi}{3}\right) - \cdots\right) \quad 3\text{-}83$$

The line voltages can thus be obtained from the phase voltages as

$$V_{ab} = V_{an} - V_{bn} \quad 3\text{-}84$$

$$V_{ab} = \frac{2\sqrt{3}V_{dc}}{\pi}\left(cos\left(\omega t + \frac{\pi}{6}\right) - \frac{1}{3}cos3\left(\omega t + \frac{\pi}{6}\right) - \frac{1}{5}cos5cos\left(\omega t + \frac{\pi}{6}\right) - \cdots\right) \quad 3\text{-}85$$

$$V_{bc} = V_{bn} - V_{cn} \quad 3\text{-}86$$

$$V_{bc} = \frac{2\sqrt{3}V_{dc}}{\pi}\left(cos\left(\omega t - \frac{\pi}{2}\right) - \frac{1}{3}cos3\left(\omega t - \frac{\pi}{2}\right) - \frac{1}{5}cos5cos\left(\omega t - \frac{\pi}{2}\right) - \cdots\right) \quad 3\text{-}87$$

$$V_{ca} = V_{cn} - V_{an} \quad 3\text{-}88$$

$$V_{ca} = \frac{2\sqrt{3}V_{dc}}{\pi}\left(cos\left(\omega t + \frac{5\pi}{6}\right) - \frac{1}{3}cos3\left(\omega t + \frac{5\pi}{6}\right) - \frac{1}{5}cos5cos\left(\omega t + \frac{5\pi}{6}\right) - \cdots\right) \quad 3\text{-}89$$

The fundamental of the line voltages is $\sqrt{3}$ times that of the phase voltage, and there is a leading phase-shift of $\frac{\pi}{6}$. The line voltages waves as shown in below have a characteristic six step

wave shape and thus the name for this inverter. The three-phase fundamental as well as the harmonic components are balanced with a mutual phase-shift angle of $\frac{2\pi}{3}$.

### 3.6.2. Three phase full-bridge inverter design and interfacing

The boost converter are step-up the photovoltaic output voltage of the PV array from 332.2V (Natural) to 680V (step up) DC outputs to feed the inverter, but the desired objective is to produce (400V ±5%) AC in ordered to require waters from the ground. An inverter is a device that changes DC to AC voltage. DC is a current that flows in only one direction, whereas AC is that which flows in both positive and negative directions. There are two basic types of inverters based on type of sources input; Voltage source (VSI) and Current Source (CSI). Voltage/Current source implies that the voltage/current level doesn't change instantly as the result of switching. Photovoltaic source and Batteries source can be used as voltage sources. It is troublesome to get ideal voltage or current sources. In practice voltage sources are simulated by voltage stiff (power supply with shunt capacitor) and hence voltage stiff inverter. Similarly, current sources are simulated by current stiff (power supply with serious inductor). In the other way Inverter may be single-phase (half bridge, full bridge) or three phase (half bridge, full bridge) but single-phase half and full bridge voltage source inverter cover low-range power applications. The main reason of these topologies is to provide a three-phase voltage source, where the amplitude, phase and frequency of the voltages can be controlled in this work.

### Photovoltaic array – Inverter interface

Totally 224 multi-crystalline silicon types, 60-cells PV modules series parallel combination is conducted in the previous topic to design 32.24kW power generator PV arrays.

A. **Nominal power:** The maximum generated power by the investigated PV array is 38.4kW at an ambient temperature of 25°C and at irradiation of 1200 W/m$^2$. However, this operating point is very seldom reached. The nominal power for the inverter is hence selected to 38.4kW / 1.2 which is 32kW, with the capability of operating at 120% power during a short time [42].
B. **Starting power:** The inverter should be able to invert even small amounts of DC power into AC power. In other words, the inverter must be able to function at very low irradiation. The European efficiency is the weighted average of efficiencies down to 5%.

Hence, the inverter should be able to operate at 5% or less of the nominal power, which is 1.6kW.

C. **Open-circuit voltage**: The worst-case open-circuit voltage across the investigated PV array is estimated to 409.2V at 1000 W/m$^2$, and a cell temperature of 25 °C. Thus, the inverter must withstand at least 409.2V without being damaged, so that 500V inverter is selected.

D. **Maximum short-circuit current**: The maximum short-circuit current generated by the investigated PV array is 97.2A. A maximum current of 100A is therefore chosen.

E. **Over-voltage protection**: The inverter must be able to resist over-voltages caused by nearby illumination. It is recommended to use a surge arrestor (Metal Oxide Varistor) with an inception voltage of 1.2 time nominal voltage [43]. The inception- and inclination-voltage should therefore be higher than 600V. So, 680V is selected.

This thesis aimed to enabled a three phase 400V by 55A of induction AC motor to pumping ground water from the borehole to the system height ($T_h$ =98m). The Output Ac voltage ($V_{rms}$) is calculated as;

$$V_{L-L} = m.\frac{V_{dc}}{2}.\sqrt{\frac{3}{2}} \quad 3\text{-}90$$

$$V_{L-L} = 0.6124 * m * V_{dc} \quad 3\text{-}91$$

Where: - $V_{dc}$ is output voltage of the boost converter, and ‘’m’’ is modulation index.

Table 3.10. Specifications of three phase H-bridge inverter [source: Author of thesis]

| Parameters | Values | Units |
|---|---|---|
| Nominal Power rating | 32 | kW |
| Input voltage, $V_{out}$ of the boost converter($V_{dc}$) | 680 | V |
| Output Ac current ($I_{rms}$) | 55 | A |
| Output Ac voltage ($V_{rms}$) | 400±5% | V |
| Modulation index(m) | 0.96 | - |
| Frequency Ac output | 50Hz | Hz |

## 3.7. LCL filters for photovoltaic system

A low-pass filter is connected to the output of inverter to supply a pure sinusoidal to the load. The factors such as efficiency, voltage and current harmonics constraints, weight, volume and

cost must be taken in to account when selecting the optimal filter design [44]. Also, the saturation of the inductor core ought to be avoided. Types of filter topologies of sine wave inverter are like L-filter, LC-filter, and LCL-filter. The full-bridge inverter output is connected to a low pass filter to supply a pure sinusoidal output voltage to the load. The factors such as efficiency, voltage and current harmonics constraints, weight, volume and cost must be taken in to account when selecting the optimal filter plan [45]. Moreover, the saturation of the inductor core should be avoided. There are a few important factors that ought to be considered when design LCL filter which contain such as: Inverter output ripple current, Inverter to load inductor ratios and filter capacitance maximum power variations. The output ripple current ($\Delta I_L$) in the design of $L_{inv}$ was expected up to 10% of the rated output current of the inverter ($L_{inv}$).

## Converter side inductor

In the worst-case scenario, the converter side inductor is specifically designed to reduce converter current ripple. The pulsed voltage generated by the converter causes this current ripple. During the switching operation, the worst case which leads to a maximum converter current ripple is obtained when the applied converter voltage varies from -$V_{dc}$ /3 to $V_{dc}$ /3. Figure 3.15 shows a waveform illustration of the converter current $I_i$ with respect to the applied converter voltage $V_i$. In this figure, $t_{on}$ and $t_{off}$ refer to the time taken by the control signal at high and low logical level, respectively. $T_{sw}$ is the switching period. According to Figure 3-16, the maximum converter side inductor and current ripple value are given by equation (3-92) and (3-93). A simplified formula for the LCL filter parameters with damping resistance may have been discussed and analyzed using the following equations, to compute the inverter side inductance ($L_{inv}$), load side inductance ($L_{Load}$), filter capacitance ($C_f$) and the damping resistance ($R_d$).

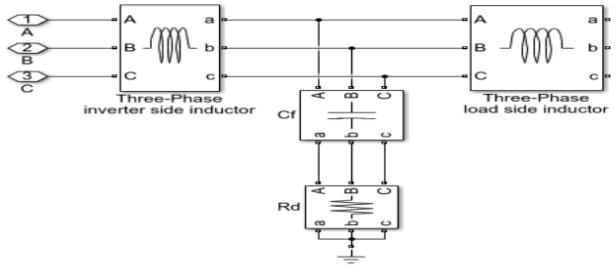


Figure 3.15. Proposed LCL filter [source: Author of thesis]

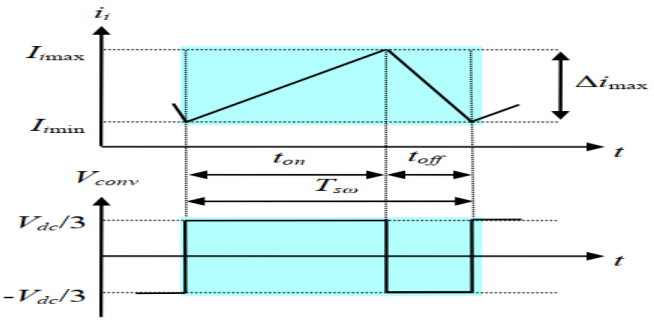


Figure 3.16. Evolution of the converter current $\boldsymbol{I_i}$ and voltage $\boldsymbol{V_i}$ [44]

First calculating filter parameters is founding $L_{inv}$, which is given as,

$$L_{inv} = \frac{V_{dc}}{6 f_{sw} \Delta I_{max}} \quad 3\text{-}92$$

$$\Delta I_{max} = \frac{V_{dc}}{6 f_{sw} L_{inv}} \quad 3\text{-}93$$

Where $\Delta I_{max}$ is the maximum converter current ripple. The output ripple current ($\Delta I_{max}$) in the design of $L_{inv}$was assumed up to 15% of the rated output current of the inverter ($I_{inv}$). The converter side current $I_{inv}$ must verify equation (3-92) in order to avoid inductor saturation problems.

$$\left| I_{imax} + \frac{\Delta I_{max}}{2} \right| < \mathrm{I_{sat}} \quad 3\text{-}94$$

Where $I_{imax} = I_{2max}$ (for high frequencies)

$$I_{2max} = \sqrt{\frac{2}{3}} * \frac{P}{V} \quad 3\text{-}95$$

## Tuning of the load side inductor

The load side inductor is designed in order to limit the load current harmonics according to standards and load requirements. According to the IEEE 519-1992 standard, the current THD value must be under 5% [46]. The relation between the converter side and the load side inductors is given by equation (3-96). The load side inductance ($L_{Load}$) is given by some constant (r) multiply by the inverter side inductance:

$$L_{Load} = r * L_{inv} \quad 3\text{-}96$$

The constant r is called the relation factor which represents the proportion between $L_{inv}$ and $L_{load}$. The voltage drop across the inductor filter ($L_{inv}$+$L_{load}$) must be less than 3% of the inverter output voltage ($V_{inv}$) [47]. Assume the two inductor proportion is 0.8 which is constant r and apply the given equations to calculate Table 3-11 parameters.

## Maximum LCL filter capacitor value

The LCL filter capacitor is designed with reactive power consumption is less than γ% of the rated power P as shown in [48] [49]. In equation 3-97, $Q_C$ refer the reactive power consumed by the filter capacitor and $\gamma$ is a positive factor chosen generally equal to or lower than 5%. According to equations (3-97) and (3-98), the maximum value of the filter capacitor can be expressed as in equation (3-99).

It should be noted that when the capacitor value is too low, the inductor values must be too high. For this reason, it is suggested to start with a capacitor value equal to one-half of the maximum value, and then if some of the constraints cannot be satisfied, increase it up to the maximum value. At that point, the value of the Rd got to be one-third of the impedance of the filter capacitor at the resonant frequency ($f_r$). The values of $f_r$ and $R_d$ are given by equations (3-100) and (3-101).

$$|Q_C| \leq \gamma\%|P| \quad (3\text{-}97)$$

$$Q_C = -V^2{}_g C_f \omega_g \quad (3\text{-}98)$$

$$C_{fmax} = 5\% \frac{P}{2\pi f_g V^2{}_g} \quad (3\text{-}99)$$

$$f_r = \frac{1}{2\pi}\sqrt{\left(\frac{L_{inv}+L_{load}}{L_{inv}*L_{load}*C_f}\right)} \quad (3\text{-}100)$$

$$R_d = \frac{1}{3}\frac{1}{2\pi f_r C_f} \quad (3\text{-}101)$$

Table 3.11. LCL filter specification [source: Author of thesis]

| Parameters | Specification |
|---|---|
| $L_{inv}$ | 5mH |
| $L_{Load}$ | 4mH |
| $C_f$ | 45µF |
| $R_d$ | 2.3Ω |

## 3.8. Motor-Pump system for photovoltaic system

The motor–pump system incorporates the motor, the pump, and the couplings. Many types of coupling are used for water pumping purposes depending on the type of application and the water demand. There are different types of pump technologies available. The choice of the

pump depends on its application. The most common commercially available configurations of motor-pump subsystems are positive displacement, centrifugal and floating point motor pump.

## Centrifugal pumps

This is frequently called a submersible centrifugal motor pump. Since it is simple to install and safe, typically the foremost common and suitable type of pumping system for village water supplies. Submerged centrifugal pump with surface mounted engine. In spite of the fact that this type of subsystem is advantageous for maintenance of the engine, the power losses in the shaft bearings and its high cost make it unattractive.

These pumps are built for a fixed head, which implies that when the pumping head deviates from the design point, their efficiency suffers. Because its vertical lifting capability is directly related to the power input, unlike volumetric pumps, a considerable decrease in a rotodynamic pump's power supply can cause it to fail at delivering water from a borehole. The finest type of equipment for a specific pumping application depends on the everyday water requirement, pumping head, suction head (for surface mounted pump-sets), and the water source. As a discussion among the pump type discussed before the volumetric pumping type is suitable for this work but the motor driving a volumetric pump requires a constant current for a given head, separated from the starting current, which tends to be higher. This condition does not match the PV characteristics where the current varies almost linearly with solar radiation. In this manner, maximum power point tracking (MPPT) controllers are used with volumetric pumps [23].

## Induction motor model

A generalized model of the induction motor (IM) can be expressed in the *abc* reference frame or in the d-q stationery or rotating reference frame. In this research, an asynchronous model available in Matlab/Simulink will be used. The parameters data of the induction motor are given Appendix B. Driving the mathematical equations of an induction motor in d-q stationery reference frame is given as shown in Figure 3.17 [50] [51]. The following are the related stationery frame equations in terms of flux linkage expressions:

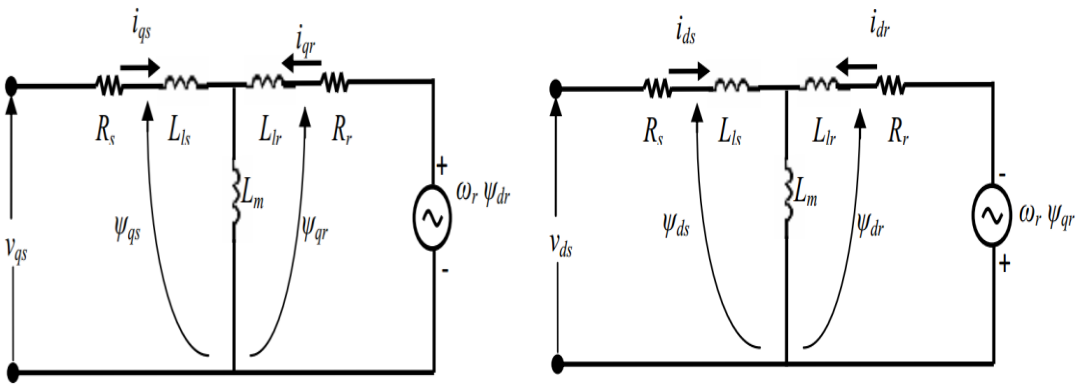


(a) q-axis equivalent circuit (b) d-axis equivalent circuit

Figure 3.17. Induction motor stationery d-q equivalent circuit model

$$v_{qs} = R_s i_{qs} + \frac{d\varphi_{qs}}{dt} \quad 3\text{-}102$$

$$v_{ds} = R_s i_{ds} + \frac{d\varphi_{ds}}{dt} \quad 3\text{-}103$$

$$0 = R_r i_{qr} + \frac{d\varphi_{qr}}{dt} - \omega_r \varphi_{dr} \quad 3\text{-}104$$

$$0 = R_r i_{dr} + \frac{d\varphi_{dr}}{dt} + \omega_r \varphi_{qr} \quad 3\text{-}105$$

The flux linkage expressions are given as below.

$$\varphi_{qs} = L_{ls} i_{qs} + L_m (i_{qs} + i_{qr}) \quad 3\text{-}106$$

$$\varphi_{qr} = L_{lr} i_{qr} + L_m (i_{qs} + i_{qr}) \quad 3\text{-}107$$

$$\varphi_{ds} = L_{ls} i_{ds} + L_m (i_{ds} + i_{dr}) \quad 3\text{-}108$$

$$\varphi_{dr} = L_{lr} i_{dr} + L_m (i_{ds} + i_{dr}) \quad 3\text{-}109$$

The electromagnetic torque and the rotor mechanical and electrical speeds are given in

$$T_e = \frac{3}{2}\left(\frac{P}{2}\right)(\varphi_{ds} i_{qs} - \varphi_{qs} i_{ds}) \quad 3\text{-}110$$

$$\frac{d\omega_m}{dt} = \frac{(T_e - T_m)}{J} \quad 3\text{-}111$$

$$\omega_r = \omega_m * \frac{P}{2} \quad 3\text{-}112$$

Table 3.12 Induction motor Parameters

| Parameters | Value | Unit |
|---|---|---|
| Rated Power | 20 | hp |
| Rated Voltage | 400 | V |
| Rated frequency | 50 | Hz |
| Rated speed | 1460 | RPM |
| Number of poles | 4 | - |
| Stator resistance | 0.2147 | Ω |
| Stator inductance | 0.000991 | H |
| Rotor referred resistance | 0.2205 | Ω |
| Magnetizing inductance | 0.06419 | H |
| Moment of inertia | 0.102 | $Kg.m^2$ |
| Friction coefficient | 0.00954 | N.m.s |
| Type | Squirrel cage | - |

# CHAPTER FOUR

# DESIGN OF CONTROLLERS FOR PV WATER PUMPING SYSTEM

## 4.1 Fuzzy logic controller structure

Fuzzy logic is work based on a mathematical model which deals with uncertainty and imprecise, ambiguous, noisy, or lost input data. It compares an analog input signal to a specified logic variable membership function or fuzzy sets with values between 0 and 1 as input. It's used in a control system to simulate human-like control decisions. Some of the basic features of fuzzy logics [52] are as follows: In fuzzy logic, exact reasoning is regarded as a limited instance of approximation reasoning. The general structure of a fuzzy controller and its main parts is shown in Figure 4.1 below. The fuzzy logic controller consists of four components: fuzzification interface, knowledge base, interface engine, and defuzzification interface.

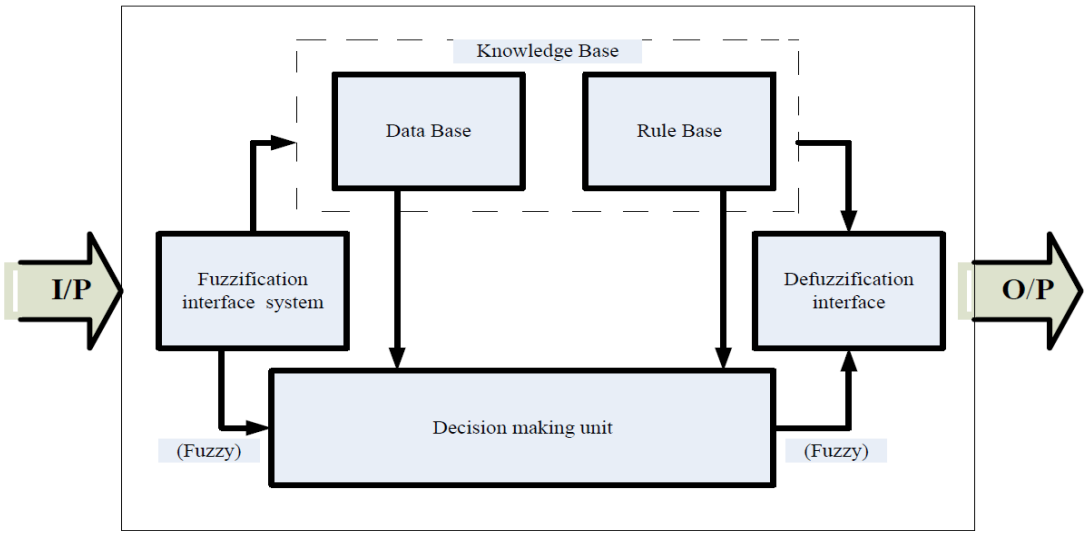


Figure 4.1 Structure of fuzzy interface system

A membership function that provides the degree of membership [53] can be used to represent a fuzzy set. In Figure 4.2, μA(x) in y-axis, is the symbol that refers to the degree of the membership function and μ(x) can be define as possibility function not probability function, and it takes value between (0, 1). Anybody can ask what is the different between probability function and possibility function. To answer this question let us see this example. If Abebe and Kebede went to visit another friend. And in the car Abebe asks Kebede, “Are you sure he is at

the home?" and Abebe answer "yes, I am sure but I do not know if he is in the bed room or on the roof". You can give him another answer. Abebe can answer him "I think 90% he is there". Look to the answer. In the first answer Abebe is sure he is in the house but he do not know where he is in the house exactly. But in the second answer Abebe is not sure he may be there and may be not there. That is the different between possibility and the probability in the possibility function the element is in the set by certain possibility and the probability in the possibility function the element is in the set by certain degree of, the probability function means that the element may be in the set or not . So if the probability of (x) = 0.8 that means (x) may be in the set by 80%. But in possibility if the possibility of (x) is 0.8 means that (x) is in the set and has degree 0.8. There is one type of membership function in the classical sets but in fuzzy sets there are different types of membership function, we now will show some of these types.

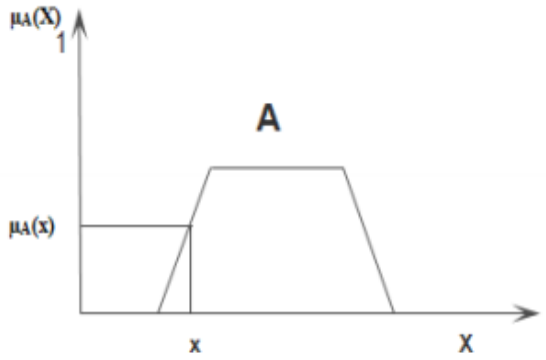


Figure 4.2 Membership function [53]

The fuzzifier transforms crisp inputs into the fuzzy subsets to obtain degrees of memberships and represent them with linguistic variables, which in turn are used to activate rules. The fuzzy inference engine process those data to obtain the desired output. The defuzzifier converts those fuzzy outputs to crisp variables to complete the desired fuzzy logic control goals. Every fuzzy are represented by its membership function. In practice the membership functions can have a number of different shapes depending on the designer interest. They are may be triangular, trapezoidal, Gaussian, bell-shaped, sigmoidal or S-curve. Some of them are shown in Figure 4.3 below. Triangular or trapezoidal MFs are mainly selected if critical dynamic variation in a short period of time is required. A Gaussian or S-curve membership function is always selected if the system requires very high control accuracy [54].

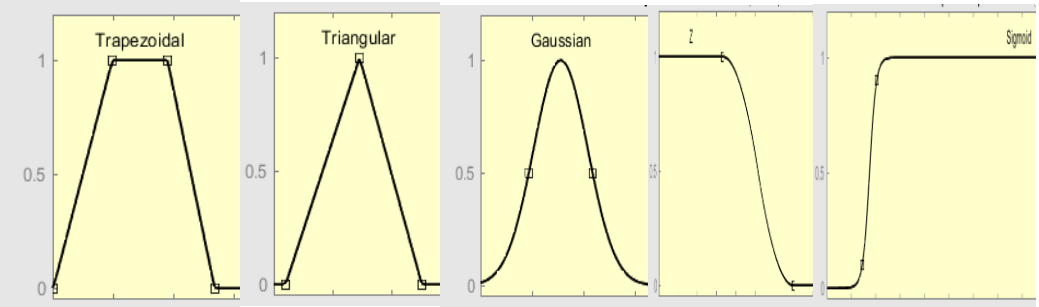


Figure 4.3 Types of membership functions [source: Author of thesis]

In fuzzy logic control, the linguistic variable is a critical concept. When fuzzy sets are used to solve a problem without analyzing the system, but human communication needs the expression of concepts and knowledge of them [32]. Humans usually don't use mathematical expressions but use linguistic expressions. For example, if you see the heavy box and you want to move it, you will say, ”I want a strong motor to move this box” we see that, we use the "strong" expression to describe the force that we need to move the box. We employ linguistic variables to characterize fuzzy sets in fuzzy sets. These variables are natural or synthetic language words or sentences. For example, if we take the universe U refer to the human age, we can take the interval between (50, 60) years and give it the name” old man this name is called a linguistic variable. We can use this name to refer to the set that contains the interval (50, 60) years.

## Knowledge base

It is the heart of the fuzzy control system and the inference basis for fuzzy control. The knowledge base defines all-important language control rules and parameters. The derivation of fuzzy rules can be performed in not mutually exclusive, and it is necessary to combine them to obtain an effective system [55]. Fuzzy uses human expert knowledge to make control decisions. Fuzzy logic may be used inside the remedy of unknown structures to model obscure data and experience knowledge.

Expert experience and control engineering knowledge: the fuzzy control rule is based on information obtained from the controlled system. Operators control actions: human controller’s actions observation in terms of input-output operating data. The number of base rules can be defined based on the number of membership in the fuzzy set and the inputs.

## Fuzzy inference system

A fuzzy interface system uses fuzzy logic to define the mapping from a given input to an output. The Mamdani approach and the Takagi-Sugeno-Kang method are the most often utilized strategies for conducting the fuzzy interface procedure in fuzzy controllers. Mamdani method is usually more popular for most control engineering applications due to its computationally more efficient and has better interpolative properties than the other interface methods [56]. In Mamdani fuzzy logic, the trapezoid or triangular fuzzy set is the most frequent, but other forms are available. The four steps that make up the mamdani method's fuzzy inference are fuzzification, rule evaluation, aggregation of rule outputs, and defuzzification [57].

## Fuzzification

Fuzzification is the initial step in fuzzy logic processing, and it involves converting crisp values to fuzzy ones. The membership function represents the process of transforming fuzzy values. For instance, if we have two inputs, input 1 and input 2, we can use the crisp inputs to determine the degree to which these inputs belong to each of the relevant fuzzy sets.

$$\text{If } \mu A_1(x) = 0.5,\ \mu A_2(x) = 0.2,\ \mu B_1(y) = 0.1,\ \mu B_1(y) = 0 \qquad 4\text{-}1$$

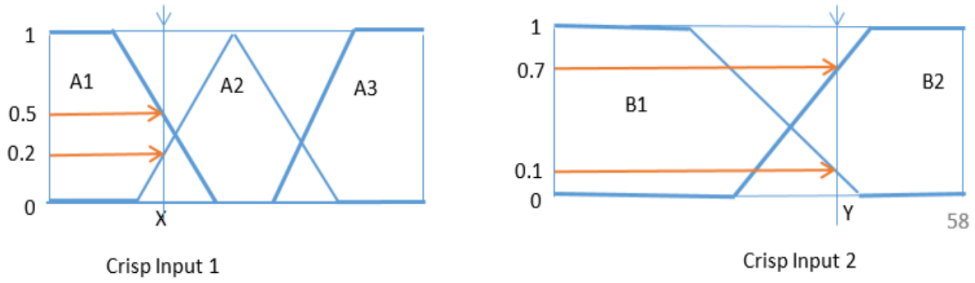


Figure 4.4 Fuzzification

## Rule evaluation

The term "fuzzy rule base" refers to a set of pre-defined instructions that relate distinct crisp values to different subsets of the fuzzy output space [57]. The fuzzified inputs are applied to the fuzzy rule's antecedents in this stage, and a fuzzy rule with several antecedents is resolved to a single integer between [0, 1] using the fuzzy operator. The fuzzy operator (AND or OR) is used to obtain this signal number. If the OR fuzzy operation is used, thus the classical fuzzy operation union is used or Maximum is used.

$$\mu_A(x) \cup \mu_B(x) = max(\mu_A(x), \mu_B(x)) \quad 4\text{-}2$$

Similarly for AND fuzzy operation minimum of the two or intersection is applied is applied.

$$\mu_A(x) \cap \mu_B(x) = min(\mu_A(x), \mu_B(x)) \quad 4\text{-}3$$

## Aggregation of the rule outputs

Following the discovery of each rule's output, the aggregation procedure is used to combine all of the rules' outputs into a single output. The combined output fuzzy set is the output of the aggregation process, as depicted in Figure 4.4 below. The aggregation technique, which takes a composite of scaled consequent membership functions as input, yields the combined output fuzzy set.

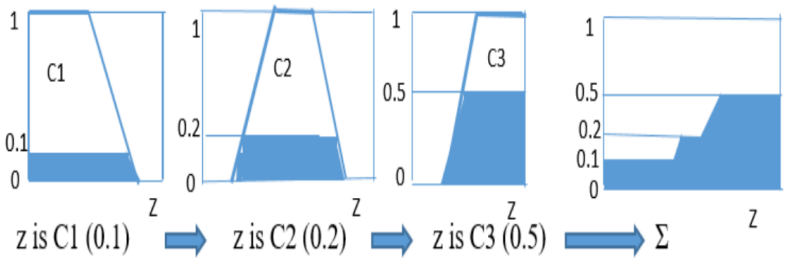


Figure 4.5 Aggregation of the rule outputs [57]

## Defuzzification

The final phase of the fuzzy interface process is defuzzification, which is the inverse of fuzzification. Defuzzification is the process of employing the membership function to convert the linguistic output from the interface engine to numerical output values. The fuzzy inference approach produces a linguistic variable based on a collection of control inputs. The ultimate output of the fuzzy control must be a precise number. As a result, defuzzification is needed to convert the fuzzy output to a crisp output that real-time application controllers can use. The mean of maximum method (MoM), height method (HM), and Center method (CM) are the most common defuzzification procedures.

## A. Mean of maximum method (MoM)

The MOM defuzzification strategy computes the average value of all the control actions whose membership functions reach the maximum.

$$\mathrm{MOM} = \sum_{i=1}^{l} \frac{W_i}{l} \qquad 4\text{-}4$$

Where; $W_i$ is the support value when the membership function reaches the maximum value $\mu_z(W_i)$, and $l$ is values of the support number.

## B. Height method (HM)

Height method is can only be applied when the output membership function is an aggregated union result of symmetrical functions.

$$Z = \frac{\sum_{j=1}^{N} w_j . \mu(w_j)}{\sum_{j=1}^{N} \mu(w_j)} \qquad 4\text{-}5$$

## C. Centre of gravity method (COG)

In real-world applications, the center of gravity method is the most often utilized defuzzification technique. The COG approach has the advantage of defuzzified values moving smoothly throughout the output fuzzy region. The COG method is a simple generic defuzzification approach that calculates the value of the abscissa of the area below the membership functions' center of gravity.

$$Z = \frac{\sum_{j=1}^{nN} w_j . \mu_z(w_j)}{\sum_{j=1}^{N} \mu_z(w_j)} \qquad 4\text{-}6$$

Where N is the number of output quantization levels.

## 4.2 Design of fuzzy logic controller for PVWPS

The most critical aspect in the MPPT of a PV system is the change of solar radiation and temperature. Because it changes on a regular and nonlinear basis, FLC-based MPPT is recommended to overcome the problem and supply the PV array's maximum available power to the load. Figure 4.6 shows a schematic of the photovoltaic array and water pumping equipment used to test the fuzzy logic controller's functionality. The error in power and the change in error are the inputs to the fuzzy control, and the output is the duty cycle variable, which controls the pulse width generating block. The fuzzy controller's error, change in error, and output are given by the equations (4-7), (4-6), and (4-7) respectively.

$$E(k) = \frac{\mathrm{P(k)-P(k-1)}}{V(k)-V(k-1)} \quad 4\text{-}7$$

$$CE(k) = E(k) - E(k-1) \quad 4\text{-}8$$

$$D(k) = D(k-1) - dD \quad 4\text{-}9$$

Most of the time the disadvantage of the fuzzy systems is not take experience from the previous information and if the input parameters to be controlled increase, the fuzzy logic controller will not be useful as successful rules cannot be determined.

The two main aspects of fuzzy systems that are used in this thesis are:

- Fuzzy systems are excellent for uncertain or approximate reasoning, especially for a system with a difficult to obtain mathematical model.
- In the presence of incomplete or uncertain evidence, fuzzy logic allows for decision-making with approximated values.

Note that there are many types of fuzzy reasoning but for this thesis, Mamdani fuzzy reasoning is the focus. Consider a simple fuzzy system with two inputs (x, y), one output (z), two rules and two membership functions per input. Let $A_1 = \mu_{A_1}$ and $A_2 = \mu_{A_2}$ be the membership functions for the first input and let $B_1 = \mu_{B_1}$ and $B_2 = \mu_{B_2}$ be the membership functions for the second input. Further, assume the input is fuzzified using the singleton fuzzifier. This means that instead of the input variable being a fuzzy set (or having a membership function), the input is a single value corresponding to the inputted value. For example, if the input is x=2 then the fuzzified input will also be x=2. Some commonly used membership functions are: triangular, trapezoidal, Gaussian, Bell or generalized Bell. To design a fuzzy logic system, no mathematical model of the system is required. This feature is beneficial because many physical systems are complex and troublesome to model. Advance, fuzzy logic is superior at handling system nonlinearities. If the fuzzy logic framework is used as a controller, it is more beneficial than the classical direct controllers such as the proportional-integral-derivative (PID) controller. The PID controller cannot control highly nonlinear systems effectively since a linear approximation around the operating point is usually performed to design a PID controller for a nonlinear system. Also, classical controllers have the downfall of being planned to control a framework at a particular operating point. If the operating point is changes, the controller needs to be re-tuned. For a fuzzy logic controller, there's a run of operating points defined by the

universe of discourse for a specific application. Hence, if the operating point changes, the fuzzy logic controller will still be effective at controlling the system under the condition that the new operating point is within the designed universe of discourse.

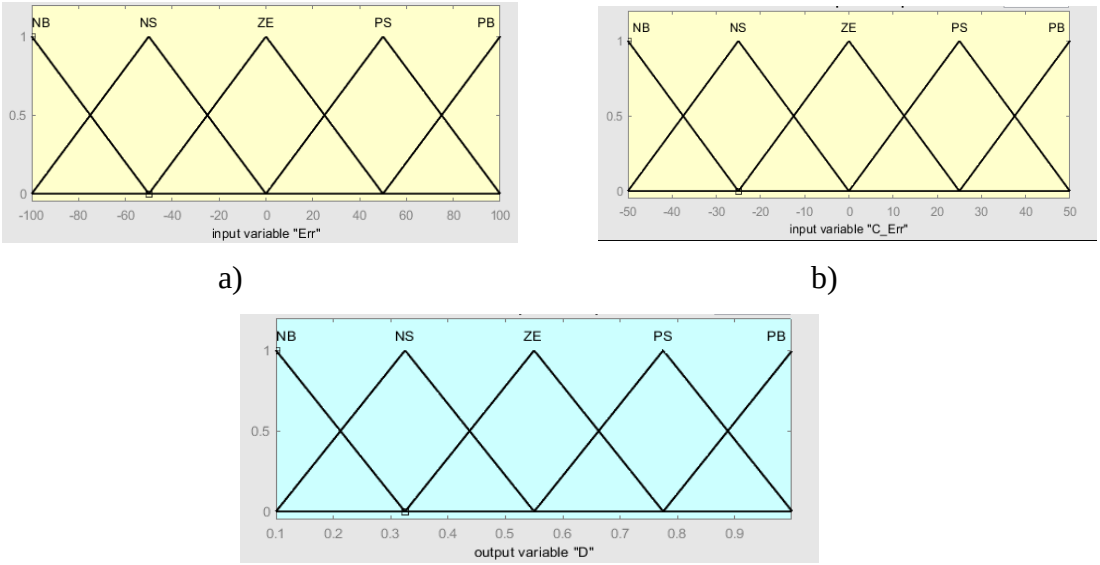


a) b)

c)

Figure 4.6. Membership functions for a) Error, b) change of error, and c) output

In literature, different membership functions (MFs) have been used. By utilizing expert knowledge, the triangular method is chosen to be the best based on its performance discussed in the literature [58]. Figure 4.5a, 4.5b, and 4.5c above shows the MFs of inputs (error and change of error), and output (Duty cycle) respectively. To develop an efficient FLC, fuzzy rules are the keys to consider. In the development of fuzzy rules in addition to the expert knowledge, there are some other parameters, e.g., error manipulation and system parameters are used that are also helpful in the definition of fuzzy rules when subjected to investigation. In this work, the proposed FLC model is simulated using the IF-THEN rule as listed in Table 4-1 below. To design FLC, the Mamdani model is utilized. The control block generates a duty cycle D, which is then fed to the boost converter as a PWM signal. Moreover, the value of D is calculated using the defuzzification algorithm referred to as the Center of Gravity (COG).

## Operation of FLC in the photovoltaic water pumping system

A fuzzy logic controller has been presented to modify the boost converter duty ratio, which adapts the PV array output voltage online to maximize output power, increasing the water pump's water discharge. It introduces a method for determining the operating point that

corresponds to maximum power for various degrees of insolation and temperatures. The proposed FLC contains two input variables and one output, as shown in Figure 4.7 below. In the fuzzification stage, numerical input variables are calculated or translated into linguistic variables based on subsets termed membership functions.

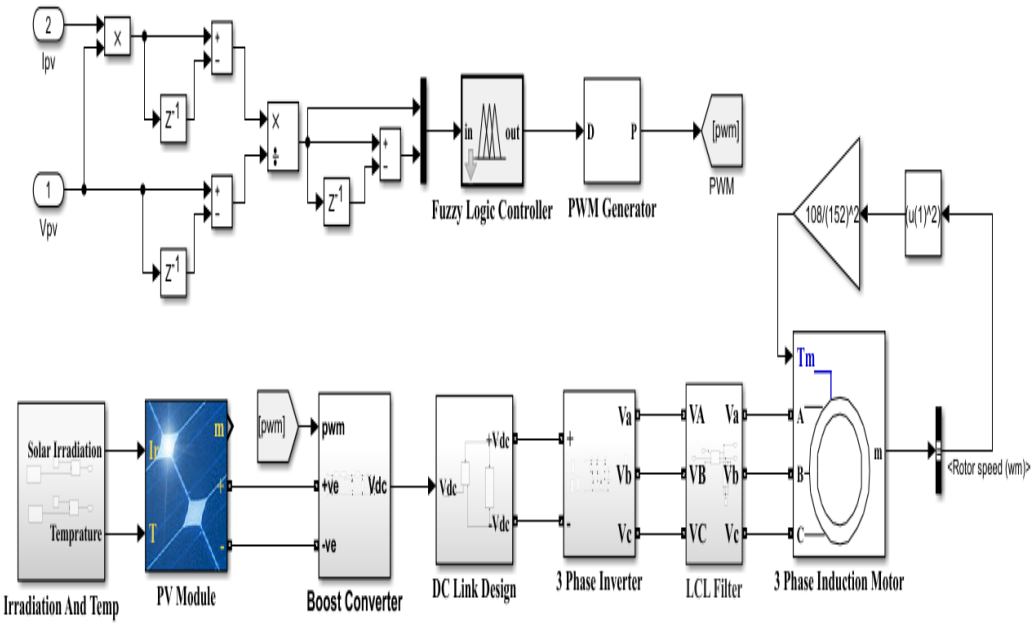


Figure 4.7. Schematic diagram of the proposed FLC MPPT based water pumping system

The input variables of the fuzzy logic controller are power variation ($\Delta P_{pv}$) and voltage variation ($\Delta V_{pv}$) at sampling instant k. The output variable is the duty ratio (D) of the boost converter. The MFs of the both inputs and output variables are represented by triangular functions and defined normalized range of input 1 (-100, 100), input 2 (-50, 50) and (0.1, 0.9) for output. The membership functions of the input variables $\Delta P_{pv}$ and $\Delta V_{pv}$, and the output variable D sets which are assigned for fuzzy sets have the same shape. The membership function of both inputs, and output variables are assigned five sets, including positive big (PB), positive small (PS), zero (ZO), negative big (NB), and negative small (NS). The fuzzy control rules have been set up using a set of IF-THEN statements that contain all information for the controlled parameters. The fuzzy control rule includes 25 rules as described in Table 4-1. These rules are used for the control of the boost converter such that the maximum power is achieved at the output of the PV array.

Table 4.1. The FLC rule base

| Error/C_Error | NB | NS | ZE | PS | PB |
|---|---|---|---|---|---|
| NB | PB | PB | PB | PS | ZE |
| NS | PB | PB | PS | ZE | NS |
| ZE | PB | PS | ZE | NS | NB |
| PS | PS | ZE | NS | NB | NB |
| PB | ZE | NS | NB | NB | NB |

## 4.3 Particle swarm optimization for tuning of FLC

Particle swarm optimization is an optimization approach that uses the interaction of individuals in a population of particles to locate optimal regions of complex search spaces [59]. Kennedy and Eberhart created it using the social behavior metaphor [60]. Many research efforts have been dedicated toward the creation and exploration of this novel technology in the previous ten years or so. One of PSO's main advantages is that its paradigm can be implemented as simple computer codes and that it is computationally cheap in terms of speed and memory needs. The PSO technique has been described as a stochastic strategy based on the swarm. [61].

Animal's social behavior including birds, insects, herds, and fishes simulated by particle swarm optimization algorithm. These swarms accommodate an agreeable way to find food, and each member within the swarms maintains changing the search pattern according to the learning experiences of its own and other members. The two types of studies are strongly related to the PSO-basic algorithm's design concept: One is an evolutionary algorithm, which allows it to simultaneously search huge parts of the optimized objective function's solution space. The other is artificial life, it studies the artificial systems with life characteristics. Fuzzy logic controllers are designed in the form of rule based behavior based on expert knowledge. In general, controller rules are set in the following format:

$$\text{if input A is } \mu_{A_1} \text{ AND input B is } \mu_{B_1} \text{ THEN output C is } \mu_{C_1} \qquad 4\text{-}10$$

Where antecedents A and B are expressed by membership functions $\mu_{A_1}$, and $\mu_{B_1}$. The process that is used to calculate the overall control action in FLC is determined by different type of defuzzification process [62].

Generally fuzzy rules expressed in Table (4-1) and the MFs can be derived from expert knowledge. However, exact rule numbers and the relationships between the antecedents *A* and *B* are difficult to derive. For example, it is difficult, sometimes to determine if a rule should be "if A AND B" or "if A OR B", or "if NOT A AND B", etc. Furthermore, in the design of MFs that involves the determination of where in the variable space each membership function should locate is also a time consuming process. The rule bases can be automatically tuned using PSO if the relationship of antecedents and consequences can be expressed using numerical values. In the MATLAB fuzzy logic toolbox the fuzzy rule expressed in Table 4-1 is compressed by numerical values as:

$$1\ 1, 1\ (1) : 3 \qquad 4\text{-}11$$

In equation (4-11) the first two 'values' represent the MF numbers associated with the two inputs (negative numbers can be used to represent the NOT function), the 'value' after the comma represents the relationship between the two inputs (1=AND and 2=OR). The value in the bracket is the weighting factor of this rule, while the last number after the colon represents the MF number associated with the output. Therefore, it is possible to automatically tune fuzzy controller using particle swarm optimization and to use PSO to find the appropriate relationships between the rules and to determine if the number of rules is adequate.

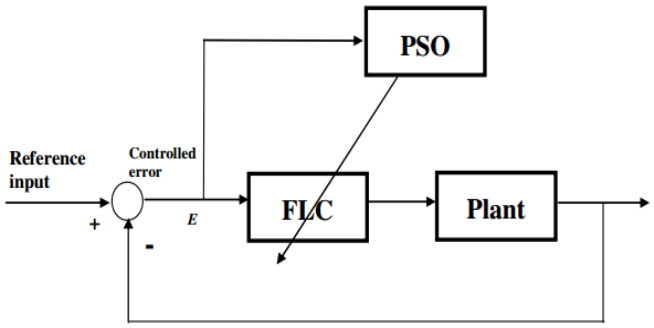


Figure 4.8. The proposed PSO based MF tuning method

The strategy of using a PSO for rule tuning in FLC can be depicted in Figure 4.8 above. In the proposed PSO process, each particle is formed to represent the rules of the FLC's. As the purpose of the PSO is to minimize the control error of the FLC, the objective (cost function) of PSO is defined as the Integral of the Squared Error (ISE) as given in Equation 4.16 below.

The nonlinear input membership function parameters must be optimized for the proposed PSO-based fuzzy logic method to be applied to the specified system. As a result, each particle in the

population has values for these parameters that correspond to a conceivable error function-minimizing solution. For the sake of this thesis, the duty cycle applied to the boost converter's MOSFET is chosen as the system output. Each particle is created as an array, with the function's center and standard deviation as columns and each row containing one membership function. Millonas presented five key concepts for how to develop swarm artificial life systems with cooperative behavior by computer while researching the behavior of social animals using artificial life theory [63] [64].

1. Closeness: For simple computations, the swarm should be able to reduce the time and space necessary.
2. Environmental Quality: The swarm should be able to detect and respond to changes in the quality of the environment.
3. Different response: In order to retain the resources within a certain range, the swarm should not limit its direction.
4. Stability: As the environment changes, the swarm's behavior should not change.
5. The ability to change: The swarm's behavior mode should only be changed when it is justified.

Note that the fourth and the fifth principle are the opposite sides of the same coin. These five fundamental principles incorporate the main characteristics of the artificial life systems, and they have become guiding principles to establish the swarm artificial life system. Particles in PSO can adjust their velocities and positions in response to changes in the environment, ensuring that it meets the proximity and quality requirements. During expansion, the swarm in PSO does not restrict its mobility; instead, it seeks out the optimal solution in the given solution space. Particles in PSO can maintain their steady mobility while changing their movement mode in response to environmental changes.

This section gives a discussion on particle swarm optimization and addresses some of the benefits of implementing it for optimization purposes. Advance, its relation to fuzzy logic controller will also be explored. Particle swarm optimization is an evolutionary algorithm that's modeled after the behavior of a flock of birds or a school of fish [65]. In the PSO algorithm, a random population is set with a number of members (called particles). Each part in the population contains a solution to the given problem. Imagine a flock of birds. Each bird in the

flock moves according to its velocity and position and is also influenced by the other birds' position. If the flock is hunting for food, one of the birds will be in the best position to find it (the global best). In order to get the meal, all other birds will modify their velocity and position based on this worldwide best position and their individual best position as outlined in Figure 4.9 below [66]. As a result, the swarm or flock gravitates toward the most optimal solution to a problem. As a result, as compared to traditional MPPT approaches, PSO usually finds the global minimum of the objective function based on the initial placements of the members in the population and enhances the tracking of the greatest power point. The population originally consists of randomly generated members. Each particle in the population has its own current position and best position called $p_{best}$, the globally best solution (called $g_{best}$) is the best solution among all of the particles $p_{best}$.

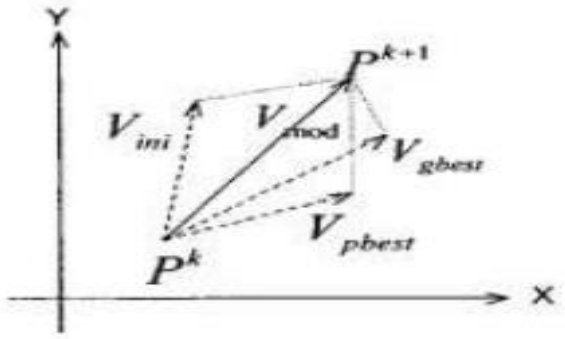


Figure 4.9 Particle position update [66]

The goal of the PSO algorithm is to move the particles towards their $p_{best}$ and the overall $g_{best}$. $P_k$ is the particles current position, $P_{k+1}$ is the particle's new update position, $V_{ini}$ is the initial velocity of the particle, $V_{mod}$ is the new velocity, $V_{pbest}$ and $V_{gbest}$ show the velocity due to personal best and global best respectively. The particle swarm optimization algorithm is discussed with its flowchart given in Figure 4.10.

1. Initialize a population of P particles with randomly generated positions and velocities.
2. For each particle, compute its fitness value according to the optimization problem.
3. Compare each particle's current fitness value with its best fitness value or $p_{best}$'s fitness. If the current value is less than the value from $p_{best}$, update $p_{best}$ with the current position.

4. Compare each particle's current fitness value with the best fitness value among all particle or $g_{best}$'s fitness. If the current value is less than the value from $g_{best}$, update $g_{best}$ with the current position.
5. Update each particle's velocity and position according to the equations (4-14) and (4-15) below.
6. Repeat steps 2-5 until a desired fitness level is achieved or a defined number of iterations is reached.

The PSO algorithm can be described as follows: Given that a swarm consists of *N* particles in a *D* dimensional problem space, the position and velocity of the *i*-th particle is presented as:

$$x_i = x_{i1} + x_{i2} + \cdots + x_{iD} \quad 4\text{-}12$$

$$v_i = v_{i1} + v_{i2} + \cdots + v_{iD} \quad 4\text{-}13$$

Where $i$=1, 2… $N$

Each particle point in the problem space, is initialized with a random position and search velocity. Its velocity and position are updated using equation (4-14) and (4-15) separately.

$$v = w * v + c_1 * rand\ (0, 1) * (P_{best} - x) + c_2 * rand\ (0, 1) * (g_{best} - x) \quad 4\text{-}14$$

$$x = x + v \quad 4\text{-}15$$

Where, *v* is the velocity of each particle, *w* is an inertia weight that reduces the effect of the previous velocity as the search progresses, $c_1$ and $c_2$ are the local and global learning rates respectively.

The PSO algorithm can be used to optimize the selection of the FLC parameters including the rule weights and the parameters of MFs. Here, the PSO algorithm has been employed to train the adjustable parameters of the FLC, such as error, change of error and duty cycle gains. Set the adjustable parameters of FLC as $k = [k_1, k_2, k_3]$. The PSO problem has been defined as a *D* dimensional problem where *D* is the total element number of *k*. Our objective is to train the parameters to be the best value $k_{best}$ so that trajectory deviation *e* approach zero.

The choice of the parameters in PSO can significantly influence the algorithm's ability to perform optimization successfully. Therefore, care must be taken in order for PSO to have the best chance at finding the optimal solution for a problem. Trial and error method can be used to determine: the ideal number of particles in the population, the inertia coefficient, the

personal and global learning rates and the limits on the particle's positions gives an explanation on how each of the parameters affects the searching ability of the PSO algorithm [66].

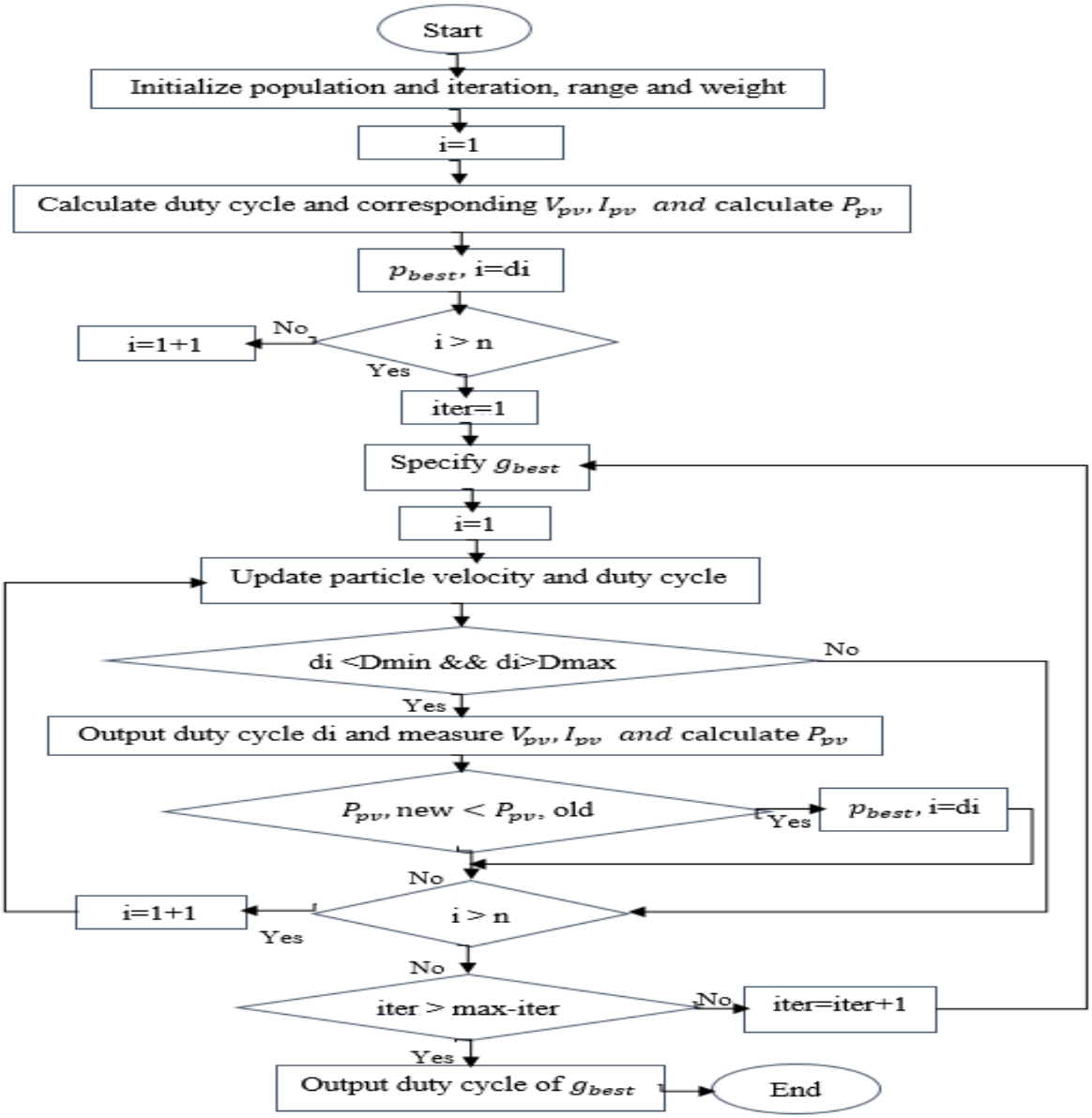


Figure 4.10 Flow chart for searching mechanism by PSO-based MPP tracker

It is important to note that limits should be set on the generated solutions in order to avoid the particle's movements outside the search space. If the position of a particle exceeds the limits, its value is set to the limits and the search continues. Generally c1=c2 rand (0, 1) is a random number between and 1 $g_{best}$ is the best position among all members (globally best position)

$p_{best}$ is the best position for a given member (personal best position) x is the current position of the particle.

## Performance specifications of MPPT controller

The dynamic response, steady-state error, and tracking efficiency would be considered for a successful design when evaluating the performance of new or modified MPPT control algorithms. This thesis compares two performance criteria, efficiency criterion and the Integral of the Squared Error, in order to evaluate the theoretical and experimental performances of presented investigations. The Reaction of the MPPT control algorithm ought to be fast to track the MPP during the fast changes in climatic conditions. The lower the tracking error and the lower the system loss, the faster the MPPT algorithm can track. The goal of most controllers is to reduce the discrepancy between the system output and the target order value. This discrepancy could be due to a shift in the system's order or other factors. As a result of these arguments, the Integral of Squared Error (ISE) is defined as follows:

$$ISE = \int_0^t [e(t)]^2 \qquad 4\text{-}16$$

Where,

$$e(t) = \frac{\Delta P_{pv}}{\Delta V_{pv}} \qquad 4\text{-}17$$

$e(t)$ is the error signal of the first input to fuzzy controller. The amount of $e(t)$ shows that the working point of a PV array used at time (t) goes to either left or right side of the MPP on the P-V curve. The ISE criterion is evaluated in the interval [0, t].

The tracking efficiency could be a very vital step, to evaluate how successfully an MPPT control algorithm tracks the MPP and to what extent it contributes to increasing the overall PV system's performance compared to other methods. According to [67] the tracking efficiency is defined as the ratio between the actual power of the PV array and the theoretical power during the same time period. The efficiency criterion $\eta_{MPPT}$ of a MPPT controller is defined by:

$$\eta_{MPPT}(\%) = \left( \int_0^t P_{MPPT}(t)dt \Big/ \int_0^t P_{ref}(t)dt \right) * 100 \qquad 4\text{-}18$$

Where $P_{MPPT}$: measured power generated by the PV panel with MPPT, $P_{ref}$ maximum power generated in the same conditions of temperature and irradiation without MPPT. Equation (4.18) is implemented in Simulink to compute the efficiency results of three proposed controllers.

# CHAPTER FIVE

# RESULTS AND DISCUSSIONS

## 5.1. Modelling of photovoltaic water pumping system using Simulink

System modeling and simulation has been undergone in MATLAB/SIMULINK. Figure 5.1 depicts the proposed system's whole SIMULINK model. The photovoltaic water pumping system is simulated in MATLAB, with an AC water pump load (22 kW) to demonstrate the feasibility and performance of the proposed Fuzzy PSO-based MPPT of the water pumping system. To carry out the tracking of MPP, Perturb and observe method, fuzzy logic, and Fuzzy PSO-based controller has been applied. Additionally, a comparison has been conducted between each proposed controller.

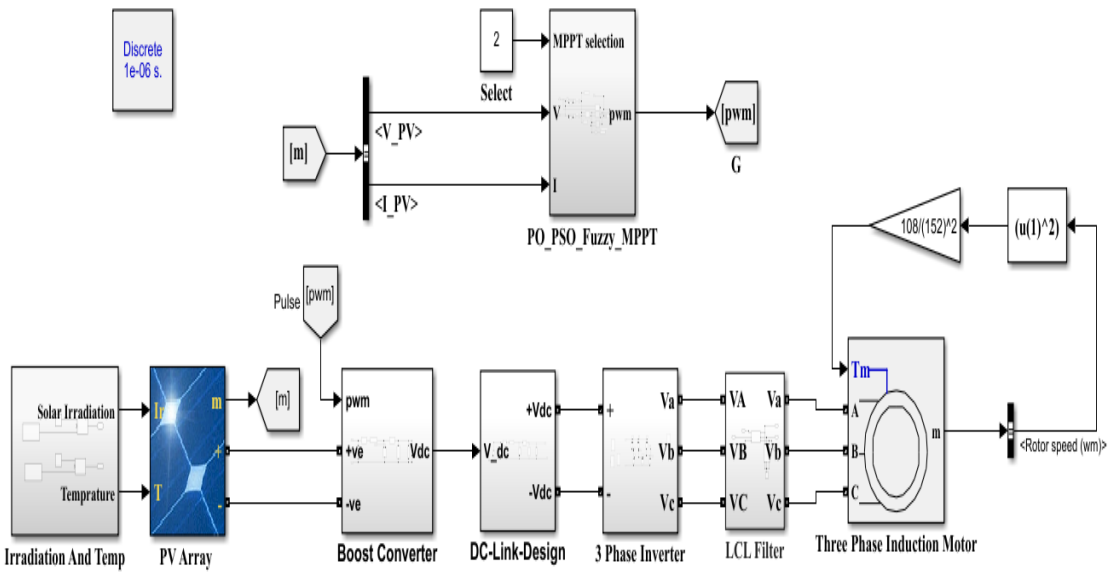


Figure 5.1 Schematic diagram of the proposed PSO-based Fuzzy Logic MPPT controller

The system design is modeled and simulated using MATLAB/SIMULINK 2019b as shown in Figure 5.1. The system consists basically of PV array model, DC/DC boost converter model used to interface PV output to the inverter to track the maximum power of the PV array, DC/AC three-phase PWM inverter model used to interface with the AC load, LCL low pass filter to supply a pure sinusoidal output voltage to the load and three-phase induction motor. The PV array used in the simulation is a 32.29 kW power i.e. 12 strings with 11 modules of 245 W

each to generate the desired power at standard conditions specified at irradiation of (G=1000 kW/m$^2$) and temperature of ($T$ =25$^0$C). Totally one hundred and thirty-two modules are executed to urge the PV control that used to create 32.29 kW for the required purpose. In this section, the results convergences towards MPP of the PV system by using three studied controllers "P&O", "Fuzzy" and "PSO-based Fuzzy" were compared. A temperature is set at 25$^0$C, while the irradiation G is rapidly variable taking the form of stairs with rising edges within a short time span. Fuzzy rules and surface view of given inputs and output are shown in Appendix B. Figure 5.2a shows variable irradiance for analysis of different MPPT techniques.

## 5.2. PV water pumping system simulation by using P&O MPPT techniques

In this PV system, the PV array has been connected to the 22kW Ac load with a P&O controller. In fact, the P&O method is commonly used for MPPT and is broadly deployed throughout the industry because it is simple and flexible. However, the P&O method shows a tradeoff between tracking accuracy and tracking speed due to the presence of an intrinsic tradeoff in choosing step size and perturbation frequency. Moreover, there is a problem of variation of value around MPP. The P&O technique works as a random system. Until the PV system modifies the duty cycle value to discover the proper value at that moment, it does not know the correct value of the duty cycle that reaches the MPP. In this way, it must spend time for this step and it causes wasting time. The system was subjected to a sudden change in solar irradiation and temperature. The simulation results of P&O MPPT techniques show that the connected system is operating far from the maximum power point at some irradiation and temperature levels. Therefore, some of the energy will be dissipated, this reduces the amount of water being discharged from the pump, and hence the system is operating at a relatively poor efficiency for various insolation and temperature levels. The average efficiency of the proposed P&O MPPT technique is 84.99%.

## 5.3. PV water pumping system simulation by using FLC controller

Fuzzy-based approaches have a high adaptability and robustness for tackling MPPT problems in solar systems, which including a large number of uncertain factors effectively. However, in the application, the general fuzzy control method depends on prior information to set control rules, membership functions, and relevant control parameters, which is difficult to meet the

real-time control requirements of the PV systems when the external environment changes greatly. The fuzzy system is better than the P & O MPPT techniques but it requires expert designers to design the fuzzy class ranges as the system wants. As the simulation, the results suggest that fuzzy logic controllers surpass P&O approaches. The average efficiency of the fuzzy logic MPPT technique is 95.65%.

## 5.4. PV water pumping system simulation by using PSO-based fuzzy control

For fuzzy rules, the adjustable parameter is the consequent constant of the rules, which is $k = [k_1, k_2, k_3]$ where $k_1, k_2, k_3$ are scaling factors of change of PV power, change of PV voltage and duty cycle respectively. Since, there are 25 fuzzy rules, which have 50 consequent constants, then set the problem space of the PSO algorithm as 50 dimension. The other PSO parameter initialized as a number of particle *N*=50; the iteration count iter*max*=10; the acceleration factors $c_1 = 1.5$, $c_2 = 1.8$; inertia weight ω declines linearly from 0.95 to 0.2 along the time.

The objective is to train the parameters to be the best value $k_{best}$, So that trajectory deviation error approaches zero. The problem is created as a minimization problem where the fitness function is based on the integral of squared error (ISE) in each iteration as shown in equation (4-14). As the simulation, the result shows PSO-based Fuzzy controller has better performance than fuzzy and P&O MPPT techniques. The average efficiency of the proposed PSO-based Fuzzy MPPT technique is 96.50%. PSO swarm algorithms are given in Appendix A.

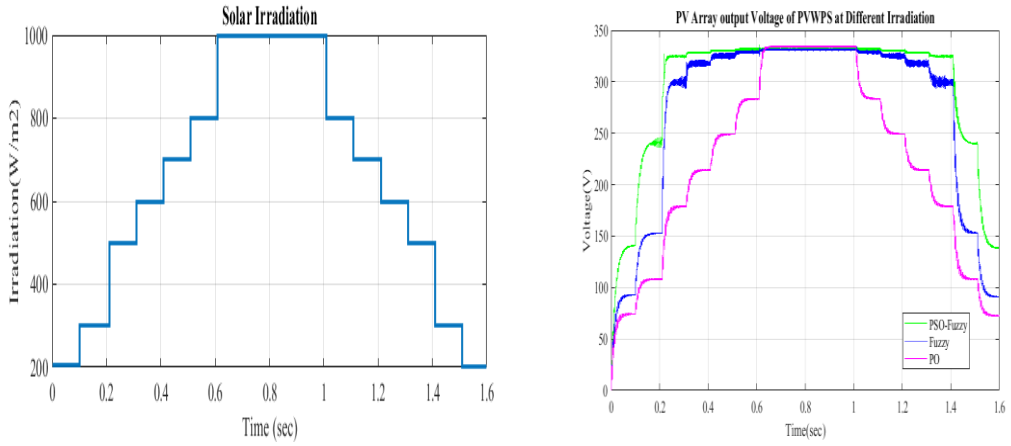


a) b)

Figure 5.2 Daily trend of a) Solar irradiation b) Module output voltage

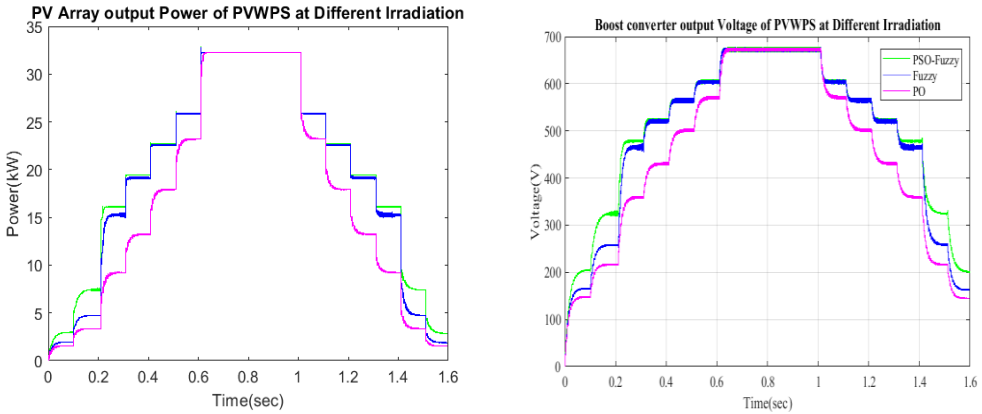


a) b)

Figure 5.3 Daily trend of a) Module output power b) Boost converter output voltage

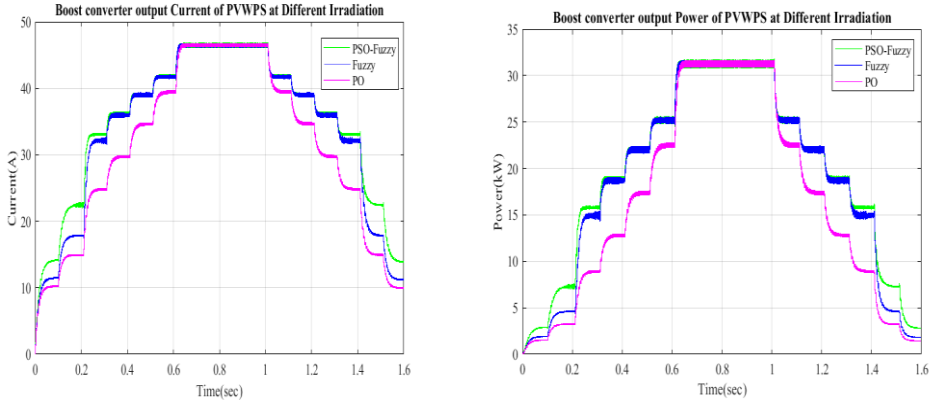


a) b)

Figure 5.4 Daily trend of boost converter output a) Current b) Power

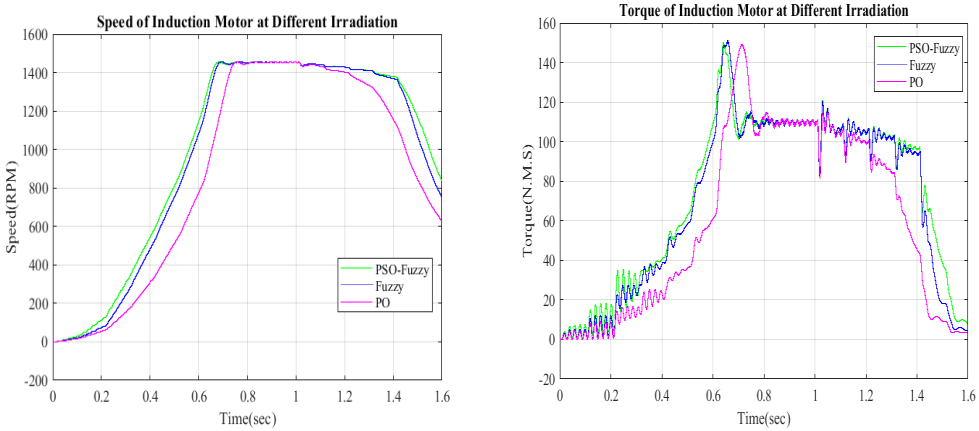


a) b)

Figure 5.5 Induction motor a) Rotor speed b) Electromagnetic torque

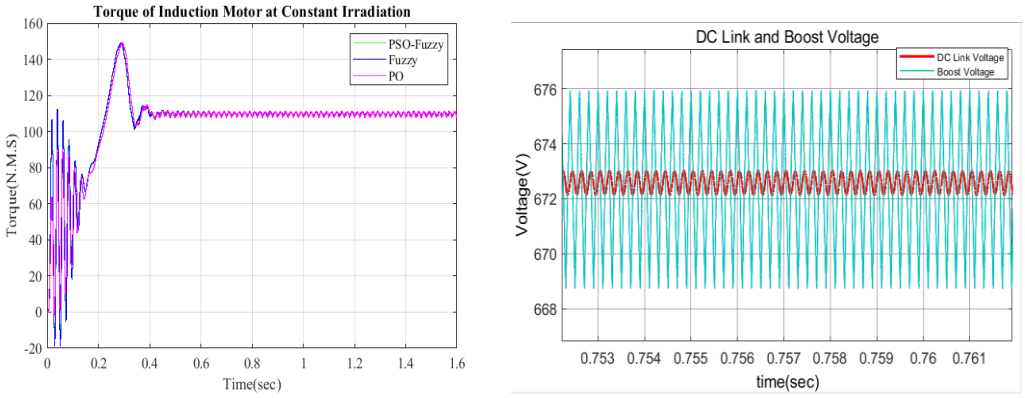


a) b)

Figure 5.6. a) Electromagnetic torque of induction motor at constant irradiation b) DC link and Boost converter voltage comparison

The simulation results of PV array and boost converter output voltage, current and power, speed, and torque of three-phase induction motor are shown in manganese, blue and green color for P & O, fuzzy logic and PSO-based fuzzy controller respectively from figure 5.2b to 5.6a. In figure 5.4b above, it shows the big difference in power from 0.2sec to 0.3sec between the two systems that can reach about 6kW. We observe that in case of sudden high and positive variations of the irradiance, the proposed PSO-based fuzzy algorithm reacts quickly and faster than the PO and fuzzy controller. In all results, the response time of the PSO-based fuzzy controller is faster than "P&O" and "Fuzzy" controllers. Figure 5.5a and 5.6a shows the rotor speed of the motor pump, which depends directly to the PV voltage. The comparison between boost voltage and DC link voltage which are shown in Figure 5.6b in cyan and red color respectively. Three-phase voltage and current of three-phase inverter and stator voltage and stator current of induction motor are shown in Figure 5.7 and 5.8 below respectively. Figure 5.9 below shows the duty cycle responses of three proposed controllers. The results showed that the use of the MPPT controller considerably and efficiently improves the performance of the PV water pumping system. A PSO-based Fuzzy controller enables to not only lower the ISE, but also increases the MPPT controller's performance $\eta_{MPPT}$, this seeks to reduce transient mode changes when compared to P & O and fuzzy logic controllers.

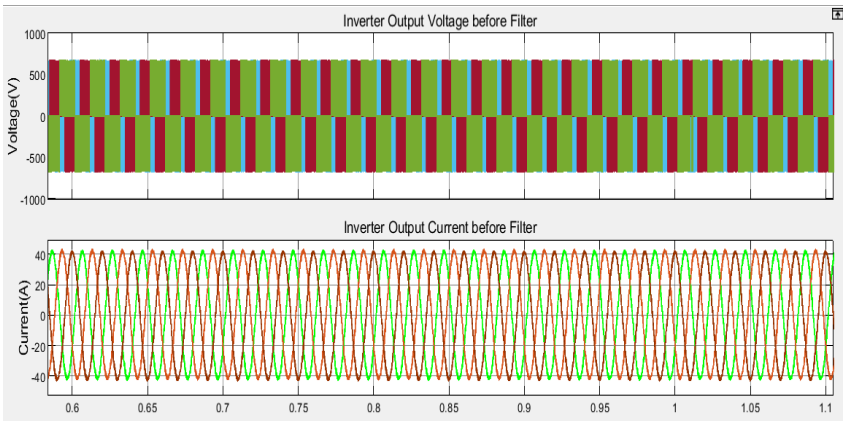


Figure 5.7. Three phase inverter output voltage and current waveform

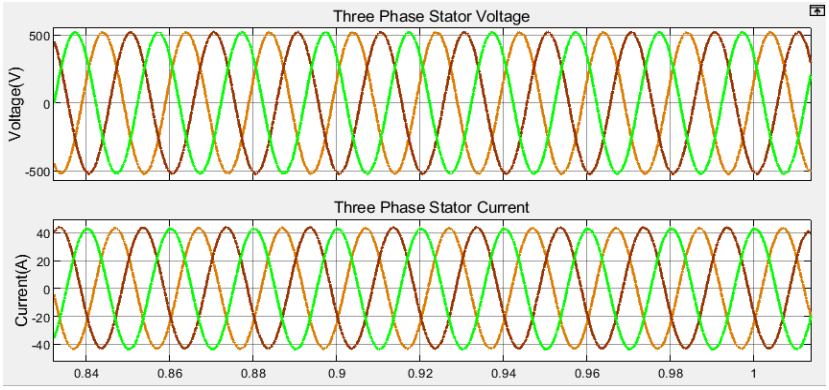


Figure 5.8 Three phase stator voltage and current of induction motor

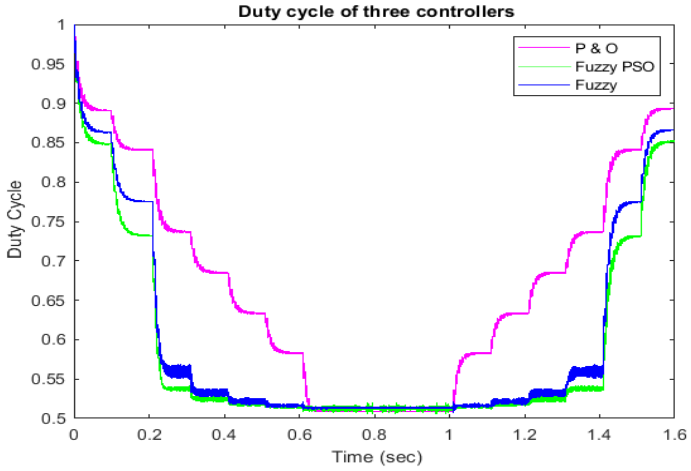


Figure 5.9. Duty cycle response of three proposed controllers

Table 5.1 PV efficiency

| Controllers | Efficiency (%) |
|---|---|
| Perturb and Observe | 84.99 |
| Fuzzy | 95.65 |
| PSO-Fuzzy | 96.50 |

## Particle swarm optimization simulation parameters

Number of variables: 3

Number of particles in the swarm: 10

Number of iterations: 5

Initial range of first variable: [1, 50]

Initial range of second variable: [0.1, 20]

Initial range of third variable: [0.1, 1]

Table 5.2 PSO Initial swarm and Best swarm matrix

| Initial swarm matrix | | | Best swarm matrix | | |
|---|---|---|---|---|---|
| 6.2260 | 8.6851 | 0.8677 | 4.7169 | 3.3274 | 0.5055 |
| 48.1330 | 18.2219 | 0.6598 | 3.6436 | 15.9063 | 0.1754 |
| 1.2271 | 3.7188 | 0.4159 | 27.0091 | 6.2932 | 0.3061 |
| 38.9706 | 5.3497 | 0.5619 | 39.1792 | 10.6178 | 0.9220 |
| 41.0479 | 2.9962 | 0.4616 | 46.7665 | 3.3964 | 0.2371 |
| 43.5660 | 2.8078 | 0.1684 | 7.3654 | 12.0794 | 0.8432 |
| 5.1374 | 17.3989 | 0.3159 | 35.5938 | 25.2877 | 1.0000 |
| 20.5893 | 11.6361 | 0.2110 | 24.0001 | 13.1162 | 0.9965 |
| 13.7336 | 11.0422 | 0.2655 | 1.5832 | 13.8154 | 0.1704 |
| 40.2034 | 2.9846 | 0.3160 | 17.5190 | 14.9882 | 0.4984 |
| Best particle 7th in Best swarm matrix | | | [35.5938179531135,25.2876854,1] | | |

# CHAPTER SIX

# CONCLUSION AND RECOMMENDATION

## 6.1. Conclusion

In this thesis work, a PV water pumping system is brought to presentation to provide the pure water in remote rural areas with a clean and sustainable supply of energy, solar irradiation. Hence, the thesis mainly focuses on the way how to improve the full system performance by implementing better controller so that the transfer of available maximum power is possible irrespective of the changing atmospheric conditions.

In this thesis, proposed system components are modelled and simulated under Matlab/Simulink 2019b, whose load is adapted by a three phase induction motor interfaced with LCL filter, VSI, and boost DC-DC converter. Three types of MPPT controllers are used to ensure MPPT: the conventional "Perturb and observe" controller, as well as intelligent controllers "Fuzzy" and "PSO-based Fuzzy controller".

The presented fuzzy PSO-based technique reaches the MPP in a shorter period, according to simulation results. In comparison to a standard technique, the Fuzzy PSO-based algorithm has benefits of high convergence speed, high precision, and can accurately track the maximum power, according to simulation results. Based on the simulated result the efficiency has been 84.99%, 95.65%, and 96.5% for P&O, FLC, and PSO-based Fuzzy respectively. So that the results confirm that the proposed MPPT method has the potential to significantly increase the total efficiency of the PV water pumping system.

## 6.2. Recommendation

In this investigation, MATLAB simulation models were proposed and used to compare the performance of MPPT techniques. The simulation results achieved in this work will hopefully incentivize future investigations involving building prototype models to test experimentally the developed MPPT techniques for the PV water pumping system, and among the three proposed controllers PSO-based Fuzzy controller shows better performance than the other two controllers so it ought to apply this controller in practical manners for PV water pumping systems.

In the current PV system, the boost converter is used as an interface to enable the MPPT process. The DC-DC converter buck-boost along with the proposed MPPT techniques to improve flexibility in the choice and configuration of PV array connection. And instead of a two-level inverter three-level inverter will smooth the output three-phase voltages. A Hybrid PSO-based Genetic algorithm could also be investigated to improve the speed of convergence and the ability to find the global optimum.

# REFERENCES


[1] I. Coimbatore, "The United Nations World Water Development Report. Water for a Sustainable World," *IEEE Internation Conference on Current Trends in Engineering and Technology*, 2015.

[2] CEO Alicia Barton, "Green strategic Outlook: Towards a clean energy Future," New york State of Opportunity, 2018.

[3] S. S. Chandel and and et.al, "Review of solar photovoltaic water pumping system technology for irrigation and community drinking water supplies," Renewable and Sustainable Energy Reviews, vol. 49, pp. 1084-1099, 2015.

[4] M. Thomson, "Reverse-osmosis desalination of seawater powered by photo voltaic without batteries:," Doctoral Thesis, Loughborough University, 2003.

[5] E. Foster and and et.al, Solar energy: renewable energy and the environment, 2009.

[6] D. V. Brian and A. N. Byron , "Analysis of off-grid hybrid wind turbine/solar PV water pumping systems," *USDA1, Agricultural Research Service, P.O. Drawer 10, Bushland, TX 79012, United States,* 2015.

[7] E. F. Robbert and C. Alma , "Solar water pumping advances and comparative economics," in *Conference: Solar World Congress, International Solar Energy SocietyAt: Cancun,*, 2015.

[8] "UNESCO, "The UN World Water Development Report,"," www.unesco.org/water /wwap/wwdr/), 2018.

[9] V. kumar and and et.al, "Design and implementation of solar PV fed BLDC motor driven water pump using MPPT," *International Journal of Scientific Engineering and Applied Science (IJSEAS) – Volume-4, Issue-03,* 2018.

[10] V. Parimala, D. Ganeshkumar and M. Divya, "Implementation of Solar Water Pumping System Using Fuzzy Logic Controller," *2020 6th International Conference on Advanced Computing and Communication Systems (ICACCS),* 2020.

[11] A. Alshamani and T. Iqbal, "Feasibility of using a Large Deep Water PV Water Pumping System: A Case Study for an Average Farm in Riyadh, Saudi Arabia," *2017 8th IEEE Annual Information Technology, Electronics and Mobile Communication Conference (IEMCON), DOI: 10.1109/IEMCON.2017.8117175,* 2017.

[12] E. Mustapha and and et.al, "Fuzzy-PI Controller for Photovoltaic Water Pumping Systems," *2019 7th International Renewable and Sustainable Energy Conference (IRSEC), DOI: 10.1109/IRSEC48032.2019.9078318,* 2019.

[13] Rajni Kumari and Ratna Dahiya, "Speed Control of Solar Water Pumping with Indirect Vector Control Technique," *2018 2nd International Conference on Inventive Systems and Control (ICISC), DOI: 10.1109/ICISC.2018.8399039,* 2018.

[14] A. Lazizi, M. Kesraoui and A. Chaib, "Fuzzy logic MPPT control for a solar PV module applied to water pumping," *International Journal of Industrial Electronics and Drives, 2016 Vol.3 No.1, pp.1 - 11, DOI: 10.1504/IJIED.2016.077676,* 2016.

[15] S. Sheik Mohammed and and et.al, "GA-Optimized Fuzzy-Based MPPT Technique for Abruptly Varying Environmental Conditions," *Journal of The Institution of Engineers (India): Series B volume 102, pages 497–508 (2021),* 2021.

[16] A. Hadjaissa and and et.al, "A GA-based optimization of a fuzzy-based MPPT controller for a photovoltaic pumping system," *IFAC(Intrnational Federation of Automatic Control) Hosting Elsevier, https://doi.org/10.1016/j.ifacol.2016.07.791,* 2016.

[17] Mustapha Errouha and and et.al, "Optimal Control of Induction Motor for Photovoltaic Water Pumping System," *Technology and Economics of Smart Grids and Sustainable Energy volume 5, Article number: 6 (2020), doi: 10.1007/s40866-020-0078-9,* 2020.

[18] S. J. Barnam , "A comparative study on converter topologies for maximum power point tracking application in photovoltaic generation," *Journal of Renewable and Sustainable Energy 6(5) DOI:10.1063/1.4900579,* 2015.

[19] B. G. Prasad and and et.al, "An Economic Rural Electrification Study Using Combined Hybrid Solar and Biomass-Biogas System," *Materials Today: Proceedings 5(1):220-225 DOI:10.1016/j.matpr.2017.11.075,* 2018.

[20] A. Hizkiel and G. Lakshmi, "Modeling and Simulation of Fuzzy logic based Hybrid power for Electrification System in case of Ashuda Villages," *electrical & electronic engineering > doi: 10.20944/preprints201810.0025.v1,* 2018.

[21] S. S. Chetan , Solar photovoltaics: fundamentals, technologies and applications, 2015.

[22] A. Dineva and and et.al, "Review of Soft Computing Models in Design and Control of Rotating Electrical Machines"," *https://doi.org/10.3390/en12061049,* 2019.

[23] N. Argaw and and et.al, Renewable Energy for Water Pumping Applications in Rural, National Renewable Energy Laboratory, 2003.

[24] T. Y. Tan, N. Kirschen and D. Jenkins, "A Model based PV Generation suitable for stability analysis," *IEEE Transactions on Energy Conversion ( Volume: 19, Issue0,* 2004.

[25] O. V. Shepovalova and and et.al, "Review of photovoltaic water pumping system research," *Energy Reports Volume 6, Supplement 6, November 2020,* 2020.

[26] A. Lázaro and and et.al, "Review of the maximum power point tracking algorithms stand-alone photovoltaic systems," *Solar Energy Materials and Solar Cells Volume 90, Issue 11, 6 July 2006 https://doi.org/10.1016/j.solmat.2005.10.023,* 2016.

[27] W. Xiao, "A modified adaptive hill climbing maximum power point tracking (MPPT) control method for photovoltaic power systems," *Master Thesis The University of British Columbia,* 2003.

[28] N. Mohan, T. M. Undeland and W. P. Robbins, Power electronics: converters, applications, and design, General & Introductory Electrical & Electronics Engineering /Power Electronics, 2007 .

[29] R. C. Neville, Solar energy conversion: the solar cell, Elsevier Science (January 1, 1728), 1995.

[30] A. Haddouche and and et.al, "Maximum Power Point Tracker Using Fuzzy Logic Controller with Reduced Rules," *International Journal of Power Electronics and Drive Systems 9(3):1381 DOI:10.11591/ijpeds.v9.i3.pp1381-1389,* 2018.

[31] H. B. Elreesh and A. Hosam, Design of ga-fuzzy controller for magnetic levitation using FPGA, 2011.

[32] L. Y. John and Reza, Fuzzy logic: intelligence, control, and information, 1999.

[33] M. M. Shebani and . T. Iqbal, "Dynamic Modeling, Control, and Analysis of a Solar Water Pumping System for Libya," *Renewable Energy https://doi.org/ 10.1155/2017/8504283,* 24 Apr 2017.

[34] "Climate Condition of Arba Minch," *http://www.weatherbase.com/weather/ weather all.php3?s=105360&units=us&cityname-Aba+Minch%2C+Southern+ Nations+ Nationalities+and+People%27s+Region%2C+Ethiopia&set=metric, accessed May 21, 2020* .

[35] "World Health Organization. How much water is needed in emergencies," *water_sanitation_health/Publication/2011,* 2017.

[36] S. Marcel and and et.al, "Solar Resource and Photovoltaic Power Potential of Nepal," *http://documents.worldbank.org.curated/en/585921519658176633/pdf,* 2017.

[37] "Engineering ToolBox. Hydraulic Diameter," *https://www.engineeringtoolbox. com/hydraulic-equivalent-diameter-d_458.html,* 2019.

[38] Aldjia Lazizi and and et. al, "Fuzzy logic MPPT control for a solar PV module applied to water pumping," *Int. J. Industrial Electronics and Drives,* 2016.

[39] C. Javier and and et.al, "On the analytical approach for modeling photovoltaic systems behavior," *https://core.ac.uk/download/pdf/148670076.pdf,* 2018.

[40] Gurhan Ertasgin and et al, "Analysis of DC Link Energy Storage for Single-Phase Grid-Connected PV Inverters," *European Conferece on Power Electronics and Applications,* 2019.

[41] O. Ojo and and et.al, "Concise Modulation strategies for four leg voltage source inverter," *2002 IEEE 33rd Annual IEEE Power Electronics Specialists Conference. Proceedings (Cat. No.02CH37289), DOI: 10.1109/PSEC.2002.1023876,* 2017.

[42] "Professor, Ph.D., Frede Blaabjerg (IET), Associate Professor John K. Pedersen (IET), Aalborg University Institute of Energy Technology, , pp.30, August 2005.," .

[43] B. Verhoeven, "Utility aspects of grid connected photovoltaic power systems Report IEA PVPS T5-01:1998".

[44] A. Tourkia, Lajnef and Slim, "Design and simulation of photovoltaic water pumping system," *International Journal of Advanced Technology and Engineering Exploration,* 2009.

[45] B. N. Remus and and et.al, "Optimal Design of High-Order Passive-Damped," *IEEE Transactions on Power Electronics, DOI: 10.1109/TPEL.2015.2441299,* 2016.

[46] J. J. Dai and F. Shokooh, "Industrial and Commercial Power System Harmonic Studies," *2021 IEEE/IAS 57th Industrial and Commercial Power Systems Technical Conference (I&CPS) 10.1109/ICPS51807.2021.9416593,* 2021.

[47] J. Wang, J. D. Yan and L. Jiang, "Delay-dependent stability of single-loop controlled grid-connected inverters with LCL filters," *IEEE TRANSACTIONS ON POWER ELECTRONICS, 31 (1). 743 - 757. ISSN 0885-8993,* 2016.

[48] M. Ben and and et.al, "Simple and systematic LCL filter design for three-phase grid-connected power converters," *Mathematics and Computers in Simulation Volume 130, December 2016, Pages 181-193,* 2016.

[49] Sanatkar Chayjani and Majid; Monfared, Mohammad, "Design of LCL and LCL filters for single-phase grid connected converters," *IET Power Electronics https://doi.org/ 10.1049/iet-pel.2015.0922,* 2016.

[50] K.Bose, Modern Power Electronics and ac Drives, 2011.

[51] P. Krause , O. Wasynczuk and S. D. Sudhoff, Analysis of Electric Machinery, 2002.

[52] . R. Machado and A. . F. d. Rocha, A hybrid architecture for fuzzy connectionist expert systems, 1992.

[53] C. W. d. Silva, Intelligent control: fuzzy logic applications, 1995.

[54] Y. Bai and and et.al, Advanced fuzzy logic technologies in industrial applications: Springer, 2007.

[55] B. Hamed and . M. Almobaied, "Fuzzy Logic Speed Controllers Using FPGA Technique for Three-Phase Induction Motor Drives," *Master Thesis, The Islamic University- Gaza,* 2008.

[56] J. Riby and and et.al, "Variable step size Perturb and observe MPPT algorithm for standalone solar photovoltaic system," *2017 IEEE International Conference on Intelligent Techniques in Control, Optimization and Signal Processing (INCOS),* 2017.

[57] I. Iancu, A Mamdani Type Fuzzy Logic Controller, 2012.

[58] A. Omar and and et.al, "Comparison betweentheEffectsof Different Typesof Membership Functions on Fuzzy Logic Controller Performance," *International Journal of Emerging Engineering Research and Technology,* 2015.

[59] M. Clerc and J. Kennedy, "The particle swarm-explosion, stability, and convergence in a multidimensional complex space," *IEEE Transactions on Evolutionary Computation ( Volume: 6, Issue: 1, Feb 2002), DOI: 10.1109/4235.985692,* 2002.

[60] J. K. R. Eberhart, "Particle Swarm Optimization," *Proceedings of ICNN'95 - International Conference on Neural Networks, DOI: 10.1109/ICNN.1995.488968,* 1995 .

[61] R. E. J. Kennedy, "A new optimizer using particle swarm theory," *MHS'95. Proceedings of the Sixth International Symposium on Micro Machine and Human Science DOI: 10.1109/MHS.1995.494215,* 1995.

[62] F. . E. Serrano and M. . A. Flores, "Automatic Fuzzy Membership Function Tuning Using the Particle Swarm Optimization," *IEEE Thirty Fifth Central American and Panama Convention,* 2015.

[63] V. d. B. F, "An analysis of Particle Swarm Optimizers," *Ph.D. dissertation, University of Pretoria, Pretoria, South Africa,* 2001.

[64] Mahdi Ajdani and Hamidreza Ghaffary, "Introduced a new method for enhancement of intrusiondetection with random forest and PSO algorithm," *https://doi.org/10.1002/spy2.147,* 2021.

[65] V. Nivetha and G. Vijaya Gowri, "Maximum power point tracking of photovoltaic system using ant colony and particle swam optimization algorithms," *2nd International Conference on Electronics and Communication Systems (ICECS),* 2015.

[66] Patrik Gilley and Yanjun Yan, "Comparison of Search Optimization Algorithms in Two-Stage Artificial Neural Network Training for Handwritten Digits Recognition," *IEEE DOI: 10.1109/SoutheastCon44009.2020.9249759,* 2020.

[67] Otmane Manari and et al, "Maximum power point tracking using fuzzy logic based controllers compared to P&O technique in photovoltaic generator," *International Conference DOI:10.1145/3128128.3128149,* 2017.

# Appendix A.

## A.1 Matlab code for perturb and observe algorithm

```
function D = PandO(Vpv, Ipv)
  persistent Dprev Pprev Vprev %save values of each
function call
  %first run
 if isempty(Vprev)
 Vprev=0;
 Pprev=0;
 Dprev=0.516; %start at duty of 0.5
 end
  %change in duty cycle and duty limits
 deltaD=0.01;
 minD=0.51;
 maxD=0.771;
  %power and delta calculations
 Ppv=Vpv*Ipv;
 deltaV=Vpv-Vprev;
 deltaP=Ppv-Pprev;
  %P&O algorithm
 if deltaP~=0
 if deltaP>0
 if deltaV<0
 D=Dprev-deltaD;
 else
 D=Dprev+deltaD;
 end
 else
 if deltaV<0
 D=Dprev+deltaD;
 else
```

```
 D=Dprev-deltaD;
 end
 end
 else
 D=Dprev;
 end
 %%limit duty cycle
 if D<minD
  D=minD;
 else
     D=Dprev;
end
 if D>maxD
 D=maxD;
 else
     D=Dprev;
end
%save values
 Vprev=Vpv;
 Pprev=Ppv;
 Dprev=D;
 end
```

## A.2 Matlab code for main PSO algorithm

```
clear all;
close all;
clc;
iter =input('Enter the iteration value:...');
Pop = input('Enter the population:...');
nVar = 3;         % Number of variables to be optimized
ub = [50, 20, 1];   % Upper bound of patricles
lb = [1,0.1,0.9];   % Lower bound of patricles
fobj = @Fitness_Evaluation_Obj;  % Objective Function
maxIter =iter;
wMax = 0.95;  % Maximum value of Inertia Weight
```

```
wMin = 0.5;   % Minimum value of Inertia Weight
c1 = 1.5;     % acceleration coefficients for c1
c2 = 1.8;     % acceleration coefficients for c2
D = length(lb);
f = NaN(Pop,1);     % Initializing fitness value
P = repmat(lb,Pop,1) + repmat((ub-lb),Pop,1).
* rand(Pop,D);      % Initial particles for PSO
v = repmat(lb,Pop,1) + repmat((ub-lb),Pop,1).*
rand(Pop,D);        % Initial Velocity for PSO
for p = 1: Pop
    f(p) = fobj(P(p,:));   % Fitness Calculation from
Objective function after simulating the model
end
pbest = P;      % Personal best for PSO particles
f_pbest = f;    % Best fitness value
[f_gbest ind] = min(f_pbest); % global best fitness
value
gbest = P(ind,:);    % Global best position of particles
for j =1 : maxIter
    for p = 1: Pop
 w =wMax - j.*((wMax - wMin)/maxIter); % Updating
inertial weight
% Updating Velocity and Position of the particles
v(p,:)  = w*v(p,:) + c1.*rand(1,D).*(pbest(p,:) -
P(p,:)) + c2.*rand(1,D).*(gbest - P(p,:));  %Updating
Velocity
P(p,:) = P(p,:) + v(p,:);  %Updating Position
P(p,:) = max(P(p,:),lb);   % Bounding Particles position
P(p,:) = min(P(p,:),ub);
```

```
f(p) = fobj(P(p,:));      % Calculating Fitness value
after updating the particle position
if f(p) < f_pbest(p)
   f_pbest(p) = f(p);  %Updating personal best fitness
value
   pbest(p,:) = P(p,:); %Updating personal best
     if f_pbest(p) < f_gbest
         f_gbest  = f_pbest(p);
         gbest = pbest(p,:);        %Updating global
best
      end
  end
end
bestfitness = f_gbest;
bestsol = gbest;
```

## A.3 Matlab code for objective function

```
function Cost = Fitness_Evaluation_Obj(k)
  out = sim('PO_PSO_FUZZY_MPPT'); % Simulation proposed
PVWPS model
  err = out.ISE;   % Integral of Squared Error
  Cost = err(length(err));
end
```

# Appendix B.

## B.1 MATLAB SIMULINK models

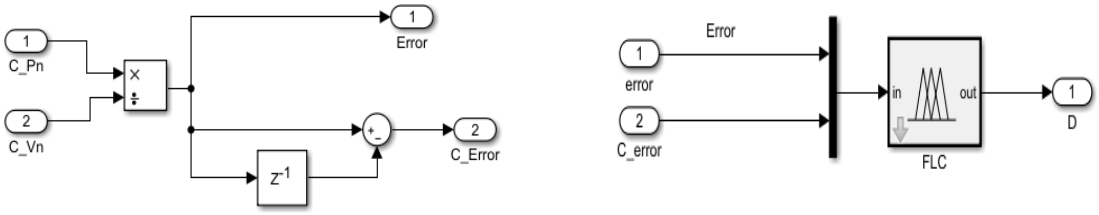


a) b)

Figure B.1 a) Error and Change of error calculation. b) Fuzzy logic controller

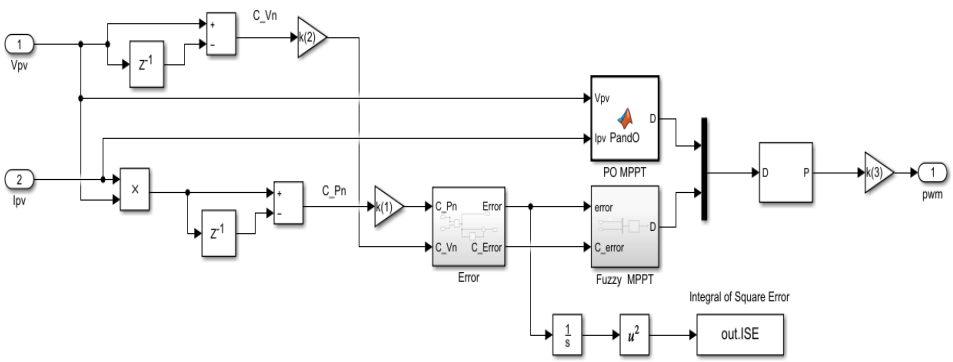


Figure B.2 MPPT techniques

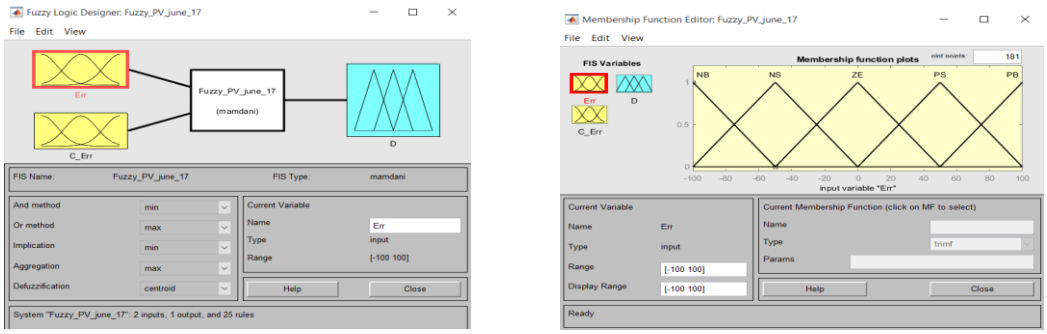


a) b)

Figure B.3 a) FIS Editor. b) Membership function of input 1

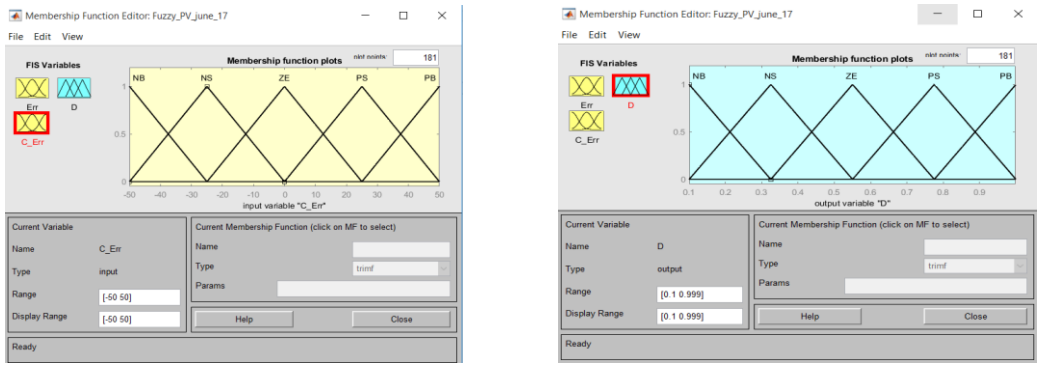


a) b)

Figure B.4 Membership function of a) input 2 b) output (Duty cycle)

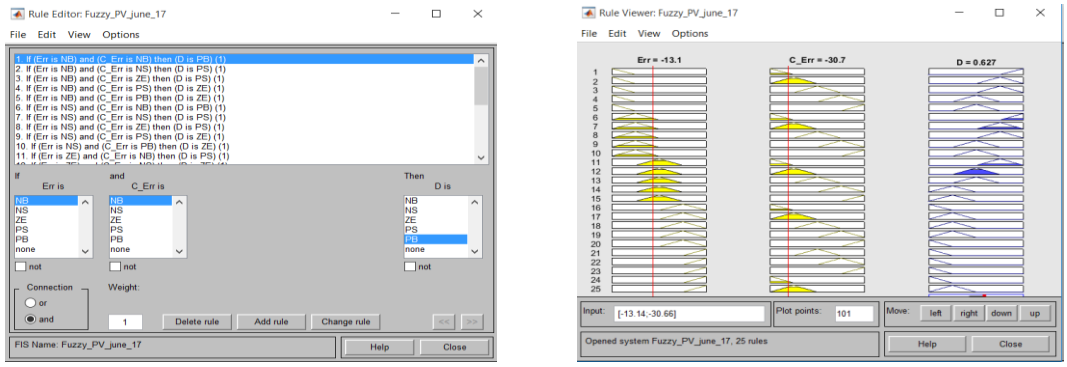


a) b)

Figure B.5 a) Rule base editor. b) Rule Viewer

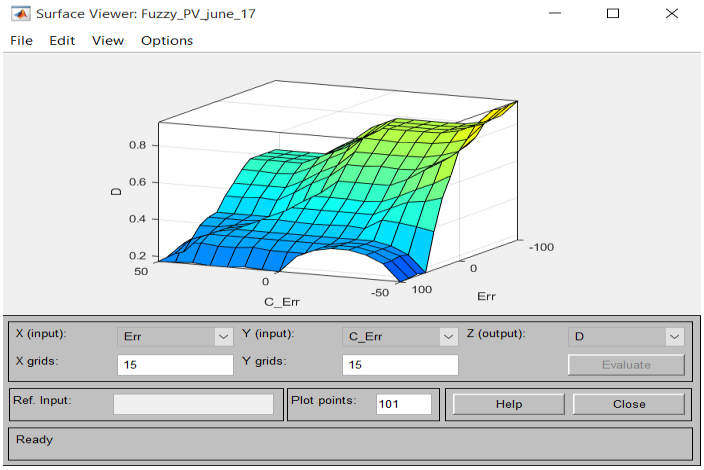


Figure B.6 Surface Viewer